GEORG-AUGUST-UNIVERSITÄT GÖTTINGEN

UNIVERSITÄTSMEDIZIN GÖTTINGEN UMG

AIRWAY EPITHELIAL CELLS AS TARGETS OF GLUCOCORTICOID THERAPY IN INFLAMMATORY LUNG DISEASES

Dissertation

in partial fulfillment of the requirements for the degree
"Doctor rerum naturalium (Dr. rer. nat.)"
of the Georg-August University Göttingen

within the "Molecular Medicine" Study Program
at the Georg-August University School of Science (GAUSS)

submitted by

Carina Klaßen

born in

Meppen, Germany

Göttingen, December 2016

Thesis Committee

Prof. Dr. Holger M. Reichardt

Institute for Cellular and Molecular Immunology

University Medical Center Göttingen

Prof. Dr. Frauke Alves

Department of Hematology and Oncology

University Medical Center Göttingen

Prof. Dr. Uwe Groß

Institute for Medical Microbiology

University Medical Center Göttingen

Additional Members of the Examination Board

Prof. Dr. Lutz Walter

Department of Primate Genetics

German Primate Center, Göttingen

Prof. Dr. mult. Thomas Meyer

Department of Psychosomatic Medicine and Psychotherapy

University Medical Center Göttingen

Prof. Dr. Hubertus Jarry

Department of Clinical and Experimental Endocrinology

University Medical Center Göttingen

Date of the oral examination: 10th February, 2017

Affidavit

I hereby declare that I have written this Ph.D. thesis entitled “Airway Epithelial Cells as Targets of Glucocorticoid Therapy in Inflammatory Lung Diseases” independently and with no other sources and aids than quoted. This thesis has not been submitted in any form to any other university.

Carina Klaßen

Göttingen, December 2016

Abstract

Glucocorticoids (GCs) have been a mainstay in the treatment of various autoimmune and allergic diseases for many decades due to their potent anti-inflammatory activities. The beneficial effects of GCs are mediated by the glucocorticoid receptor (GR) mainly through modulation of target gene expression via transactivation or transrepression. Despite their therapeutic potency, the use of GCs is limited as their broad activity profile may lead to the development of severe side effects. Therefore, a better understanding of the precise mode and site of GC-action could help to improve this therapeutic regimen.

Allergic airway inflammation (AAI) as a model of asthma was induced in GR^{dim} mice to dissect the molecular mechanisms of GCs. These mice carry a point mutation that impairs GR-dimerization and thus interferes with gene transactivation. Treatment of AAI with dexamethasone (Dex) failed to diminish clinical symptoms in the airways of GR^{dim} mice, indicating that an intact GR-dimerization interface was essential for therapeutic efficacy in this disease model. As previous data had revealed that GCs presumably target structural cells of the lung in the treatment of AAI rather than immune cells, it was tested whether airway epithelial cells (AECs) were essential targets. Hence, AAI was induced in GR^{spc} mice that specifically lack the GR in alveolar type II epithelial (AT-II) cells. Dex repressed AAI in GR^{spc} mice only partially, highlighting that AT-II cells play a crucial role for the efficacy of GC-therapy. Notably, GC-treatment of acute lung injury (ALI), another pulmonary disease, was not impaired in GR^{spc} mice.

A potential link between GC-target site and mode of action was confirmed by expression analysis of various inflammatory genes in the lung, which revealed that GR^{dim} and GR^{spc} mice behaved similarly with regard to transcriptional control. Furthermore, antibody-conjugated betamethasone nanoparticles were investigated as a novel vehicle for AT-II cell-directed delivery of GCs in AAI but did not show any efficacy in improving disease symptoms.

Taken together, the findings reported in this thesis bring about a novel concept of GC-therapy of allergic asthma, indicating that its efficacy depends on GR-dependent gene regulation in AECs. This notion paves the way for a future cell-directed delivery of GCs as an interesting approach for the improvement of GC-therapy in allergic asthma with fewer side effects.

Table of Contents

1. Introduction

The lung is one of the largest organs of the human body. The blood-air barrier in the alveoli of the lung allows direct contact of the blood circulation with oxygen from the environmental air. Therefore, the lung is highly susceptible to both exogenous and endogenous insults such as infectious bacteria and viruses, allergens or air pollutants. As consequence, the development of various lung diseases like asthma or acute lung injury (ALI) is very common. Many of these diseases are not curable and treatment is still very challenging. Despite their many side effects, glucocorticoids (GCs) are often the first- or last-line treatment.

1.1 The Airway Epithelium as Frontline Defense Against Inflammatory Lung Diseases

Most lung diseases are characterized by airway dysfunction and an extensive distortion of the lung architecture, frequently involving the epithelial lining of the lung. Over the past few decades, airway epithelial cells (AECs) were shown to be key mediators in the development of inflammatory lung diseases and important targets for novel therapeutic approaches.

1.1.1 Composition of the Airway Epithelium

The respiratory tract represents one of the largest surfaces of the human body covering an area that exceeds 120 m^2 (Hasenberg et al., 2013). It can be divided in two compartments according to their distinct functions. The conducting airways consist of the nose, the trachea and bronchi. Inhaled air is warmed, moistened and filtered from foreign particles and pathogens. The main function of the conducting airways is to transport air to the lung parenchyma where the gas exchange occurs. The lung parenchyma or the respiratory surface is comprised of the respiratory bronchi and alveoli (Hollenhorst et al., 2011; Holt et al., 2008).

Several secretory and ciliated epithelial cells with different morphologies and functions are forming the characteristic pseudostratified epithelium of the conducting airways (Camelo et al., 2014; Hollenhorst et al., 2011; Whitsett and Alenghat, 2014) (**fig. 1**).

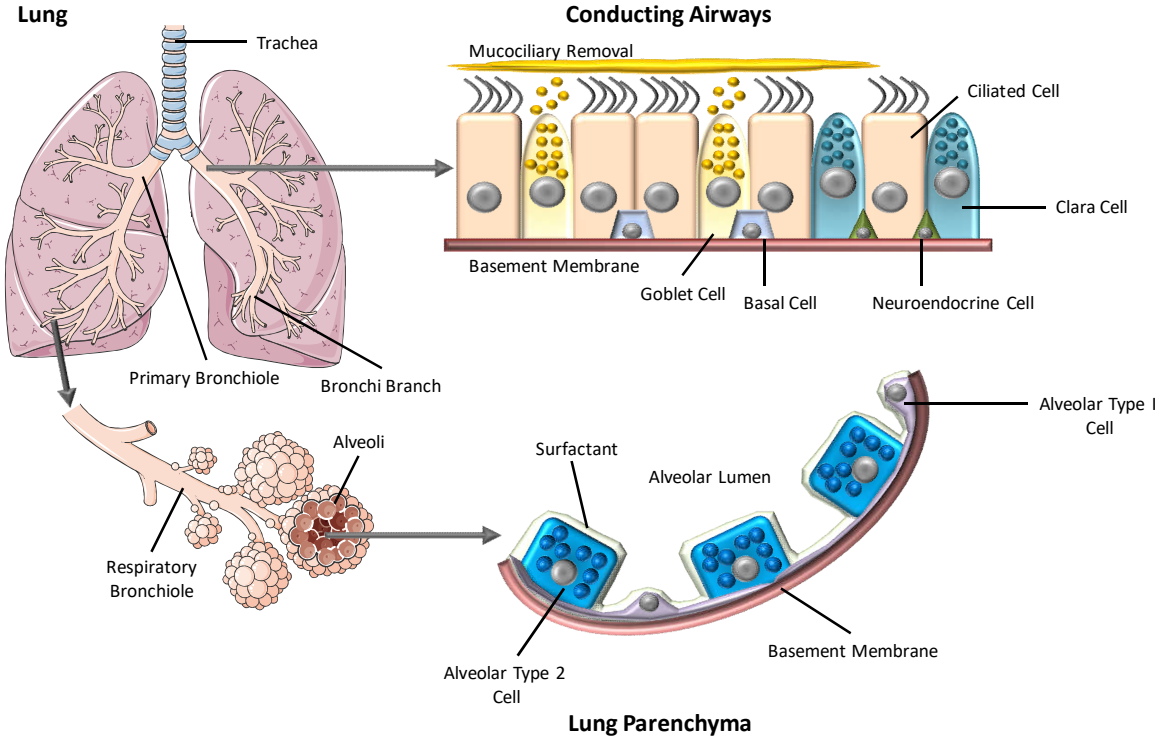

Figure 1: Cell types of the airway epithelium. The conducting airways are lined by a pseudostratified epithelium with various ciliated and secretory epithelial cells like goblet cells, clara cells, basal cells and neuroendocrine cells. In contrast, the alveoli in the lung parenchyma are formed only by AT-I and AT-II cells.

Mucous cells or goblet cells contain membrane-bound mucin granules. They produce and release mucus into the airway lumen to trap foreign particles (Camelo et al., 2014; Knight and Holgate, 2003). Ciliated epithelial cells are the most common cell type within the airways and account for 50% of all epithelial cells (Knight and Holgate, 2003). Foreign particles that are trapped in mucus are cleared from the airways by beating their motile cilia in the ascending direction (Camelo et al., 2014; Hollenhorst et al., 2011). The amount of mucus and the efficacy of the mucociliary clearance are influenced by injury or infection (Whitsett and Alenghat, 2014). Basal cells are widely distributed throughout the airways. They are located beneath the surface epithelium and directly attached to the epithelial basement membrane which forms a barrier to the underlying mesenchymal compartment. Serving as stem cells for ciliated and secretory cells, basal cells play a crucial role in the regeneration of the airway epithelium following inflammatory insults (Knight and Holgate, 2003; Whitsett and Alenghat, 2014). Pulmonary neuroendocrine

cells are found as single cells or in clusters as neuroepithelial bodies (NEBs). They are thought to sense stimuli such as hypoxia and to contribute to the regulation of growth and regeneration of other AECs (Knight and Holgate, 2003; Rock et al., 2011). Clara cells, also known as club cells, are additional secretory cells of the conducting airways and often reside close to NEBs. They contribute to the maintenance and repair of bronchioles i.e. clara cells metabolize xenobiotics, produce bronchial surfactants and specific anti-proteases (Knight and Holgate, 2003; Zheng et al., 2013).

Progressive branching of bronchioles eventually gives rise to alveolar ducts and alveoli that are part of the lung parenchyma. The distinct arrangement of the alveolar compartment directly reflects its main function as respiratory surface (Hasenberg et al., 2013). A large contact area is maintained at the blood-air barrier thereby requiring minimal place (Hollenhorst et al., 2011). The alveolar compartment comprises two types of alveolar epithelial cells: alveolar type I (AT-I) cells and type II (AT-II) cells. Squamous AT-I cells cover approximately 90% of the alveolar surface, which is due to their flattened phenotype (Camelo et al., 2014). Together with microvascular endothelial cells they form the blood-air barrier, which is also known as alveolar-capillary barrier, and facilitate efficient gas exchange. Moreover, AT-I cells have an important role in the fluid homeostasis of the lung as they are involved in ion and water transport (Hollenhorst et al., 2011). In contrast to AT-I cells, AT-II cells are smaller in size but higher in number in the alveoli (Hollenhorst et al., 2011). Their main function is the production and recycling of surfactant proteins which are stored in lamellar bodies. Surfactant reduces the surface tension of the alveoli thereby preventing it from collapsing, thus allowing efficient gas exchange (Hasenberg et al., 2013; Hollenhorst et al., 2011; Rock et al., 2011). AT-II cells are believed to serve as progenitor of AT-I cells and allow the repair of alveolar damage (Hasenberg et al., 2013; Hollenhorst et al., 2011).

The integrity and permeability of the airway epithelium are sustained by tight junctions, which are composed of various transmembrane proteins like occludin, claudin, junctional adhesion molecules (JAMs), and E-cadherin, as well as adaptor proteins such as β-catenin and zonula occludens (ZO) (Arora and Kale, 2013; Holgate, 2007). The different proteins interact to form a tight connection between neighboring AECs enabling adhesion and intercellular communication. In addition, tight junctions also prevent the entry of foreign material and bacteria (Camelo et al., 2014). Furthermore, epithelial integrity involving

cell-cell and cell-extracellular matrix (ECM) interactions is supported by desmososomes, hemidesmosomes and adherens junctions (Arora and Kale, 2013; Camelo et al., 2014). Notably, damage of tight junctions is a major hallmark of many lung diseases like asthma or ALI, and may cause increased epithelial permeability and inflammatory responses in the airways (Whitsett and Alenghat, 2014).

Importantly, many cell types of the innate and adaptive immune system reside within the airway epithelium. The conducting airways contain dense networks of antigen-presenting cells (APCs) such as macrophages and dendritic cells (DCs). Intraepithelial T cells, mast cells, plasma cells and to some extent naïve B cells reside in the lamina propria underneath the epithelial basement membrane. In the lung parenchyma, it is mainly alveolar macrophages which are present, as well as minor DC and T cell populations (Holt et al., 2008).

1.1.2 AECs in Innate and Adaptive Immune Responses

For many years, AECs were believed to exclusively function as a physical barrier against potential pathogens which are subsequently removed from the airways by mucociliary clearance. In recent years, it has become evident that AECs secrete a plethora of different regulatory and effector molecules that are involved in the frontline defense against these pathogens. Protease inhibitors, enzymes like lysozyme, defensins, mucins, lactoferrin, pentraxins, small molecules such as reactive oxygen species (ROS) and nitric oxide (NO), and many more are known to play a crucial role in neutralizing pathogens (Holt et al., 2008; Kato and Schleimer, 2007; Schleimer et al., 2007). Secretion of these anti-microbial mediators is thought to be regulated by pattern recognition receptors (PRRs) including Toll-like receptors (TLRs) and Nod-like receptors (NLRs) (**fig. 2**). AECs are able to sense pathogen-associated molecular patterns (PAMPs) or danger-associated molecular patterns (DAMPs) via expression of PRRs (Whitsett and Alenghat, 2014). TLR4 is involved in sensing inhaled allergens and thus contributes to the development of a T helper type 2 (T_H2) cell-driven immune response. Other TLRs like TLR3, TLR7, TLR8 and TLR9 are involved in the recognition of viral antigens, e.g. from respiratory syncytial virus (RSV) or influenza A virus (IAV) (Holtzman et al., 2014). NLRs including NOD1 and NOD2, as well as

the NLPR3 inflammasome complex sense viral and fungal antigens (Holtzman et al., 2014; Kato and Schleimer, 2007).

Activation of PRRs leads to the production and secretion of AEC-derived cytokines and chemokines, which serves to regulate the immune responses in the airways. Most importantly, secretion of type I and III interferons (IFNs) including IFN-β and IFN-λ improves antiviral defense mechanisms and prevents the development of respiratory diseases. Moreover, secretion of interleukin (IL)-10 and transforming growth factor-β (TGF-β) acts as a negative feedback mechanism in response to pro-inflammatory cytokines and suppresses inflammatory responses in the airways (Holtzman et al., 2014; Kato and Schleimer, 2007; Weitnauer et al., 2016).

AEC-derived cytokines and chemokines mediate the recruitment and activation of both innate and adaptive immune cells to further modulate immune responses in the lung.

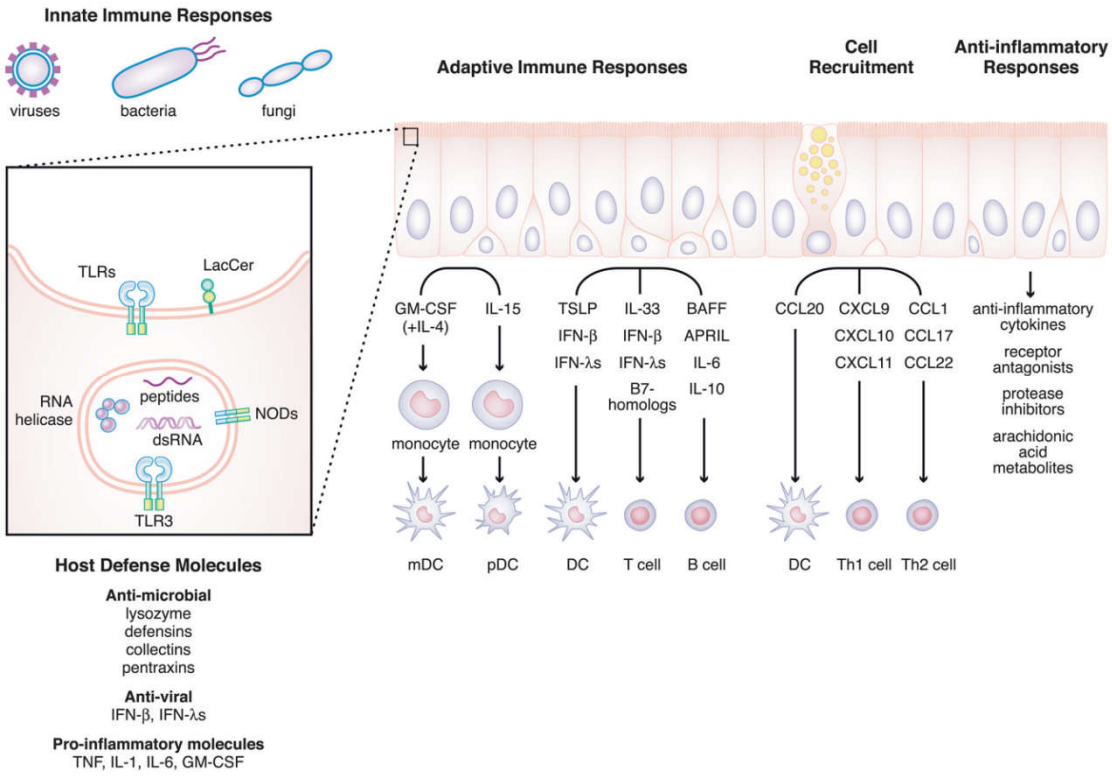

Figure 2: AECs as modulators of innate and adaptive immune responses in the lung. AECs express a wide array of PRRs including TLRs and NLRs. In response to PRR activation, they secrete a plethora of anti- and pro-inflammatory cytokines and chemokines that drive the recruitment of various immune cells like DCs, T cells and B cells in the airways. Figure taken from Kato and Schleimer, 2007.

The recruitment and local survival of DCs is mainly mediated by the secretion of CCL20 and GM-CSF. The latter also drives monocyte differentiation into the myeloid and

plasmacytoid DC subsets. Moreover, secretion of thymic stromal lymphopoietin (TSLP) by AECs drives DCs to initiate a T_H2 immune response (Kato and Schleimer, 2007; Schleimer et al., 2007).

In response to different inflammatory stimuli, AECs mediate the recruitment of distinct T cell subsets into the airways. T_H1 cells migrate into the airways in response to CXCL9, CXCL10 and CXCL11 whereas recruitment of T_H2 cells is mediated by CCL17 and CCL22. Furthermore, AECs are able to interact with T cells via the secretion of cytokines and expression of various surface molecules like CD40, Fas and Fas-ligand (FasL). AECs express B7 homologs that act as co-stimulatory molecules and are important regulators for the activation of T cells. Secretion of IL-33 by AECs enhances the T_H2 immune response by initiating the production of T_H2-specific cytokines (Kato and Schleimer, 2007; Schleimer et al., 2007).

B cells can be activated following secretion of IL-6 and TGF-β by AECs. Moreover, AECs express B cell activating factor of the tumor necrosis factor (TNF) family (BAFF) as well as a proliferation inducing ligand (APRIL) that both play crucial roles in the activation, differentiation and survival of B cells. BAFF and APRIL induce class-switch recombination (CSR) and mediate production of immunoglobulin (Ig) A and IgM in the airways. Polymeric forms of these Igs bind to the polymeric Ig receptor (pIgR), which mediates the transport across the airway epithelium into the airway lumen. This forms a crucial mechanism for the neutralization of potential antigens in the airways (Kato and Schleimer, 2007; Schleimer et al., 2007).

1.1.3 AT-II Cells as Defender of the Alveolar Compartment

In recent years, a lot of research particularly focused on the role of AT-II cells in regulating immune responses in the airways. AT-II cells are primarily known for their production of the four surfactant proteins SP-A, SP-B, SP-C and SP-D that regulate the surface tension of the alveoli. Noteworthy, SP-A and SP-D play crucial roles in innate immune responses in the airways. Both surfactant proteins are collectins that either directly bind bacterial lipopolysaccharides (LPS) or bind to the surface of pathogens which causes pathogen aggregation and subsequently removal by secretion of further antimicrobial substances like lysozyme (Fehrenbach, 2001; Hasenberg et al., 2013; Mason, 2006). In addition, surfactant proteins can act as opsonins and thereby enhance phagocytosis by local

immune cells such as alveolar macrophages (Fehrenbach, 2001; Hasenberg et al., 2013; Mason, 2006). Innate immune responses are supported by AT-II cells through the expression of TLRs, especially TLR2 and TLR4, as well as expression of complement factor C3 (Mason, 2006; Weitnauer et al., 2016).

Like other AECs, AT-II cells secrete a variety of cytokines and chemokines including IL-1β, TNF-α, IL-6 and IL-8 that can modulate the differentiation and recruitment of various immune cells (Mason, 2006). AT-II cells have been shown to secrete monocyte chemotactic protein 1 (MCP-1) and RANTES (regulated on activation, normal T cell expressed and secreted) that both attract macrophages. SP-A is also able to regulate macrophage functions including the secretion of ROS or NO (Fehrenbach, 2001).

Interestingly, AT-II cells express both major histocompatibility complex (MHC)-I and MHC-II. In the context of autoimmunity, AT-II cells were found to be able to present antigens to $CD4^+$ T cells via MHC-II molecules (Gereke et al., 2009). Nevertheless, the antigen-presenting function of AT-II cells remains controversial and needs to be further evaluated. Moreover, activation and proliferation of T cells were shown to be decreased by SP-A and SP-D, as well as by the secretion of TGF-β (Fehrenbach, 2001). In addition, T cell tolerance towards non-pathogenic antigens in the alveoli was found to be induced by AT-II cells (Lo et al., 2008).

1.2 Asthma - A Heterogeneous Disease

Asthma is a highly prevalent disease of the airways leading to bronchoconstriction and chronic inflammation, and is associated with mucus hypersecretion and most importantly airway hyperresponsiveness (AHR) (Ishmael, 2011; Shifren et al., 2012). AHR refers to a condition in which the airways contract too easily, either spontaneously or in response to stimulation. Typical triggers are cold air, physical exercise, emotional stress, inhaled allergens and respiratory infections (Drazen et al., 2015; Ishmael, 2011). Asthma patients suffer from recurrent episodes of clinical symptoms comprising wheeze, cough, chest tightness and breathlessness (Drazen et al., 2015; Holgate, 2011a). Asthma symptoms are mostly intermittent and reversible, but in some patients they may persist with irreversible airway damage (Holgate, 2011a; Nakawah et al., 2013).

Asthma can develop at any age, but first symptoms most often appear already during childhood. Most likely due to endocrine factors, women are more often affected than

men (Drazen et al., 2015; Langen et al., 2013; Martinez and Vercelli, 2013). During the last decades, asthma has become a major health problem in many countries worldwide with high socioeconomic importance due to the high increases in global prevalence and morbidity (Langen et al., 2013; Martinez and Vercelli, 2013). The World Health Organization (WHO) estimates that approximately 235 million people (*status: 2013*) worldwide suffer from asthma. In addition, it is the most common chronic disease in children. Due to the fact that asthma is often undiagnosed or undertreated especially in developing countries, the true number of asthma patients could be significantly higher (Martinez and Vercelli, 2013, WHO Asthma Fact Sheet No. 307, 2013).

In the past, asthma was often believed to be a single disease entity. In recent years, however, it has become clear that asthma is a heterogeneous disease which involves a complex interplay of genetic and environmental factors (Campo et al., 2013; Ishmael, 2011; Martinez and Vercelli, 2013). On the one hand, genome-wide association studies (GWAS) identified variations in a number of different genes related to a higher risk for the development of asthma (Martinez and Vercelli, 2013). On the other hand, the increased environmental exposure to certain allergens (house dust mite, pollen, animal dander, mould), tobacco smoke, chemicals and air pollution, is also a critical risk factor (Galli et al., 2008; Holgate, 2011a; Martinez and Vercelli, 2013). Moreover, urbanization and Western-lifestyle with excessive hygiene behavior ("*hygiene-hypothesis*") have been proposed to be disadvantageous (Liu, 2015; Ponte et al., 2016).

Because of the heterogenic origin of asthma, several disease variants with different etiologic and pathophysiological outcomes exist (Campo et al., 2013; Ishmael, 2011; Rothe, 2013; Shifren et al., 2012; Wenzel, 2012). Occupational asthma, obesity-induced asthma, as well as intrinsic and non-atopic asthma are the best known examples (Campo et al., 2013; Rothe, 2013; Wenzel, 2012). Allergic or atopic asthma, however, is the most common variant accounting for about 60% of all cases. Furthermore, asthma phenotypes can be further subdivided into so-called endotypes based on distinct pathophysiological mechanisms including distinct biomarkers (Campo et al., 2013; Rothe, 2013).

Noteworthy, asthma is often mistaken for chronic obstructive pulmonary disease (COPD). In contrast to asthma, COPD is characterized by permanent obstruction of the airways predominantly occurring in elderly people. In rare cases, asthma patients develop COPD

which is also known as asthma-COPD overlap syndrome (ACOS) (Drazen et al., 2015; Nakawah et al., 2013).

1.2.1 Allergic Pathophysiology of Asthma

Up to now, the exact mechanism underlying the development of the allergic inflammation in asthma is not fully understood. A complex interplay of cells of the innate and adaptive immune system together with structural cells of the lung and a plethora of inflammatory mediators initiates and drives the allergic cascade (**fig. 3**).

Various birth cohort studies revealed that rhinovirus infections in infants are a major cause for the development of the allergic airway inflammation. Early viral infections lead to a substantial damage of the airway epithelium which makes it more susceptible to certain triggers (Guilbert and Denlinger, 2010; Martinez and Vercelli, 2013). Inhaled allergens are able to escape from mucociliary clearance and penetrate the disrupted airway epithelium. Professional APCs such as DCs recognize these allergens and subsequently phagocytose them. DCs migrate to local lymph nodes where they process them into small allergenic peptides which are presented to naïve T cells (Bloemen et al., 2007; Galli et al., 2008; Verstraelen et al., 2008). Interaction of DCs with T cells is mediated via MHC-II molecules together with co-stimulatory molecules including B7-1 and B7-2 (CD80 and CD86) (Holgate, 2012a). Naïve T cells undergo clonal expansion and differentiate into T_H2 cells under the influence of polarizing cytokines, in this case mainly IL-4. This in turn leads to the production and secretion of T_H2 cell-specific cytokines, most importantly IL-3, IL-4, IL-5, IL-9, IL-13 and GM-CSF that drive the following steps of the allergic cascade (Holgate, 2011a; Verstraelen et al., 2008). In addition, allergen-triggered AECs can also activate T cells and DCs by the secretion of IL-25, IL-33 and TSLP, which cause their migration into the airways. At the same time, these cytokines can also activate type 2 innate lymphoid cells (ILC2) that are another important source of T_H2-specific cytokines and amplify the T_H2 cell-specific responses in asthma (Holgate, 2012a; van Rijt et al., 2016; Scanlon and McKenzie, 2012). In comparison to T_H2 cells, the exact role of ILC2 cells as source of T_H2-specific cytokines is unknown (Fahy, 2015). ILC2 cells have been hypothesized to orchestrate the immune responses between AECs and cells of innate and adaptive immunity (van Rijt et al., 2016).

T_H2 cells induce CSR in B cells mainly through secretion of IL-4 and IL-13, but also via the co-stimulatory molecule CD40L (Holgate, 2012a). During the allergic cascade, plasma cells mainly secrete IgE antibodies. IgE enters the systemic circulation and binds to its high-affinity receptor FcεRI on mast cells and basophils (Bloemen et al., 2007; Galli et al., 2008). Binding of IgE to mast cells, sensitizes them for future allergen re-exposure. Each IgE antibody, which is bound to a single mast cell, is specific for a distinct allergen (Galli et al., 2008). Thus, mast cells are the major effector cells during allergen sensitization and also in the early-asthmatic responses. These early-phase reactions usually occur within minutes after allergen re-exposure.

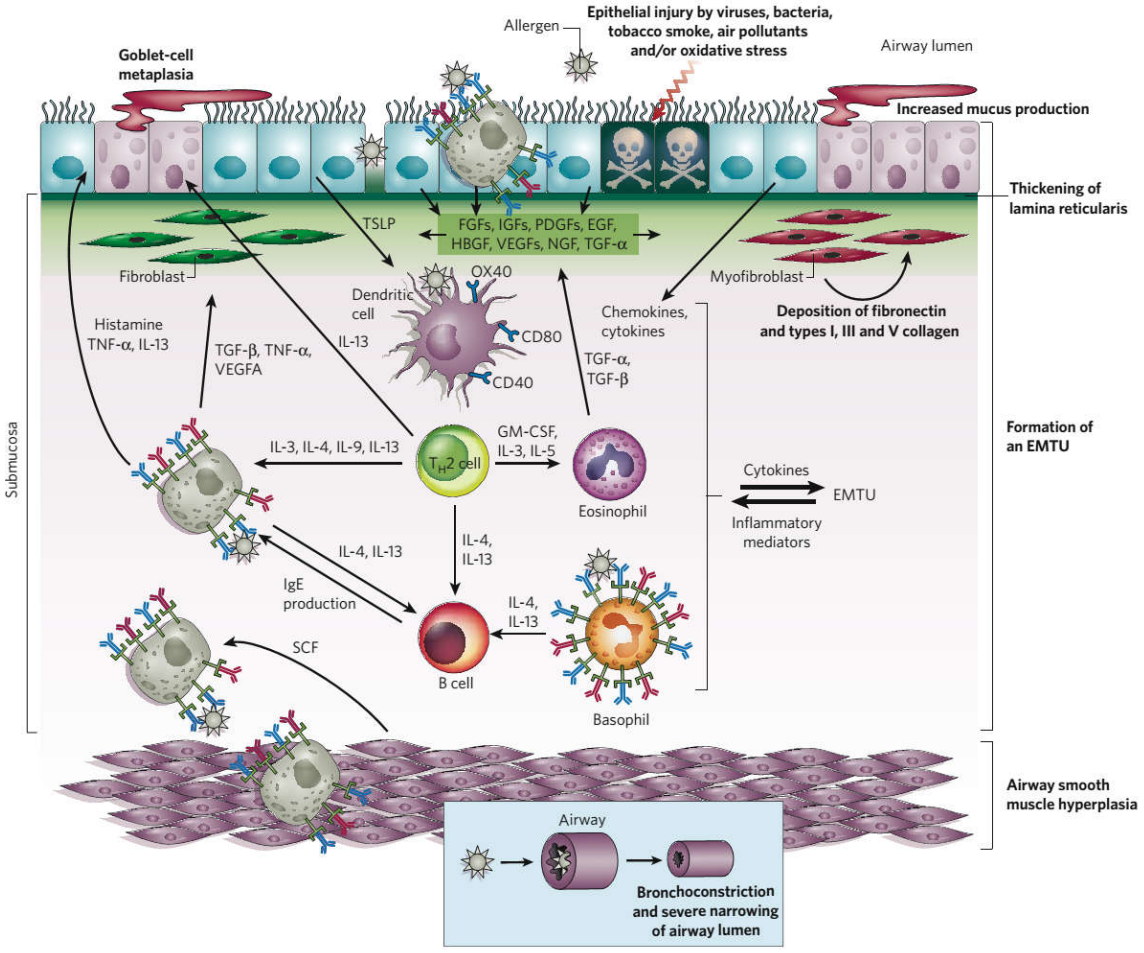

Figure 3: Immunological pathways involved in the pathogenesis of allergic asthma. Following allergen sensitization, the early-phase response is mainly characterized by mast cell degranulation. This initiates the recruitment of additional inflammatory cells that secrete further pro-inflammatory mediators. During the late-phase response, eosinophils become the major effector cells of airway damage and dysfunction in allergic asthma. Eosinophil-dominated inflammation is induced and maintained by T_H2 cells. Continuing allergen exposure leads to the development of chronic inflammation which is characterized by substantial damage of structural cells of the lung. Taken from Galli et al., 2008.

Allergens cross-link mast cell-bound IgE antibodies which leads to FcεRI aggregation and causes mast cell degranulation (Galli et al., 2008; Verstraelen et al., 2008). Subsequently, preformed inflammatory mediators such as histamine, serine proteases, TNF-α, prostaglandins and leukotrienes, as well as chemokines like IL-8 are released. The rapidly secreted mediators cause immediate symptoms like cough, bronchoconstriction and increased mucus secretion (Bloemen et al., 2007; Galli et al., 2008; Verstraelen et al., 2008). Furthermore, mast cell degranulation also contributes to the initiation of the late-phase asthmatic response, which occurs several hours after allergen re-exposure. Mast cell-derived inflammatory mediators promote the activation and recruitment of further inflammatory cells to the site of action (Galli et al., 2008).

Allergen-stimulated T_H2 cells are not only important in the induction of the allergic cascade, but also play a substantial role in the ongoing inflammation by excessive secretion of cytokines. Together with IL-4 and IL-13, IL-9 is known to mediate the generation of more mast cells and directly contributes to AHR and mucus hypersecretion (Bloemen et al., 2007). IL-5 and GM-CSF mediate eosinophil maturation and migration to inflamed sites (Bloemen et al., 2007; Holgate, 2012a; Verstraelen et al., 2008). As mentioned earlier, eosinophils are the major effector cells in this late-phase response. Secretion of eosinophil granule proteins such as major basic protein (MBP), eosinophil cationic protein (ECP), eosinophil-derived neurotoxin (EDN) and eosinophil peroxidase (EP) cause major tissue damage especially to endothelial cells and the ECM (Bloemen et al., 2007). Together with T_H2 cytokines, these eosinophil-derived mediators promote the recruitment of more eosinophils and T_H2 cells to the inflammatory site, which fosters an ongoing eosinophil-driven inflammation in the allergic airways (Bloemen et al., 2007; Verstraelen et al., 2008).

A chronic airway inflammation develops when allergen exposure is either repetitive or continuous. Then, airway remodeling occurs due to the persistent interaction between inflammatory cells and structural cells of the lung (Bloemen et al., 2007; Galli et al., 2008; Verstraelen et al., 2008). The formation of the so-called epithelial-mesenchymal trophic unit (EMTU) is the consequence of continuous damage to AECs and the underlying mesenchymal cells. This unit is thought to regulate airway remodeling by sustaining the T_H2-specific response, e.g. through secretion of TSLP (Galli et al., 2008). Structural changes in the allergic airways include hyperplasia of goblet cells along with increased

mucus hypersecretion, deposition of ECM proteins such as fibronectin and collagen, as well as airway wall thickening which includes the airway epithelium, airway smooth muscle cells and the lamina reticularis. Moreover, subepithelial fibrosis and vascular permeability are induced (Bloemen et al., 2007; Galli et al., 2008; Verstraelen et al., 2008). Eventually, airway remodeling substantially affects lung function and can lead to irreversible damage (Galli et al., 2008).

1.2.2 Traditional and Novel Concepts for the Treatment of Asthma

Current therapeutic approaches have little or no effect on the natural history of asthma, meaning they cannot prevent the development of the disease. Furthermore, these approaches are not able to cure asthma (Holgate, 2012b).

As allergen sensitization is the crucial step in the development of asthma, allergen avoidance should be a good prophylactic strategy. However, this strategy is controversially discussed and had only limited success in the past (Holgate, 2013). Avoidance of common allergens such as house dust mite did not reduce asthma symptoms in adults whereas it seemed to be effective in children (Martinez and Vercelli, 2013).

In line with this notion, there has been only limited success with allergen-specific immunotherapy. Here, patients receive multiple injections of a distinct allergen to induce immunological tolerance towards that allergen. Once tolerance has been established, it can last for several years thereby preventing the development of asthma symptoms. Nevertheless, this method is only effective in patients that are sensitized to a single allergen (e.g. animal dander or pollen). Most asthma patients, however, are sensitized to multiple allergens (Holgate, 2013; Holgate and Polosa, 2008). Thus, environmental control and immunotherapy are less suitable approaches for asthma management, and symptom-relieving and controller therapies are still required to interfere with the inflammatory responses and airway remodeling processes (Holgate and Polosa, 2008). Pharmacological strategies include the use of anti-inflammatory agents and bronchodilators.

For decades, inhaled GCs (ICs) have been a mainstay in the treatment of asthma. Despite the complexity of the disease, ICs effectively control asthma symptoms by suppressing the inflammatory responses in the allergic airways (Barnes, 2011a; Martinez and Vercelli,

2013). They are often used in combination with long-acting β2-agonists (LABAs) that are the most effective bronchodilators. LABAs like salmeterol and formoterol directly induce airway smooth muscle relaxation irrespective of the inciting bronchoconstricting stimulus (Barnes, 2011a, 2012). LABAs can potentiate GC-actions and vice versa. Both are very effective in improving lung function and in reducing asthma exacerbations (Barnes, 2012; Holgate and Polosa, 2008). Nevertheless, LABAs should never be used without GCs as this can worsen the inflammatory responses and lead to severe asthma exacerbations (Barnes, 2011a, 2012). In contrast to LABAs, short-acting β2-agonists (SABAs) like salbutamol and terbutaline are used alone (without GCs) and provide quick relieve of sudden asthma exacerbations (Holgate and Polosa, 2008).

Other anti-inflammatory approaches include the use of leukotriene receptor antagonists. Leukotrienes are pro-inflammatory mediators that are mainly secreted by mast cells to promote tissue damage. Antagonists like montelukast have been shown to improve asthma symptoms by mediating airway smooth muscle relaxation and diminishing mucus secretion. Unfortunately, these beneficial effects are not as effective as those mediated by ICs (Barnes, 2011a; Holgate, 2012b; Martinez and Vercelli, 2013).

An advanced understanding of the pathophysiological mechanisms of asthma has led to the development of biologic agents targeting distinct aspects of the allergic cascade.

Omalizumab is currently the only monoclonal antibody for the treatment of asthma that has been approved by the Food and Drug Administration (FDA) and European Medicines Agency (EMA) (Barnes, 2012; Campo et al., 2013). It targets the Fcε3 region of IgE antibodies that is required for binding to the high-affinity receptor FcεRI. Hence, mast cell-mediated effects in the early-phase and late-phase of the allergic cascade can be blocked (Holgate, 2012b, 2013). Treatment with omalizumab has been shown to be very effective in reducing asthma symptoms, although part of the patients responded only moderately or were even completely refractory (Holgate, 2012b, 2013). So far, no biomarkers have been identified to distinguish between responders and non-responders of omalizumab (Barnes, 2012). Additional limiting factors are the large doses that are required to treat patients, as well as the resulting high costs of asthma treatment (Martinez and Vercelli, 2013).

T_H2 cytokines have been of major interest for the development of monoclonal antibodies in the treatment of asthma (Holgate, 2012a). They play crucial roles in different steps of

the allergic cascade and contribute to inflammation by interaction with other immune cells, as well as structural cells of the lung.

Mepolizumab targets IL-5 which is an essential cytokine for eosinophil maturation and recruitment. Use of this antibody was found to reduce sputum and circulating eosinophils whereas airway-resident and bone marrow eosinophils were only reduced to half. Importantly, only selected patients showed improved symptoms (Holgate, 2012a, 2012b; Martinez and Vercelli, 2013).

Pitrakinra is a mutated form of IL-4 that blocks binding of both IL-4 and IL-13 to the IL-4Rα receptor subunit. Treatment showed minor effects in the late-phase responses in selected patients. Thus, clinical studies with pitrakinra have been largely disappointing (Barnes, 2012; Holgate, 2013; Martinez and Vercelli, 2013).

IL-13 can be blocked by lebrikizumab, but again, symptoms were only improved in selected patients (Barnes, 2012; Holgate, 2012a; Martinez and Vercelli, 2013). In this case, however, the identification of periostin as a biomarker has been of major interest as it allows to distinguish between responders and non-responders to lebrikizumab treatment. High levels of periostin, an AEC-derived ECM protein, were found in those patients who responded well to the treatment (Holgate, 2012a; Martinez and Vercelli, 2013).

Currently, many other monoclonal antibodies e.g. specific for IL-25, IL-33 and GM-CSF, are being tested in clinical trials for their use in asthma (Barnes, 2012). Nevertheless, these monoclonal antibodies mostly work in distinct endotypes of asthma with the expression of distinct biomarkers. Moreover, it is unlikely that interference with one single cytokine is sufficient for effective treatment as a plethora of inflammatory mediators is involved in the allergic responses of asthma (Barnes, 2012).

1.2.3 Murine Models of Allergic Airway Inflammation

The knowledge of the exact pathophysiology and immunomechanisms involved in the development of asthma is still incomplete. For obvious ethical reasons, comprehensive studies in asthma patients are restricted to morphological and *in vitro* analyses (Kips et al., 2003). *In vitro* models with specific cell lines seem to be informative for studying the asthma pathogenesis. However, their use is limited because they often do not reflect the *in vivo* situation sufficiently enough. In asthma, complex interactions between immune cells and structural cells of the lung, as well as other biological and chemical processes

throughout the whole human body, mediate the outcome of the disease (Zosky and Sly, 2007).

For more than 100 years, animal models have been extensively used to investigate the different pathophysiological mechanisms in asthma. So far, most knowledge has been derived from numerous studies with animals although different aspects of the human situation are missing. Moreover, animal models are the best tool for developing and testing potential therapeutic approaches for asthma (Bates et al., 2009; Shin et al., 2009; Zosky and Sly, 2007).

Mice are the most popular species for mimicking allergic responses in the airways. Amongst others, this is due to various practical advantages like low costs and a short gestation period (Bates et al., 2009; Shin et al., 2009). Furthermore, the availability of genetically characterized inbred strains allows good reproducibility (Kips et al., 2003). Different processes or molecules can easily be manipulated in mice by a wide range of immunological and molecular biological tools, allowing to gain a better understanding of their importance in asthma. This can be done by using transgenic technologies or by using distinct antagonists or agonists to interfere with that distinct molecule or process (Bates et al., 2009; Kips et al., 2003; Zosky and Sly, 2007).

Under normal circumstances, mice do not develop asthma naturally. An allergic airway inflammation (AAI) needs to be induced which mimics the main features of the human disease (Kips et al., 2003; Nials and Uddin, 2008). Mice can be sensitized with different compounds to which they are normally not exposed. Model allergens include house dust mite, cockroach antigens, and aspergillus fumigatus, although ovalbumine (OVA) is most commonly used (Zosky and Sly, 2007). Mice are usually sensitized several times by intraperitoneal (i.p.) injections of the respective model allergen together with an adjuvant. In case of the AAI model, aluminium hydroxide (alum) is used to boost a T_H2-response. Following sensitization, allergen exposure is performed either by using aerosols or by nasal instillation of the respective allergen (Bates et al., 2009; Kips et al., 2003; Nials and Uddin, 2008). This strategy leads to a strong T_H2-cell mediated inflammation in the airways characterized by elevated IgE levels, eosinophilia and structural changes like goblet cell hyperplasia and epithelial hypertrophy (Nials and Uddin, 2008; Zosky and Sly, 2007). Of note, mice develop AHR only in response to bronchoconstricting stimuli like metacholine (Shin et al., 2009; Zosky and Sly, 2007). Another limiting factor is the lack of

chronicity in this acute model. Human asthma is characterized by chronic lung inflammation. In mice, however, approaches with long-term exposure to allergens failed to induce any chronic inflammation. Extended exposure rather led to decreased inflammatory responses in the airways with the development of immune tolerance towards the model allergen (Bates et al., 2009; Nials and Uddin, 2008; Zosky and Sly, 2007). Unfortunately, there is no uniform model for allergen sensitization and exposure as different time points and durations of treatment can significantly influence the severity and outcome of inflammation (Bates et al., 2009). Additional limiting factors are obvious differences in human and murine lung physiology, as well as immunological differences (Zosky and Sly, 2007).

Although murine models of AAI can provide promising results for future therapeutic approaches, interpretation and extrapolation to human asthma remain very challenging.

1.3 ALI and Acute Respiratory Distress Syndrome - A Paradigm Shift

In 1967, Ashbaugh and colleagues were the first to use the term "acute respiratory distress syndrome" (ARDS) to describe a group of critically ill patients with acute onset of respiratory failure (Ashbaugh et al., 1967). ARDS is not a distinct pulmonary disease but rather the most severe manifestation of a continuous inflammatory process that is known as acute lung injury (ALI) (Butt et al., 2016; Mackay and Al-Haddad, 2009). ALI can be the consequence to a plethora of inflammatory insults to the lung that can be either direct or indirect. Typical direct causes are pneumonia, gastric aspiration, contusion or pulmonary embolism. Indirect insults include sepsis, trauma, pancreatitis, blood transfusions and drug abuse (Howell and Bellingan, 2009). Most cases of ALI are associated with sepsis (Mackay and Al-Haddad, 2009). Of note, patients with similar insults would never show the same course of the disease since environmental factors such as age, sex, predisposing pulmonary diseases and smoking history substantially affect the pathogenesis (Howell and Bellingan, 2009). Currently, a lot of research is dealing with the role of genetic factors regarding the susceptibility and disease course of ALI. Certain polymorphisms in genes encoding for angiotensin converting enzyme (ACE), IL-10 or vascular endothelial growth factor (VEGF) were shown to be protective concerning mortality (Reddy and Kleeberger, 2009; Sharp et al., 2015).

The multi-factorial origin of ALI extensively hinders its diagnosis. In general, ALI is characterized by its acute onset with bilateral pulmonary infiltrates of leukocytes, edema formation and hypoxia. Differential diagnosis is indispensable because of the non-specific symptoms. Other pulmonary diseases, as well as many cardiac diseases present with similar symptoms and need to be considered to allow correct diagnosis of ALI (Saguil and Fargo, 2012). Due to these diagnostic difficulties, ALI and ARDS remain underdiagnosed. Thus, ALI has a remarkable impact on public health care as there is a higher incidence than reported (Rubenfeld et al., 2005). It is estimated that approximately 17-34 persons per 100.000 develop ALI every year in the USA. Around 70% of all ALI patients suffer from ARDS and the mortality rate in ALI patients is between 35-40% (Laycock and Rajah, 2010; (Mackay and Al-Haddad, 2009). Importantly, patients mostly die due to complications of the underlying insult or multi-organ failure (Laycock and Rajah, 2010).

1.3.1 Pathophysiology of ALI

Regardless of the exact inflammatory insult, ALI patients show a similar pathophysiology which is incompletely understood (Mackay and Al-Haddad, 2009). The immune responses taking place in ALI are not locally restricted to the lung. Namely, the innate immune system plays a crucial role in regulating communication systemically between the lung and other organs that are directly involved in the progression of the disease (Han and Mallampalli, 2015).

The acute or exudative phase of ALI starts a few hours after the initial direct or indirect inflammatory insult to the lung (**fig. 4**). Alveolar macrophages sense PAMPs and DAMPs via TLR-signaling. In response, they secrete a broad range of cytokines, most importantly IL-1β, IL-6, IL-8, IL-10 and TNF-α, which leads to the recruitment and activation of circulating monocytes and neutrophils, as well as other leukocytes (Butt et al., 2016; Han and Mallampalli, 2015; Johnson and Matthay, 2010).

The excessive recruitment and activation of neutrophils is mediated by IL-8 and represents a major hallmark of the pathogenesis of ALI. Degranulation of neutrophils leads to the secretion of various pro-inflammatory mediators like leukotrienes, proteases, platelet-activating factors (PAFs), elastase and ROS. This results in hypoxemia and provokes massive epithelial and endothelial injury thus reducing the lung compliance. In

addition, accumulation of neutrophils at inflamed tissue sites leads to the formation of so-called neutrophil-extracellular traps (NETs). On the one hand, NETs can build a barrier to inhibit further spread of pathogens. On the other hand, increased NETosis initiates cell death mechanisms and may cause additional tissue damage (Butt et al., 2016; Han and Mallampalli, 2015; Narasaraju et al., 2011; Sharp et al., 2015). Epithelial and endothelial cell injury and death provokes the disruption of the alveolar-capillary barrier integrity.

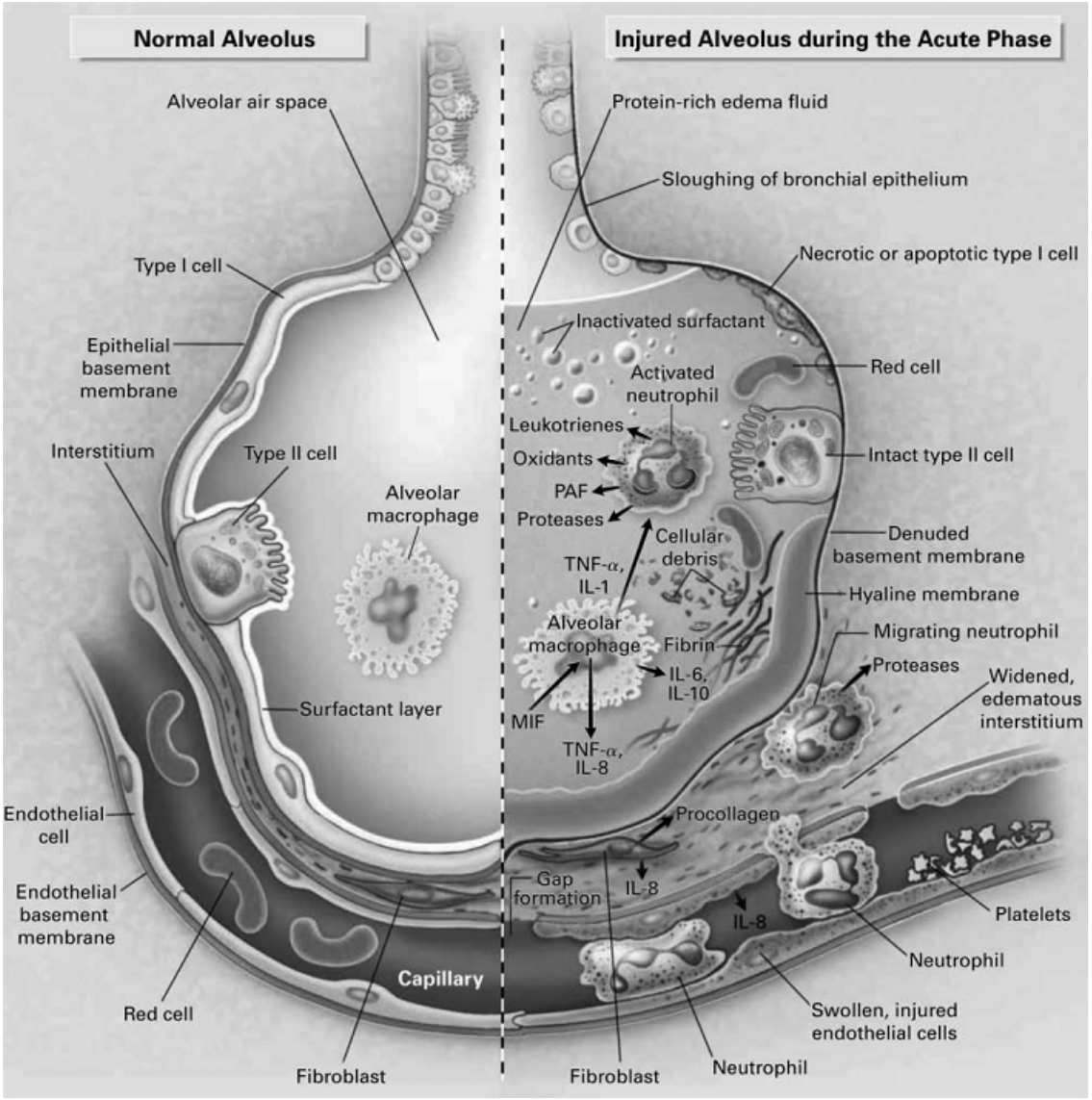

Figure 4: An alveolus in a healthy and injured state during ALI. An insult to the lung leads to massive infiltration of leukocytes into the airways which is dominated by neutrophils. Alveolar macrophages secrete a plethora of inflammatory cytokines promoting tissue damage and airway dysfunction. Damage to the epithelial and endothelial barrier causes vascular leakage and the development of pulmonary edema. In addition, coagulation is initiated whereas fibrinolysis is impaired. Fibroblasts further promote alveolar damage by inducing fibrosis in the alveolar epithelium and endothelium. Figure taken from Johnson and Matthay, 2010.

Downregulation of sodium channels and sodium-potassium pumps impairs fluid transport in the alveoli (Johnson and Matthay, 2010; Sharp et al., 2015). Vascular leakage occurs and protein-rich edema fluid enters the alveoli and interstitium leading to the formation of hyaline membranes. Consequently, there is a loss in surfactant production by alveolar epithelial cells (Johnson and Matthay, 2010).

In addition to the formation of pulmonary edema, platelet- and fibrin-rich thrombi are formed by impaired fibrinolysis and increased coagulation (Laycock and Rajah, 2010). The amount of neutrophils in the injured lung correlates with the severity of alveolar and capillary permeability, as well as hypoxemia. Enhanced neutrophilia serves as marker for poor survival (Mackay and Al-Haddad, 2009; Sharp et al., 2015).

One week after disease onset, the proliferative phase occurs which is characterized by more pronounced damage of the alveolar-capillary barrier. AT-I cells undergo necrosis which denudes the epithelial basement membrane. This results in massive proliferation of AT-II cells (Howell and Bellingan, 2009; Mackay and Al-Haddad, 2009; Sharp et al., 2015). Moreover, fibrinous exudates are replaced by collagen fibrils mediating the invasion of fibroblasts into the alveolar lumen and interstitium (Howell and Bellingan, 2009).

In some patients resolution of ALI can be observed which is not yet understood. The alveolar and capillary barrier is repaired, which results in the removal of protein-rich edema fluid from the alveoli. Furthermore, clearance of neutrophils is a prerequisite for this process (Sharp et al., 2015).

Despite the potential resolution of ALI, most patients progress to the fibrotic and chronic phase of the disease starting approximately two weeks after onset (Sharp et al., 2015). While neutrophils are the major effector cells during disease onset, fibroblasts are the key players in this fibrotic phase. Excessive fibroblast proliferation leads to deposition of ECM and collagen. This contributes to epithelial and endothelial fibrosis which is known as fibrosing alveolitis (Laycock and Rajah, 2010). The dense fibrosis may cause pulmonary hypertension which worsens the impaired lung compliance and gas exchange, and may contribute to multi-organ failure in ALI patients (Howell and Bellingan, 2009; Sharp et al., 2015). In the past, it was thought that these three disease phases progress sequentially. However, recent studies revealed that the three phases can also occur simultaneously (Howell and Bellingan, 2009).

1.3.2 Therapeutic Intervention for ALI

Due to the incomplete understanding of its pathophysiology, treatment of ALI is very difficult. In general, it is essential to provide good supportive care while maintaining oxygenation. Furthermore, the underlying cause of ALI needs to be identified and immediately treated to inhibit further complications. Therapeutic strategies are thus based on ventilatory, non-ventilatory and pharmacological approaches.

The use of many pharmacological approaches is debatable. Various studies have shown that most pharmacological agents are not effective in decreasing mortality.

Application of exogenous lung surfactant improves oxygenation and alveolar surface tension (Howell and Bellingan, 2009). Inhaled nitric oxide (NO) has been shown to increase vasodilation in aerated areas of the lung which leads to the redistribution of the blood flow to these aerated areas (Diaz et al., 2010; Howell and Bellingan, 2009). The use of NO, however, is dangerous because it can react with ROS to form reactive nitrogen species which is highly cytotoxic to the alveolar epithelium (Diaz et al., 2010). More approaches include low-molecular weight heparin to prevent thromboembolism (Saguil and Fargo, 2012) and β_2-agonists like salbutamol to increase alveolar fluid clearance by upregulating alveolar sodium channels and sodium-potassium pumps (Howell and Bellingan, 2009; Johnson and Matthay, 2010).

GCs are popular due to their potent anti-inflammatory and anti-fibrotic activities. Studies, however, revealed a controversial role of GCs in the treatment of ALI. On the one hand, ALI symptoms were not improved after GC-treatment (Hough, 2014). On the other hand, GCs were shown to prevent the progression to ARDS and to reduce the mortality (Diaz et al., 2010; Marik et al., 2011). Many clinical trials are currently trying to assess the treatment parameters for more effective GC-treatment in ALI.

If though treatment was successful, ALI survivors tend to have a lower quality of life. They have cognitive deficits, suffer from post-traumatic stress disorder and have a decreased lung function due to remarkable damage of the lung (Howell and Bellingan, 2009; Mackay and Al-Haddad, 2009; Saguil and Fargo, 2012).

Thus, more research needs to be done to obtain a better understanding of ALI and subsequently to develop better strategies to treat this disease while preventing complications at the same time.

1.3.3 Murine Models of ALI

Similar to asthma, mice are the most popular species to study the pathomechanisms of ALI. Murine models mimic major characteristics of human ALI like the disrupted alveolar-capillary barrier, damaged epithelial and endothelial cells, massive influx of inflammatory cells into the airways, and signs of fibrosing lung tissue.

A frequently employed ALI model is the use of bacterial endotoxins. LPS are glycolipids that are found in the outer membrane of gram-negative bacteria. They activate CD14/TLR4 receptors on monocytes and other myeloid cells that subsequently secrete various pro-inflammatory mediators (Matute-Bello et al., 2008). In addition, LPS plays a crucial role in bacterial sepsis which is one of the most common predisposing conditions of ALI. In general, LPS exposure primarily affects the endothelium. Apoptosis of endothelial cells leads to further tissue damage which is characterized by injured AT-I and AT-II cells, as well as accumulation of neutrophils (Matute-Bello et al., 2008). Noteworthy, the route of LPS administration in mice can determine the severity of the lung injury. Intraperitoneal injection of LPS leads to a mild form of ALI but instead causes a systemic inflammation in mice (Bastarache and Blackwell, 2009). In contrast, intratracheal application of LPS leads to massive influx of neutrophils and other inflammatory cells into the airways (Bastarache and Blackwell, 2009; Matute-Bello et al., 2008).

Oleic acid (OA) is the most common free fatty acid in the human body that is present in plasma, cell membranes and adipose tissue. Intravenous administration of OA in mice favorably targets the lung as it comprises around 85% free fatty acids (Gonçalves-de-Albuquerque et al., 2015). In contrast to LPS, OA induces necrosis of endothelial cells by direct toxic effects (Matute-Bello et al., 2008). In addition, an injured alveolar epithelium leads to a disturbed barrier function and subsequent pulmonary edema formation. This is accompanied by microvascular thrombosis (Gonçalves-de-Albuquerque et al., 2015; Matute-Bello et al., 2008). Pulmonary emboli in trauma patients contain approximately 50% OA (Matute-Bello et al., 2008). Therefore, the OA model has widely been used to model trauma-related lung injury.

Up to now, no single murine model is able to replicate all pathogenic characteristics of ALI (Bastarache and Blackwell, 2009; Matute-Bello et al., 2008). Thus, murine models with

more than one injurious insults to the lung may reflect of the human situation better (*"two-hit hypothesis"*) (Matute-Bello et al., 2011).

1.4 Glucocorticoids in Inflammatory Lung Diseases

It has been 70 years since Hench and colleagues discovered the powerful use of the GC cortisone to treat symptoms of rheumatoid arthritis, a discovery that revolutionized the field of medicine (Kadmiel and Cidlowski, 2013). Since then cortisone and its synthetic analogues such as prednisolone, dexamethasone (Dex) and budesonide have been widely used to treat various inflammatory disorders like asthma, multiple sclerosis, dermatitis and ulcerative colitis (Buttgereit, 2012; Cruz-Topete and Cidlowski, 2015). Up to now, GCs have been the most prescribed drug worldwide due to their broad availability, cost-efficacy and potent anti-inflammatory activities (Cruz-Topete and Cidlowski, 2015; Stahn and Buttgereit, 2008).

GCs such as cortisol in humans and corticosterone in rodents belong to the family of steroid hormones. The so-called hypothalamus-pituitary-adrenal (HPA)-axis dynamically regulates their synthesis in a circadian and ultradian manner (Kadmiel and Cidlowski, 2013). In response to stressful stimuli including inflammation, the hypothalamus secretes corticotrophin-releasing hormone (CRH), which in turn acts on the pituitary gland to secrete adrenocorticotropic hormone (ACTH) (**fig. 5**). Subsequently, ACTH induces the release of GCs such as cortisol by the adrenal cortex (Cruz-Topete and Cidlowski, 2015; Gupta and Bhatia, 2008; Rhen and Cidlowski, 2005).

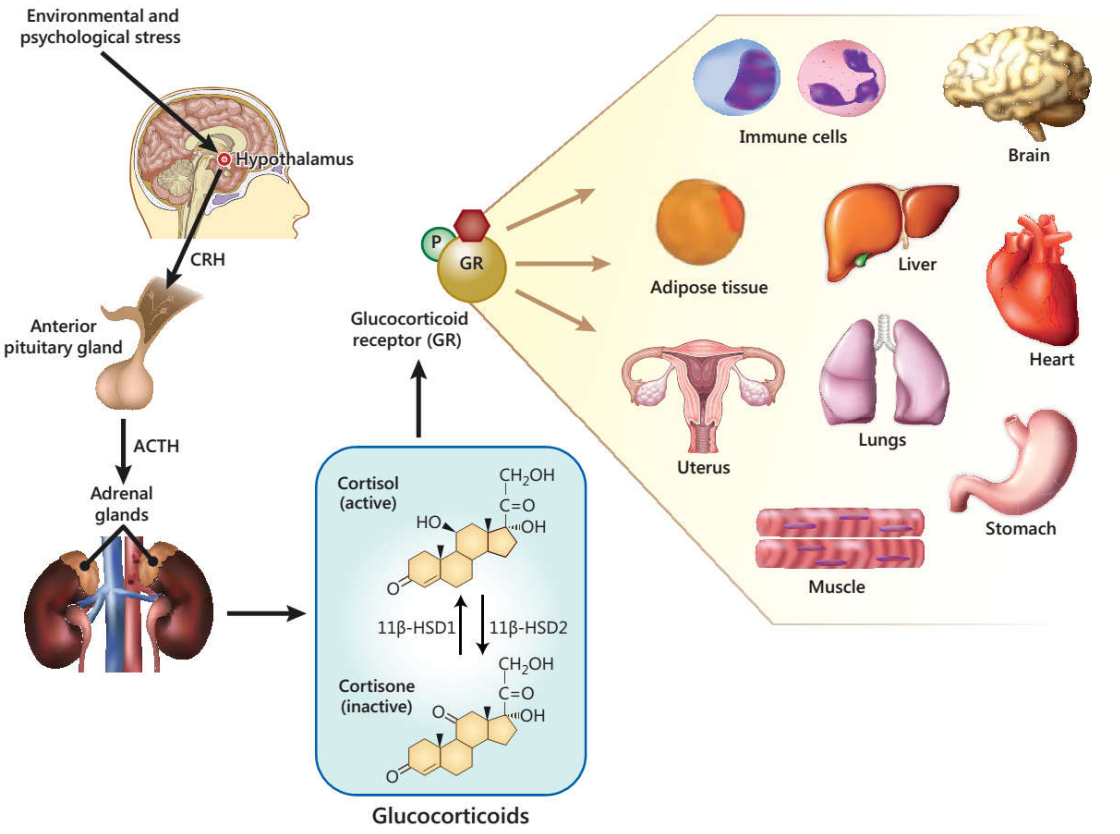

Figure 5: GC release is mediated by the HPA-axis. The hypothalamus secretes CRH, which stimulates the pituitary gland to release ACTH. This leads to secretion of cortisol (in humans) by the adrenal cortex. Biologically active cortisol can be converted to inactive cortisone by type 2 11β-HSD and vice versa by type 1 11β-HSD. GCs modulate many fundamental processes in the body by interacting with the GR, which is expressed in virtually all cell types. Figure taken from Cruz-Topete and Cidlowski, 2015.

After having its release, most cortisol is bound to corticosteroid-binding globulin in blood. However, only free cortisol represents the biologically active form of the hormone (Rhen and Cidlowski, 2005). Cortisol can be converted to the biologically inactive form cortisone by type 2 11β-hydroxysteroid dehydrogenase (HSD). Conversely, cortisone can be converted to active form cortisol by type 1 11β-HSD (Cruz-Topete and Cidlowski, 2015; Rhen and Cidlowski, 2005). In addition, circulating cortisol can act on the hypothalamus and the pituitary gland to inhibit the secretion of further CRH and ACTH thereby constituting a negative feedback mechanism. Hereby, cortisol homeostasis is achieved (Gupta and Bhatia, 2008; Rhen and Cidlowski, 2005).

Almost all GC-effects are mediated by the glucocorticoid receptor (GR), which is ubiquitously expressed throughout the human body in virtually all cell types and tissues.

Hereby, GCs control many biological processes such as immune responses, development, reproduction or metabolic homeostasis (Vandevyver et al., 2013).

1.4.1 Genomic and Non-Genomic Effects

The GR belongs to the nuclear receptor family of ligand-activated transcription factors. It is encoded by the NR3C1 gene, which is located on chromosome 5q 31-32 in humans (Kadmiel and Cidlowski, 2013; Rhen and Cidlowski, 2005). The GR is composed of three functional domains comprising an N-terminal transactivation domain (NTD), DNA-binding domain (DBD), C-terminal ligand-binding domain (LBD), and a flexible hinge region linking the DBD and LBD (**fig. 6 A**). The NTD contains an activation function (AF-1), which is important for the recruitment of co-regulators and the transcriptional machinery (Cruz-Topete and Cidlowski, 2015; Kadmiel and Cidlowski, 2013). Furthermore, the AF-1 comprises most residues of the GR that are target of post-transcriptional modifications (PTMs) such as the phosphorylation of serine residues (Cruz-Topete and Cidlowski, 2015). The DBD contains two zinc finger motifs that are required for DNA binding. Specific DNA sequences in GC-target genes are recognized and bound by the DBD (Cruz-Topete and Cidlowski, 2015; Kadmiel and Cidlowski, 2013). Besides, dimerization of the GR relies on the second zinc finger motif (Vandevyver et al., 2013). The LBD has an ligand-dependent AF-2 that interacts with transcriptional co-regulators (Kadmiel and Cidlowski, 2013; Tan and Wahli, 2016). Nuclear localization signals present in the DBD, LBD and hinge region mediate the GR's translocation into the nucleus (Kadmiel and Cidlowski, 2013).

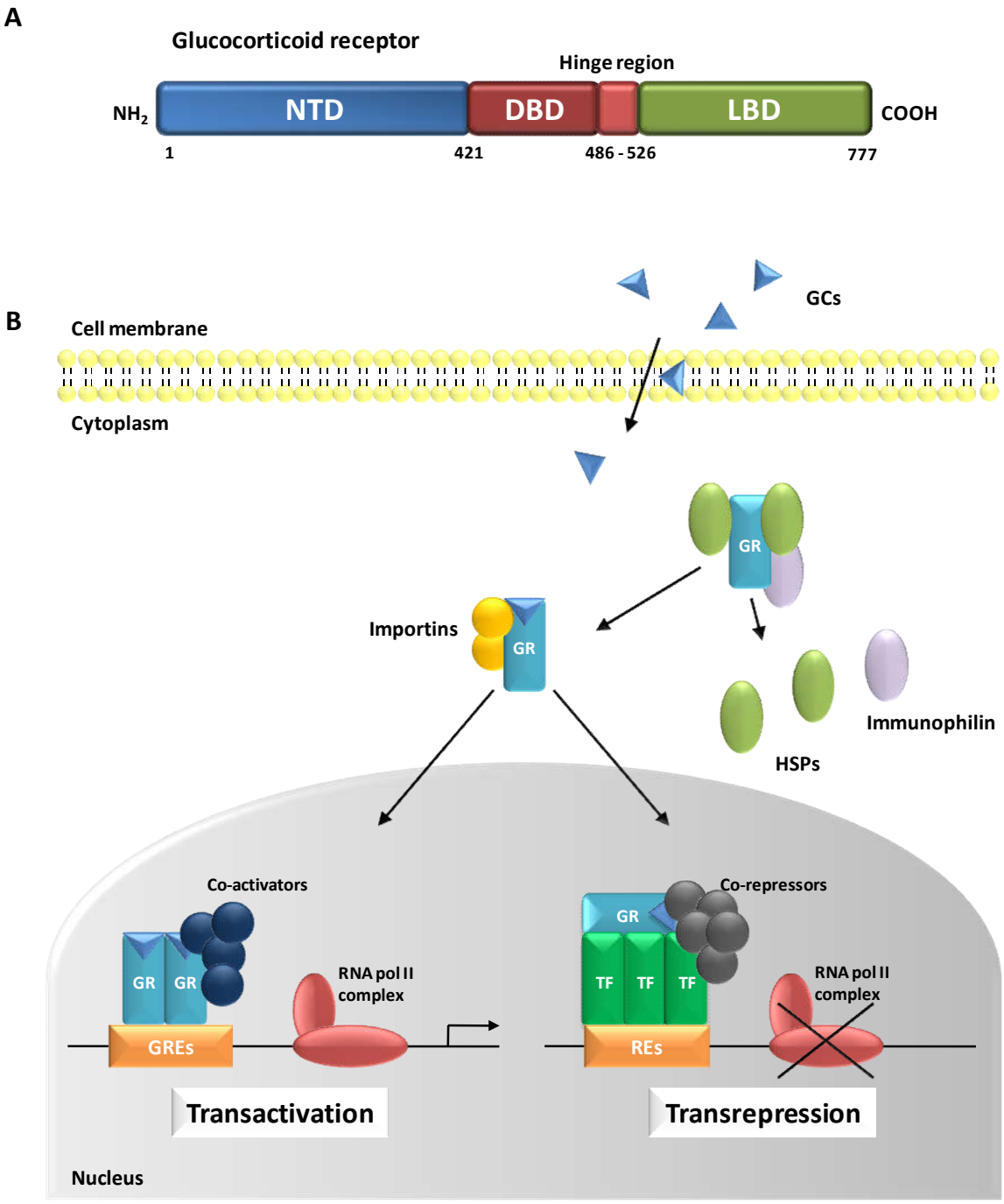

Figure 6: Structure of the GR and its mechanisms of transcriptional regulation. The GR contains several functional domains: NTD, DBD, hinge region and LBD (A). Following ligand binding, the GR is released from a multi-protein complex consisting HSPs and immunophilins, and then translocates into the nucleus guided by importins. Control of target gene expression is regulated in a transactivating manner by GR dimers recruiting co-activators, or in a transrepressing manner by GR monomers interacting with other transcription factors (TF) and recruiting co-repressors. Besides these two major modes of GC-action, additional ones exist (not shown).

In absence of ligands, the GR resides in the cytoplasm within a multimeric protein complex comprised of chaperone proteins such as heat shock proteins (hsp90 and hsp70), immunophilins (FKBP51 and FKBP52) and other inhibitory proteins (p23 and SRC) (Cruz-Topete and Cidlowski, 2015; Stahn and Buttgereit, 2008). This multimeric protein complex inhibits degradation of the GR (Vandevyver et al., 2013). Due to their lipophilic properties, GCs can easily diffuse across the cell membrane. Upon GC binding in the cytoplasm, the GR undergoes conformational changes, which mediate its dissociation from the protein complex. Nuclear import proteins importin-α and importin-13 bind to the GC-GR complex allowing the complex to move into the nucleus (Barnes, 2011b; Kadmiel and Cidlowski, 2013; Stahn and Buttgereit, 2008).

In the nucleus, the GR is able to either enhance or repress transcriptional activity of GC-target genes by different mechanisms (**fig. 6 B**). The GC-GR complex is able to form homodimers that bind with high affinity to GC-responsive elements (GREs) present in the promoter region of GC-responsive genes (Barnes, 2011b; Kadmiel and Cidlowski, 2013; Stahn and Buttgereit, 2008). Once bound to a GRE, the transactivation domains serve as docking platforms for transcriptional co-activators like CREB (cAMP response element-binding protein)-binding protein. These ones have an intrinsic histone-acetyltransferase (HAT) activity which mediates chromatin remodeling and association of RNA polymerase II. Subsequently, transcription of anti-inflammatory and regulatory proteins is switched-on in a transactivating manner (Barnes, 2011b; Kadmiel and Cidlowski, 2013).

Alternatively, the GR is able to interact with other transcription factors such as NF-κB, AP-1 or STAT3 that regulate the transcription of pro-inflammatory genes, which proceeds in similar manner as GR-mediated transactivation (Barnes, 1998; Kadmiel and Cidlowski, 2013). In this case, however, the ligand-bound GR binds as a monomer to these pro-inflammatory transcription factors via so-called tethering mechanisms to form a protein-protein complex thereby initiating the recruitment of co-repressors (Barnes, 1998; Vandevyver et al., 2013). These co-repressors are often histone-deacetylases (HDACs) that prevent chromatin-remodeling and activation of RNA-polymerase II. Consequently, inflammatory gene transcription is repressed in a transrepressing manner (Barnes, 2011b).

Less commonly, the homodimerized GR is also capable to repress target gene expression. This is mediated by binding to inverted palindromic negative GREs (nGREs) which leads to

co-repressor recruitment (Barnes, 2011b; Kadmiel and Cidlowski, 2013; Vandevyver et al., 2013). Moreover, the monomeric GR can directly bind to GREs by interacting with neighboring DNA-bound transcription factors. This composite mechanism can initiate both activation and repression of target genes (Cruz-Topete and Cidlowski, 2015).

PTMs including phosphorylation, acetylation or ubiquitination contribute to the diversity of GR-mediated actions. Transcriptional activity can either be increased or decreased by distinct PTMs (Kadmiel and Cidlowski, 2013; Tan and Wahli, 2016). Dimerization and DNA-binding have been shown to be modulated by phosphorylation of AF-1 in the NTD, for example (Tan and Wahli, 2016).

Of note, GCs are able to exert some of their effects more rapidly in a way that is independent of changes in target gene expression. These non-genomic mechanisms are mediated by the cytosolic GR or a membrane-bound GR (Stahn and Buttgereit, 2008). Mainly signal transduction pathways like the MAPK/ERK pathway are thought to be modulated by these mechanisms (Kadmiel and Cidlowski, 2013). A well described non-genomic effect is the influence of GCs on endothelial NO synthase (eNOS) in human endothelial cells. The GC-bound GR activates PI3K (phosphatidylinositol-3-kinase), which in turn phosphorylates Akt. Subsequently, Akt phosphorylates eNOS which triggers the production of NO. Vasodilation and vascular permeability can be influenced by this mechanism (Rhen and Cidlowski, 2005). Nevertheless, the non-genomic mechanisms are not fully elucidated and their biological implications remain unclear.

1.4.2 Anti-Inflammatory Effects of GCs in Respiratory Diseases

In general, GCs control inflammatory processes in the airways by interfering with the expression of both anti-inflammatory and pro-inflammatory genes. Interestingly, inhibition of the pro-inflammatory transcription factor NF-κB can be mediated by both GR mechanisms. GCs directly suppress NF-κB expression via the transrepressing mechanism while it can be indirectly suppressed by upregulation of the inhibitor IκB-α via the transactivating mode of action (Barnes, 1998). A plethora of anti-inflammatory and pro-inflammatory genes encoding for cytokines, chemokines, proteins, enzymes or adhesion molecules can be influenced by GC-treatment in the airways, as listed in **table 1**.

Increased Transcription by Transactivation	
Dual Specificity Protein Phosphatase 1 (DUSP1)	Inhibitor of MAPK-Pathway
Glucorticoid-Inducible Leucine Zipper (GILZ)	Transcriptional Regulator of GC Function
IL-1R, IL-10, IL-12	Anti-Inflammatory Cytokines
IκB-α	Inhibitor of NF-κB
Lipocortin-1	Inhibitor of Prostaglandin Formation
Secretory Leukocyte Inhibitory Protein (SLPI)	Inhibitor of Serine Proteases
β_2-Adrenoceptors	Mediator of Airway Smooth Muscle Relaxation

Decreased Transcription by Transrepression	
CCL1, IL-8, RANTES, MIP-1α, MCP-1/-3/-4,	Chemokines
ICAM-1, VCAM-1, E-Selectin	Adhesion Molecules
IL-1, IL-2, IL-4, IL-5, IL-6, IL-9, IL-13, TNF-α, GM-SCF, TSLP	Pro-Inflammatory Cytokines
iNOS, Cyclo-Oxygenase (COX)-2	Inflammatory Enzymes
MUC2, MUC5a	Mediators of Mucus Secretion

Table 1: Transactivation and transrepression of inflammatory cytokines associated with respiratory diseases. Adapted from Barnes, 2011b.

By suppressing various inflammatory mediators, GCs exert profound effects on nearly all cells of the immune system. The numbers of immune cells in the inflamed airways, such as eosinophils, mast cells, DCs, macrophages, B cells or T cells, can be reduced by different mechanisms (Barnes, 1998, 2011b; Kadmiel and Cidlowski, 2013). Migration to the site of inflammation is mainly inhibited by repression of adhesion molecules and chemokines (**table 1**), but GCs can also induce apoptosis of immune cells, mainly of eosinophils and T cells (Barnes, 2003). Eosinophil survival is mediated by secretion of IL-5 in the airways which is suppressed by GCs (Barnes, 1998). GCs promote T cell apoptosis although the pro-apoptotic mechanisms are not fully understood. In contrast, GCs can also promote survival of anti-inflammatory cells like regulatory T (T_{reg}) cells and increase their numbers in the inflamed airways (Kadmiel and Cidlowski, 2013).

Moreover, GCs can influence various immune cells functions. Antigen-presentation of DCs is dampened by suppressing DC maturation (Barnes, 1998; Kadmiel and Cidlowski, 2013). GCs also decrease the antibody-production of B cells and inhibit the release of further pro-inflammatory mediators by other immune cells (Kadmiel and Cidlowski, 2013).

GCs also have immunomodulatory and immunosuppressive effects by interfering with the maturation, activation and proliferation of immune cells (Barnes, 1998, 2003, 2011b; Kadmiel and Cidlowski, 2013). Nevertheless, the exact mechanisms and target sites of GCs remain unclear and remain to be investigated for each lung disease.

1.4.3 These Days Pessimism Towards GCs: Adverse Effects and GC-Resistance

Despite their potent anti-inflammatory activities, GCs can also induce numerous adverse effects. The development and incidence of side effects is determined by the duration and dose of the treatment, the mode of application and the individual susceptibility (Schäcke et al., 2002). Prolonged GC-treatment has been shown to be a major risk factor while high-dose treatment seemed to be less problematic. Systemic exposure to GCs is directly related to the development and severity of side effects (Dahl, 2006; Schäcke et al., 2002). However, topic GCs are also known to cause not only local, but systemic side effects as well. ICs for instance may be absorbed in the airways and reach the circulation where they can affect other organs than the lung (Dahl, 2006; Rhen and Cidlowski, 2005). Of note, pharmacokinetic parameters like the clearance rate, half-life, distribution and accumulation play a crucial role regarding the systemic exposure of topic GCs (Dahl, 2006).

A particular serious side effect is the imbalance of the HPA-axis. Prolonged GC-treatment leads to a downregulation of ACTH production thereby disturbing basal cortisol secretion. The adrenal gland is no longer able to produce sufficient amounts of cortisol that are required for daily physiology (Gupta and Bhatia, 2008). Suppression of the HPA-axis can lead to adrenal crisis ("*Addison's disease*"), whereas excess GCs lead to an upregulation of ACTH that causes excessive cortisol release from the adrenal gland ("*Cushing's syndrome*") (Dahl, 2006; Rhen and Cidlowski, 2005). GC-treatment can cause further endocrine and metabolic disturbances including growth retardation in children, increased body weight and fat redistribution, as well as the development of diabetes. Other adverse effects are skin thinning and impaired wound repair, osteoporosis, hypertension and myopathy. Of note, there is an increased risk of infections due to the excessive immunosuppression (Dahl, 2006; Rhen and Cidlowski, 2005; Schäcke et al., 2002; Stahn and Buttgereit, 2008).

Dependent on the treatment regimen and particular patient, single or multiple adverse effects can develop in different organs with different prevalence (Schäcke et al., 2002). Adverse effects may be mediated by genomic or non-genomic mechanisms of GCs. Nevertheless, many side effects were found to be associated with the transactivating mode of action (Schäcke et al., 2002; Stahn and Buttgereit, 2008).

It is noteworthy that adverse effects are a limiting factor for the GC-treatment of various inflammatory diseases; therefore the benefit-risk ratio needs to be carefully taken into account for each patient.

Another limiting factor for the use of GCs is the occurrence of GC-resistance. Most clinical symptoms of patients with inflammatory diseases are well controlled by low dose GC-treatment. However, a number of patients fail to respond to GCs even at high doses, and multiple mechanisms have been speculated to contribute to the development of this resistance (Barnes, 2013).

GC-resistance was identified in families of non-responders. This familial GC-resistance (FGR) is characterized by high levels of circulating cortisol without symptoms of Cushing's syndrome (Barnes, 1998, 2011b). Furthermore, distinct polymorphisms of the NR3C1 gene with modified transcripts of the GR were shown to influence the sensitivity to GCs (Barnes, 2011b; Kadmiel and Cidlowski, 2013). Defective GR-binding and translocation also contribute to GC-resistance which is mainly due to altered phosphorylation by kinases such as p38 MAPK (Kadmiel and Cidlowski, 2013). An additional mechanism is an increased histone acetylation with reduced HDAC activity (Barnes, 2011b; Kadmiel and Cidlowski, 2013). Hyperactivity of pro-inflammatory transcription factors like AP-1 was also found to be a critical mechanism, as GR-binding to GREs and other transcription factors is impaired (Barnes, 2013; Kadmiel and Cidlowski, 2013). Moreover, many GC-resistant patients show altered lymphocyte functions. In response to GCs, T_{reg} cells for instance fail to secrete IL-10 whereas increased numbers of T_H17 cells increase IL-17 production simultaneously (Barnes, 2013).

A better understanding of the mechanisms leading to the GC-mediated adverse effects and GC-resistance is substantial for the development of novel drugs that maintain the beneficial effects of GCs and at the same time overcome these limiting factors.

2. Objectives

GCs have been a mainstay in the treatment of asthma for many years despite the severe side effects they can induce. However, the exact mechanisms of GCs have not been fully elucidated.

Previous findings indicated that the anti-inflammatory effects of GCs in allergic asthma rely on the transactivating mechanism of the GR as shown by the analysis of AAI in GR^{dim} mice carrying a point mutation that impairs GR-dimerization (unpublished data). Further experiments had revealed that the therapeutic effects of GCs depended on the control of cells other than those of hematopoietic origin (unpublished data). From this it was concluded that structural cells of the lung rather than immune cells might be crucial targets for GC-treatment.

In particular AECs play an important role in the pathogenesis of asthma by secreting various pro- or anti-inflammatory mediators that modulate the immune responses in the asthmatic lung. Therefore, it was hypothesized that AECs might be potential targets in the treatment of asthma with GCs.

To test a possible connection between mechanism and site of action, RNA sequencing (RNA-seq) analysis should be performed with AECs from wild type and GR^{dim} mice. Differences in the transcriptome should be identified during the allergic response, as well as following subsequent treatment with Dex. To this end, a protocol for the isolation and purification of AECs should be established. Newly identified candidate genes should be examined in detail by quantitative real-time PCR (qRT-PCR).

To further investigate the role of AECs as potential targets for the GC-treatment in asthma, AAI should be induced in GR^{spc} mice. These mice are GR-deficient specifically in AT-II cells. Different experimental approaches should be employed to address the GC-efficacy.

GCs are also used in other inflammatory lung diseases such as ALI. Thus, AECs should also be investigated as potential targets of the GC-treatment in murine ALI. Various experimental approaches should be used to test the relevance of AECs in the GC-treatment of ALI.

3. Material and Methods

3.1 Material

3.1.1 General Equipment

Instrument	Manufacturer
Anesthetic Machine VS 4255	VisualSonics, Toronto, Canada
Camera Colorview	Olympus, Tokio, Japan
Centrifuges:	
Centrifuge 5804-R	Eppendorf, Hamburg Germany
Multifuge 4 KR	Heraeus, Hanau, Germany
Centrifuge 2-5	Sigma Laborzentrifugen, Osterode am Harz, Germany
Microfuge 5417R	Eppendorf, Hamburg, Germany
Minifuge Rotilabo	Carl Roth, Karlsruhe, Germany
Chemiluminiscence Imaging System Chemocam Imager	Intas, Göttingen, Germany
Electrophoresis Chamber Systems:	
Horizontal System Type 40-0708, 40-1214, 40-1410	Peqlab Biotechnology, Erlangen, Germany
Vertical System Mini-Protean Tetra Cell	BioRad, München, Germany
Electrophoresis Power Supplies:	
EPS 301	Amersham Biosciences, Freiburg, Germany
Power Pac Basic	BioRad, München, Germany
Flow Cytometer FACS Canto II	BD Biosciences, Heidelberg, Germany
Gel Documentation System Gel iX Imager	Intas, Göttingen, Germany
Incubator Hera Cell 240	Heraeus, Hanau, Germany
Light Microscopes:	
Primo Star	Zeiss, Jena, Germany
BX 51	Olympus, Tokio, Japan
Magnetic Cell Separator (MACS) autoMACS	Miltenyi Biotec, Bergisch-Gladbach, Germany
Microplate Reader and Spectrophotometer Power Wave 340	BioTek Instruments, Bad Friedrichshall, Germany
Microtome SH2000R	Leica Biosystems, Wetzlar, Germany
Neubauer Improved Hemocytometer	Henneberg-Sander, Giessen, Germany
Photometer Nanodrop 2000	Peqlab Biotechnology, Erlangen, Germany

Table 2: List of general equipment.

Instrument	Manufacturer
Pipettes:	
Micropipette 0.1-2.5 µl, 2-20µl, 20-200µl and 100-1000 µl Research	Eppendorf, Hamburg, Germany
Micropipette 0.5-10 µl Reference	Eppendorf, Hamburg, Germany
Multichannel Pipette S-12 20-200 µl	Brand, Wertheim, Germany
Pipetting Aid Easypet 3	Eppendorf, Hamburg, Germany
Real-Time PCR System 7500	Applied Biosystems, Foster City, CA, USA
Scales:	
Acculab ALC-3100.2	Sartorius, Göttingen, Germany
MC1 RC6011	Sartorius, Göttingen, Germany
Shaker GFL 3006	Gesellschaft für Labortechnik, Burgwedel, Germany
Sterile Bench Hera Safe	Heraeus, Hanau, Germany
Thermocycler Mastercycler EP Gradient	Eppendorf, Hamburg, Germany
Thermomixer Comfort	Eppendorf, Hamburg, Germany
Tissue Embedding System EG1160	Leica Biosystems, Wetzlar, Germany
Tissue Homogenizer Ultra Turrax T18 Basic	IKA, Staufen, Germany
Tissue Processor TP1020	Leica Biosystems, Wetzlar, Germany
Vortex Genie-2	Scientific Industries, Bohemia, NY, USA
Water Bath W12	Labortechnik Medingen, Dresden, Germany
Water Purification System Arium 611	Sartorius, Göttingen, Germany

Table 3: List of general equipment continued.

3.1.2 Consumables

Consumable	Manufacturer
6-Well and 48-Well Suspension Culture Plates Cellstar	Greiner BioOne, Frickenhausen, Germany
96-Well Flat Bottom Plate Nunc Maxisorp	eBioscience, San Diego, CA, USA
96-Well Optical Reaction Plate MicroAmp	Applied Biosystems, Foster City, CA, USA
Activated Charcoal Adsorption Filter Vaporguard	VetEquip, Livermore, CA, USA
Animal Feeding Needle 20G x 1.5"	Fine Science Tools, Foster City, CA, USA
Blotting Paper Whatman GB005	Sigma-Aldrich, Taufkirchen, Germany
Cannula Sterican 26G x ½" (0.45 x 12 mm)	B. Braun, Melsungen, Germany
Cell Culture Dish Cellstar 100 x 20 mm	Greiner BioOne, Frickenhausen, Germany
Cell Strainer 40 µm and 100 µm	Greiner BioOne, Frickenhausen, Germany
Centrifuge Tubes 15 ml and 50 ml	Greiner BioOne, Frickenhausen, Germany

Table 4: List of consumables.

Consumable	Manufacturer
FACS Tubes 5 ml	BD Biosciences, Heidelberg, Germany
Glass Pipettes 5 ml, 10 ml, 20 ml and 25 ml	Brand, Wertheim, Germany
MACS Columns autoMACS	Miltenyi Biotec, Bergisch-Gladbach, Germany
Microscope Cover Slips 24 x 60 mm	Menzel-Gläser, Braunschweig, Germany
Microscope Slides SuperFrost Plus	Menzel-Gläser, Braunschweig, Germany
Nitrocellulose Membrane Hybond-ECL	Amersham Biosciences, Freiburg, Germany
Optical Adhesive Cover MicroAmp	Applied Biosystems, Foster City, CA, USA
Parafilm	Bemis, Neenah, WI, USA
Pasteur Pipettes Labsolute 3 ml	Th. Geyer, Renningen, Germany
PCR Tubes Multiply-µStrip Pro 8-Strip	Sarstedt, Nümbrecht, Germany
Pipette Tips:	
Clear 0.1-10 µl	Greiner BioOne, Frickenhausen, Germany
Yellow 10-200 µl	Greiner BioOne, Frickenhausen, Germany
Blue 100-1.000 µl	Greiner BioOne, Frickenhausen, Germany
Round Bottom Culture Tube 14 ml	Greiner BioOne, Frickenhausen, Germany
Safe-Lock Tubes 1.5 and 2 ml	Greiner BioOne, Frickenhausen, Germany
Serological Pipettes Cellstar 5 ml, 10 ml and 25 ml	Greiner BioOne, Frickenhausen, Germany
Syringes:	
Diabetic Syringe Micro-Fine + Demi 0.3 ml 30G x 8 mm	BD Medical Diabetes Care, Le Pont de Claix Cedex, France
Diabetic Syringe Micro-Fine + Demi 1 ml 29G x 12.7 mm	BD Medical Diabetes Care, Le Pont de Claix Cedex, France
Syringe Injekt-F Tuberculin 1 m	BD Biosciences, Heidelberg, Germany
Syringe Discardit II 2 ml, 10 ml and 20 ml	BD Biosciences, Heidelberg, Germany
Tissue Cassettes MacrOflow	Microm International, Walldorf, Germany
Tissue Culture Dish 60 x 15 mm	Sarstedt, Nümbrecht, Germany
Venous Catheter Venflon Pro 0.9 x 25 mm	BD Infusion Therapy, Helsingborg, Sweden

Table 5: List of consumables continued.

3.1.3 Chemicals and Reagents

Name	Manufacturer
5x Phusion Reaction Buffer HF with 7.5 mM Magnesium Chloride	Genaxxon Biosciences, Ulm, Germany
10x PCR Buffer S with 1.5 mM Magnesium Chloride	Genaxxon Biosciences, Ulm, Germany
Acetic Acid Glacial	Sigma-Aldrich, Taufkirchen, Germany
Agarose Ultra Low Gelling Temperature Type IX-A	Sigma-Aldrich, Taufkirchen, Germany
Agarose Ultrapure	Invitrogen, Carlsbad, CA, USA
Albumine from Chicken Egg White, Grade V (Ovalbumine; OVA)	Sigma-Aldrich, Taufkirchen, Germany
Alhydrogel 2% (Alum)	InVivoGen, Toulouse, France
Ammonium Persulfate (APS)	Sigma-Aldrich, Taufkirchen, Germany
Bovine Serum Albumine (BSA)	Carl Roth, Karlsruhe, Germany
Bradford Reagent	Sigma-Aldrich, Taufkirchen, Germany
Bromophenol Blue	Merck, Darmstadt, Germany
Chloroform	Sigma-Aldrich, Taufkirchen, Germany
Citric Acid Monohydrate	Merck, Darmstadt, Germany
Dexamethasone (Dex) Dexa-Ratiopharm Injection Solution	Ratiopharm, Ulm, Germany
Dimethyl Sulfoxide (DMSO)	Carl Roth, Karlsruhe, Germany
Disodium Hydrogen Phosphate	Sigma-Aldrich, Taufkirchen, Germany
Dispase 50 U/ml	BD Biosciences, Heidelberg, Germany
DNase I 2000 U/mg	Sigma-Aldrich, Taufkirchen, Germany
dNTP Mix PCR	Genaxxon Biosciences, Ulm, Germany
Entellan	Merck, Darmstadt, Germany
Eosin Y Yellowish	Merck, Darmstadt, Germany
Ethanol	Carl Roth, Karlsruhe, Germany
Ethidium Bromide Solution	Carl Roth, Karlsruhe, Germany
Ethylendiaminetetraacetic Acid (EDTA)	Sigma-Aldrich, Taufkirchen, Germany
Fetal Bovine Serum (FBS)	Invitrogen, Carlsbad, CA, USA
Forene 100% (v/v) (Isoflurane)	Abbvie, Ludwigshafen, Germany
Generuler DNA Ladder 1 kb	Fermentas, St.-Leon-Rot, Germany
Glycerol	Carl Roth, Karlsruhe, Germany
Hemalum Solution Acid acc. to Mayer	Carl Roth, Karlsruhe, Germany
Hydrogen Peroxide 30%	Carl Roth, Karlsruhe, Germany
Igepal CA-630	Sigma-Aldrich, Taufkirchen, Germany

Table 6: List of chemicals and reagents.

Name	Manufacturer
Isopropanol	Carl Roth, Karlsruhe, Germany
Lipopolysaccharide (LPS) from *e. coli* (055:B5)	Sigma-Aldrich, Taufkirchen, Germany
Luminol	Serva Electrophoresis, Heidelberg, Germany
Methanol	Carl Roth, Karlsruhe, Germany
Nanoparticles:	
Betamethasonephosphate Nanoparticles (BNPs); $ZrO[(BMP)_{0.9}(FMN)_{0.1}]$	Prof. Claus Feldmann, Karlsruhe Institute of Technology, Karlsruhe, Germany
Betamethasonephosphate Nanoparticles with Anti-SP-C Antibody (BNPs-SPC)	Prof. Claus Feldmann, Karlsruhe Institute of Technology, Karlsruhe, Germany
Oleic Acid (OA)	Sigma-Aldrich, Taufkirchen, Germany
Orange G Sodium Salt	Sigma-Aldrich, Taufkirchen, Germany
Paraffin Wax for Histology	Sigma-Aldrich, Taufkirchen, Germany
p-Coumaric Acid	Carl Roth, Karlsruhe, Germany
Penicillin/Streptomycin 10.000 U/ml	Invitrogen, Carlsbad, CA, USA
PfuS DNA Polymerase	Own Production
Protease Inhibitor Cocktail	Sigma-Aldrich, Taufkirchen, Germany
Protein G Plus Agarose	Santa Cruz Biotechnology, Heidelberg, Germany
Protein Marker Prestained Broad Range 7-175 kDa	New England Biolabs, Frankfurt, Germany
Proteinase K	Applichem, Darmstadt, Germany
Roti Histofix 4% (Paraformaldehyde; PFA)	Carl Roth, Karlsruhe, Germany
Rotiphorese 30 (30% Acrylamide/Bisacrylamide Solution)	Carl Roth, Karlsruhe, Germany
Sodium Azide	Sigma-Aldrich, Taufkirchen, Germany
Sodium Carbonate	Merck, Darmstadt, Germany
Sodium Chloride	Merck, Darmstadt, Germany
Sodium Dodecylsulfate (SDS)	Carl Roth, Karlsruhe, Germany
Sodium Fluoride	Merck, Darmstadt, Germany
Sodium Hydroxide	Sigma-Aldrich, Taufkirchen, Germany
Sodium Molybdate	Sigma-Aldrich, Taufkirchen, Germany
Sodium Orthovanadate	Sigma-Aldrich, Taufkirchen, Germany
Sodium Hydrogen Carbonate	Merck, Darmstadt, Germany
Streptavidin Microbeads for MACS	Miltenyi Biotec, Bergisch-Gladbach, Germany
Sulfuric Acid	Merck, Darmstadt, Germany
Tamoxifen Free Base	Sigma-Aldrich, Taufkirchen, Germany
Taq DNA Polymerase 5 U/µl	Genaxxon Biosciences, Ulm, Germany

Table 7: List of chemicals and reagents continued.

Name	Manufacturer
Tetramethylbenzidine (TMB)	Sigma-Aldrich, Taufkirchen, Germany
Tetramethylethylenediamine (TEMED)	Carl Roth, Karlsruhe, Germany
Tetrasodium Pyrophosphate	Sigma-Aldrich, Taufkirchen, Germany
Thioglycolate	Sigma-Aldrich, Taufkirchen, Germany
Tris Pufferan	Carl Roth, Karlsruhe, Germany
Trypan Blue	Carl Roth, Karlsruhe, Germany
Tween-20	Carl Roth, Karlsruhe, Germany
Xylene	Carl Roth, Karlsruhe, Germany
β-Mercaptoethanol	Carl Roth, Karlsruhe, Germany

Table 8: List of chemicals and reagents finished.

3.1.4 Commercial Assays

Name	Manufacturer
BsrGI Enzyme Set	New England Biolabs, Frankfurt, Germany
iScript cDNA Synthesis Kit	BioRad, München, Germany
Mouse IL-6 ELISA MAX Standard Set	BioLegend, San Diego, CA, USA
Power SYBR-Green PCR Mastermix	Applied Biosystems, Foster City, CA, USA
Quick-RNA Mini Prep	Zymo Research, Irvine, CA; USA
RNeasy Plus Universal Kit	Qiagen, Hilden, Germany

Table 9: List of commercial assays.

3.1.5 Buffers and Solutions

3.1.5.1 General Buffers and Solutions

H_2O

For all experiments demineralized or deionized water was used, if not stated otherwise.

PBS

80 g	Sodium Chloride
29 g	Disodium Hydrogen Phosphate
2 g	Potassium Chloride
2 g	Potassium Dihydrogen Phosphate
1000 ml	H_2O

(pH 7.2-7.3)

PBS/BSA

0.1% BSA in PBS.

PBS-Tween

0.05% Tween-20 in PBS.

TAC Buffer

20 mM	Tris
155 mM	Ammonium Chloride
1000 ml	H_2O
(pH 7.2)	

FACS Buffer

0.1%	BSA
0.01%	Sodium Azide
500 ml	PBS

MACS Rinse Buffer

2 mM	EDTA
1000 ml	PBS

MACS Buffer

0.5% BSA in MACS Rinse Buffer.

Trypan Blue Solution

0.5% Trypan Blue in PBS.

Tail Extraction Buffer

5 mM	Tris
100 mM	Sodium Chloride
100 mM	EDTA
1%	SDS
1000 ml	H_2O

TE Buffer

10 mM	Tris
1 mM	EDTA
1000 ml	H_2O
(pH 8.0)	

Orange G Loading Dye

100 mg	Orange G Sodium Salt
30%	Glycerol
100 ml	H_2O

50x TAE Buffer

4.8 g	Tris
1.1 g	Acetic Acid Glacial
0.29 g	EDTA
1000 ml	H_2O

Ripa Buffer

10 mM	Tris
5 mM	EDTA
150 mM	Sodium Chloride
10 mM	Sodium Fluoride
1 mM	Tetrasodium Pyrophosphate
1000 ml	H_2O
(pH 7.4)	

Laemmli Buffer

62.5 mM	Tris
20%	Glycerol
2%	SDS
5%	β-Mercaptoethanol
0.025%	Bromophenol Blue
100 ml	H_2O

10% NP-40 solution

5 mg	Igepal CA-630
45 ml	H_2O

Protein Lysis Buffer

1%	NP-40 Solution 10%
1 mM	Sodium Orthovanadate (50 mM)
10 µM	Sodium Molybdate (10 mM)
2.5%	Protease Inhibitor Cocktail
50%	Ripa-Buffer
1 ml	H_2O

3.1.5.2 SDS-PAGE and Western Blot Reagents

SDS-Running Buffer

25 mM	Tris
192 mM	Glycerol
3.5 mM	SDS
1000 ml	H_2O

Lower Buffer

1.5 mM	Tris
14 mM	SDS
1000 ml	H_2O

Upper Buffer

0.5 mM	Tris
14 mM	SDS
1000 ml	H_2O

10% SDS-Running Gel

1.95 ml	Lower Buffer
2.7 ml	Rotiphorese 30
7.5 µl	TEMED
49.95 µl	APS
3.3 ml	H_2O

10% SDS-Stacking Gel

938 µl	Upper Buffer
600 µl	Rotiphorese 30
3.75 µl	TEMED
32.5 µl	APS
2.205 ml	H_2O

10x Blotting Buffer

0.5 M	Tris
0.4 M	Glycerol
13 mM	SDS
15 mM	Sodium Azide
1000 ml	H_2O

Blotting Buffer

10%	10x Blotting Buffer
20%	Methanol
1000 ml	H_2O

Blocking Solution

5%	BSA
0.01%	Sodium Azide
50 ml	PBS-Tween

Solution A

0.1 M	Tris
250 mg/l	Luminol
100 ml	H_2O

Solution B

1.1 mg	p-Coumaric Acid
10 ml	DMSO

Western Blot Developing Solution

4 ml	Solution A
400 µl	Solution B
1.2 µl	Hydrogen Peroxide 30%

3.1.5.3 ELISA Reagents

Coating Buffer

0.1 M	Sodium Carbonate
1000 ml	H_2O
(pH 9.5)	

Assay Diluent

10% FBS in PBS.

TMB Solution

1% TMB in DMSO.

Substrate Buffer

0.1 M	Citric Acid
0.2 M	Disodium Hydrogen Phosphate
1000 ml	H_2O

TMB-Substrate Solution

1%	TMB Solution
0.2%	Hydrogen Peroxide 3.5%
10 ml	Substrate Buffer

Stop Solution

2N Sulfuric Acid

3.1.6 Media

DMEM (Dulbecco's Modified Eagle Medium)

DMEM + GlutaMAX (Invitrogen, Carlsbad, CA, USA)

DMEM^{++}

10%	FBS
1%	Penicillin/Streptomycin
500 ml	DMEM

3.1.7 List of Antibodies

3.1.7.1 For Flow Cytometry

Specificity	Clone	Isotype	Conjugation	Manufacturer
CD3ε	17A2	Rat IgG2a, κ	APC	BioLegend
CD4	RM4-5	Rat IgG2a, κ	PerCp	BD Biosciences
CD8α	53-6.7	Rat IgG2a, κ	APC	BioLegend
CD11b	M1/70	Rat IgG2a, κ	PE-Cy7	BioLegend
CD16/CD32 (TruStain fcX)	93	Rat IgG2a, λ		BioLegend
EpCAM (CD326)	G8.8	Rat IgG2a, κ	APC or APC-Cy7	BioLegend
F4/80	BM8	Rat IgG2a, κ	FITC	BioLegend
GR-1 (Ly-6C/G)	RB6-8C5	Rat IgG2a, κ	APC-Cy7	BD Biosciences
MHC-II (I-Ab)	AF6-120.1	Mouse Balb/C IgG2a, κ	PE	BioLegend
Siglec F	E50-2440	Rat IgG2a, κ	PE	BD Biosciences

Table 10: List of antibodies for flow cytometry.

3.1.7.2 For Cell Separation

Specificity	Clone	Isotype	Conjugation	Manufacturer
CD3ε	145-2C11	Hamster IgG1, κ	Biotin	BD Biosciences
CD11b	M1/70	Rat IgG2a, κ	Biotin	BioLegend
CD11c	N418	Rat IgG2a, κ	Biotin	BioLegend
CD45R (B220)	RA3-6B2	Rat IgG2a, κ	Biotin	BD Biosciences
F4/80	BM8	Rat IgG2a, κ	Biotin	BioLegend
Siglec F	ES22-10D8	Rat IgG1	Biotin	Miltenyi Biotec

Table 11: List of antibodies for cell separation.

3.1.7.3 For ELISA

Specificity	Clone	Isotype	Conjugation	Manufacturer
Mouse IgE	Polyclonal	Goat	HRP	Southern Biotech
Mouse IgG1	Polyclonal	Goat	HRP	Southern Biotech
Mouse IgG2a	Polyclonal	Goat	HRP	Southern Biotech

Table 12: List of antibodies for ELISA.

3.1.7.4 For Western Blot and Nanoparticles

Specificity	Clone	Isotype	Conjugation	Manufacturer
GR (M-20)	Polyclonal	Rabbit IgG	Purified	Santa Cruz Biotechnology
ERK-1 (K23)	Polyclonal	Rabbit IgG	Purified	Santa Cruz Biotechnology
SP-C (FL-197)	Polyclonal	Rabbit IgG	Purified	Santa Cruz Biotechnology
Goat Anti-Rabbit IgG (H+L)	Polyclonal	Goat IgG	HRP	Pierce Biotechnology

Table 13: List of antibodies for western blot and nanoparticles.

Manufacturer Information:

BioLegend	San Diego, CA, USA
BD Biosciences	Heidelberg, Germany
Miltenyi Biotec	Bergisch-Gladbach, Germany
Pierce Biotechnology	Rockford, IL, USA
Santa Cruz Biotechnology	Heidelberg, Germany
Southern Biotech	Birmingham, AL, USA

3.1.8 Oligonucleotides

Name	Forward Primer Sequence	Reverse Primer Sequence
ATF6	CGAGTTGTGAGGGAGAGGTG	ACAACGTCGACTCCCAGTCT
CD163	GAAGCCCACAAAGAAAGCTG	TGCACACGATCTACCCACAT
Claudin 5	GAGATCCTGGGGGCACTAGA	TGCCCTTTCAGGTTAGCAGG
Cre	GGAAATGGTTTCCCGCAGAA	ACGGAAATCCATCGCTCGAC
ELANE	CAGAGGCGTGGAGGTCATTT	CCGGAAATTTAGGCCGTTCAC
GRflox (flox1, flox4/flox8)	GGCATGCACATTACTGGCCTTCT	GTGTAGCAGCCAGCTTACAGGA CCTTCTCATTCCATGTCAGCATGT
GRquant	CAGCAACGGGACCACCTCCC	GTGCTGTCCTTCCACTGCTCTC
GT3'-GT5'	CCATTACCTTCCAGGTTCATTC	GTGTCTTGATGATAGTCTGCT
HPRT	GTCCTGTGGCCATCTGCCTA	GGGACGCAGCAACTGACATT
IL-13	CCCCTGTGCAACGGCAGCAT	CGGGGAGGCTGGAGACCGTA
IL-1b	GCCACCTTTTGACAGTGATG	GCTCTTGTTGATGTGCTGCT
IL-33	TCAATCAGGCGACGGTGTGGA	AAGGCCTGTTCCGGAGGCGA
IL-5	TGCTGAAGGCCAGCGCTGAAG	GGGACAGGAAGCCTCATCGTCTCAT
iNOS	CCGCACCCGAGATGGTCAGG	GCAAGGCTGGGAGGGGTCCT
ITGAE (CD103)	CAAAGACTCAGGACCACACTGA	GCGGCCACGGTTACATTTTC
MCP-1	AGCACCAGCCAACTCTCACT	CGTTAACTGCATCTGGCTGA
Occludin	CCTCCACCCCCATCTGACTA	CTTCAGGCACCAGAGGTGTT
RANTES	GTGCCCACGTCAAGGAGTAT	GGAAGCGTATACAGGGTCA

Table 14: List of oligonucleotides. All oligonucleotides were designed using Primer-Blast software and purchased from Metabion (Martinsried, Germany).

3.1.9 Mice

3.1.9.1 BALB/c Mice

BALB/c is an inbred albino laboratory mouse strain. Mice were bred in the animal facilities at the European Neuroscience Institute (ENI) in Göttingen or purchased from Charles River (Sulzfeld, Germany).

3.1.9.2 C57BL/6 Mice

C57BL/6 is an inbred mouse strain with characteristic black fur. Mice were obtained from Janvier Labs (Le Genest-Saint-Isle, France) or bred in the animal facilities at the ENI in Göttingen.

3.1.9.3 GR^{dim} Mice

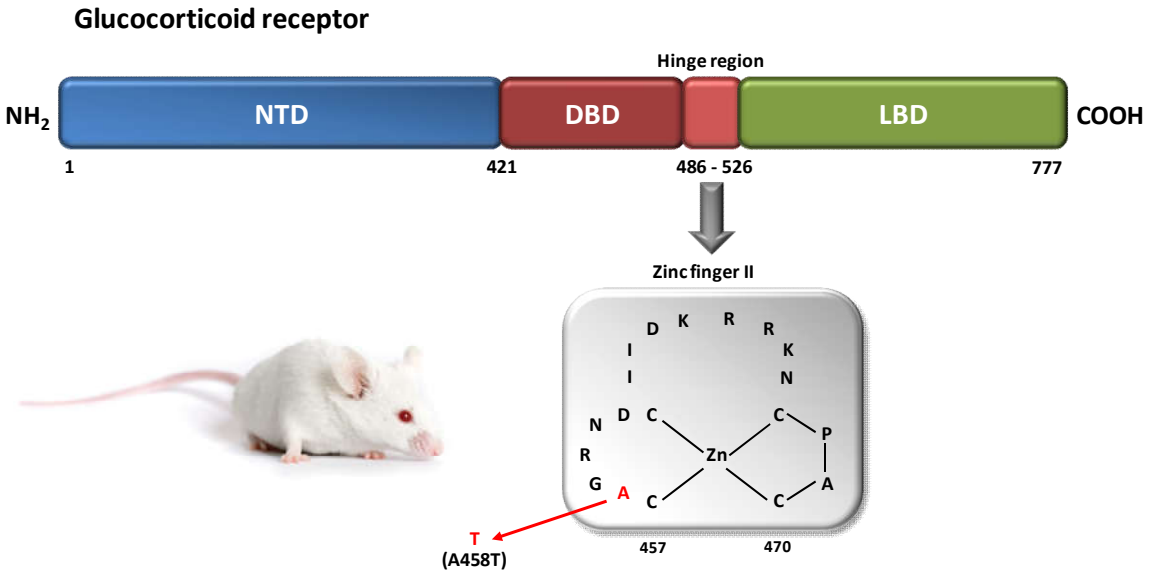

Figure 7: Schematic representation of GR^{dim} mutation.

GR$^{dim/dim}$ mice (Nr3c1^{tm3GSc}; designated GR^{dim}) carry a single point mutation in the DBD of the GR gene, which was introduced via homologous recombination of mouse embryonic stem cells (ES cells) (Reichardt et al., 1998). Alanine is replaced by threonine (A458T) in the D-loop of the second Zinc-finger in the DBD (**fig. 7**). This mutation impairs GR-dimerization and thus the transactivating mode of action whereas the transrepressing mechanism remains intact. GR^{dim} mice have been backcrossed to the BALB/c background for more than 10 generations.

3.1.9.4 GR^{spc} Mice

GR$^{flox/flox}$Sftpc^{CreERT2} mice (Nr3c1^{tm2GSc}Sftpc$^{tm1(cre/ERT2)Blh}$; designated GR^{spc}) carry a specific and inducible deletion of the GR in AT-II cells. The conditional knock-out was achieved by employing a tamoxifen-inducible Cre/loxP recombination system. GR$^{flox/flox}$ mice (Tronche et al., 1999) were intercrossed with Sftpc^{CreERT2} mice (Rock et al., 2011) that have been kindly provided by Prof. Brigid Hogan (Duke University, Durham, NC, USA). The Cre-recombinase in these mice is expressed under the control of the human surfactant protein C (SftpC) promoter which is exclusively expressed in AT-II cells. Experiments were

performed with mice that have been backcrossed to a C57BL/6 background for at least 10 generations.

3.1.10 Software

Name	Manufacturer
analySIS	Olympus, Tokio, Japan
Intas GDS	Intas, Göttingen, Germany
Intas Chemostar	Intas, Göttingen, Germany
Nanodrop 2000 Software	Thermo Scientific, Wilmington, DE, USA
Microsoft Office 2007 and 2010	Microsoft, Redmond, WA, USA
Primer-Blast Software	http://www.ncbi.nlm.nih.gov/tools/primer-blast/
BD FACS Diva Software 6.1.2	BD Biosciences, Heidelberg, Germany
Gen 5 1.09.8	BioTek Instruments, Bad Friedrichshall, Germany
GraphPad Prism 5.02	GraphPad Software, La Jolla, CA, USA
FlowJo 7.6	TreeStar, Ashland, OR, USA
Zotero 4.0.29.10	Center for History and New Media, Fairfax, VA, USA
7500 System SDS Software 1.4.0.25	Applied Biosystems, Foster City, CA, USA

Table 15: List of software.

3.2 Methods

3.2.1 Animal Experimentation

Mice were housed and bred under specific pathogen-free (SPF) conditions in the animal facilities at the ENI or the University Medical Center in Göttingen (ZTE). Mice were kept in individually ventilated cages (IVCs) with a 12 hour light-dark cycle. Food and drinking water were provided *ad libitum*. All animal experiments were performed according to the ethical standards of humane animal care and approved by the Lower Saxony State Office for Consumer Protection and Food Safety (LAVES). Due to breeding limitations, mice were neither age- or sex-matched. Mice were sacrificed by CO_2 inhalation.

3.2.2 Genotyping of GR^{dim} and GR^{spc} Mice

Genomic DNA used for genotyping was isolated from mouse tail biopsies. The tissue was incubated in 800 µl tail extraction buffer together with 20 µg proteinase K at 56°C under constant agitation overnight. Afterwards, 280 µl saturated sodium chloride solution were added and samples were incubated for 5 min at room temperature (RT). This was followed by centrifugation of the samples at >20.000 x g (V_{max}) for 10 min. Supernatants were transferred to new tubes. The DNA present in the supernatant was precipitated by addition of 600 µl isopropanol. Samples were incubated for 3 min at RT which was followed by 10 min centrifugation at V_{max}. Supernatants were discarded and 500 µl 70% ethanol were added to each pellet. Samples were centrifuged again, the supernatant removed and the DNA pellet dried at 50°C for at least 1 hour. Finally, the DNA pellet was dissolved in 100 µl TE buffer.

For genotyping of GR^{dim} and GR^{spc} mice, a PCR was performed with PfuS DNA polymerase. GR^{dim} mice were characterized by using GT3'-GT5' primers whereas Cre-primers were used for GR^{spc} mice.

Standard Reaction		**PCR Protocol**		
0.5 µl	DNA	98.5°C	2 min	
4 µl	5x Buffer HF	98.5°C	20 sec	
1 µl	dNTPs	64°C	15 sec	30 Cycles
1 µl	Primermix (10 µM)	72°C	20 sec	
0.3 µl	PfuS DNA Polymerase	72°C	2 min	
13.2 µl	H_2O	4°C	∞	

An additional GR^{flox}-specific PCR was performed for GR^{spc} mice to distinguish between the GR^{flox}-, the GR^{null}-, and the GR^{wt}-allele. This PCR was done using Taq DNA polymerase.

Standard Reaction		**PCR Protocol**		
1 µl	DNA	95°C	5 min	
2.5µl	10x PCR Buffer	95°C	30 sec	35 Cycles
1 µl	dNTPs	60°C	1 min	
0.5 µl	Primermix (10 µM)	72°C	1 min	
0.2 µl	Taq DNA Polymerase	72°C	10 min	
19.8 µl	H_2O	4°C	∞	

Enzymatic digestion of the GR^{dim} PCR products was performed with BsrGI. A restriction site for BsrGI was present in the amplicon from DNA containing the A458T point mutation in GR^{dim} mice (Reichardt et al., 1998) which allows to distinguish between wild type- and dim-allele.

Standard Reaction

10 µl	PCR Product
0.5 µl	BsrGI (10.000 U/ml)
2 µl	NEBuffer 2.1
2 µl	10x BSA
5.5 µl	H_2O

The PCR products were digested at 37°C for 2 hours.

The lengths of the PCR products were evaluated by agarose gel electrophoresis. Seven µl of orange G DNA loading dye were added to each sample that was loaded on a 1.5% (w/v) agarose gel in 1x TAE buffer (from 50x TAE buffer; containing 1 µg/ml ethidium bromide). In a separate lane, 13 µl of a DNA standard (Generuler 1 kb DNA ladder) were loaded. Electrophoresis was performed at 120 Volt and DNA bands were visualized under UV-light.

After restriction of the GR^{dim} PCR product with BsrGI, the wild type-allele resulted in a band of 240 bp. In the case of the dim-allele, two smaller bands of approximately half of this size were obtained.

The Cre PCR product in GR^{spc} mice had a length of 225 bp. Depending on the genotype, the GR^{flox} PCR products resulted in bands of 390 bp lengths for the GR^{null}-allele, 225 bp for the GR^{wt}-allele, and 275 bp for the GR^{flox}-allele.

3.2.3 Induction of Recombination by Tamoxifen Treatment

GR^{spc} mice were treated with tamoxifen to induce the GR-deletion in AT-II cells. Tamoxifen was prepared in a mixture of 70% ethanol together with sunflower oil (1:20 ratio). The mixture was warmed at 37°C and agitated until the tamoxifen was completely dissolved. Tamoxifen was applied to mice with the help of a feeding needle by oral gavage. Tamoxifen was administered three times at a concentration of 20 mg/ml in 150 µl every other day (Lee et al., 2012). GR^{spc} and wild type GR^{flox} mice both received tamoxifen to exclude any potential side effects.

3.2.4 Induction of AAI

For the induction of AAI, mice were sensitized i.p. with 10 µg OVA together with 2 mg of the adjuvant alum in a total volume of 200 µl in PBS over a period of 4 weeks on days 0, 7, 14 and 21 (**fig. 8**). Mice underwent allergen exposure on days 28 and 29 (Brandt et al., 2007). To this end, 20 µl of 250 µg OVA solubilized in PBS were applied intranasally under slight isoflurane anesthesia. Part of the mice was i.p. injected with the synthetic GC Dex at a dose of 10 mg/kg body weight. In case of the GR^{spc} mice, gene recombination was induced prior to the first immunization on days -14, -12 and -10; tamoxifen treatment was repeated on days 14, 16 and 18. In all experiments, mice were sacrificed on day 31 and different samples were taken for further *ex vivo* analyses.

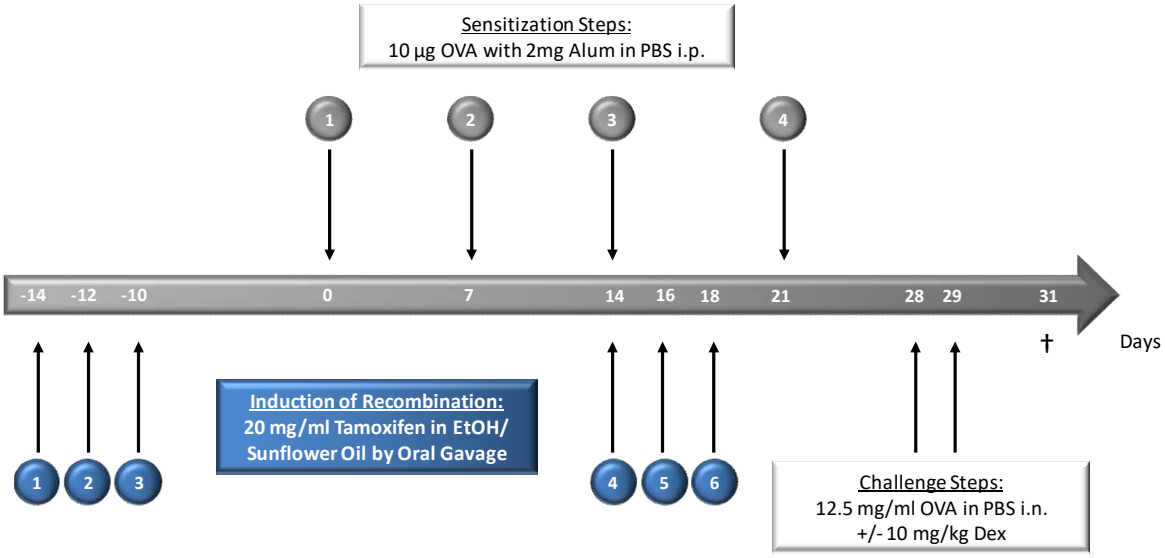

Figure 8: Induction of AAI. Mice were immunized four times by i.p. injections of OVA in alum and PBS followed by two intranasal challenges with OVA in PBS. Part of the mice was treated i.p. with Dex on the same days as the challenges. In case GR^{spc} were investigated, they were treated with tamoxifen two weeks prior to the first immunization and again four weeks later. Mice were sacrificed on day 31.

3.2.5 Induction of ALI

ALI model was induced by combined treatment with LPS and OA with slight modifications as described by Zhou (Zhou et al., 2005). Mice were injected i.p. with 10 mg/kg bodyweight LPS (**fig. 9**). In the case of GC-treatment, mice received i.p. injections of 10 mg/kg Dex simultaneously with the LPS injections. Thirty minutes afterwards, OA was applied intravenously (i.v.) at a concentration of 2.6 µl/g body weight. OA was prepared as a 4%-solution in 0.1% PBS/BSA. Control mice were treated with PBS only. Mice were sacrificed 15 hours later and different samples were taken for further analyses.

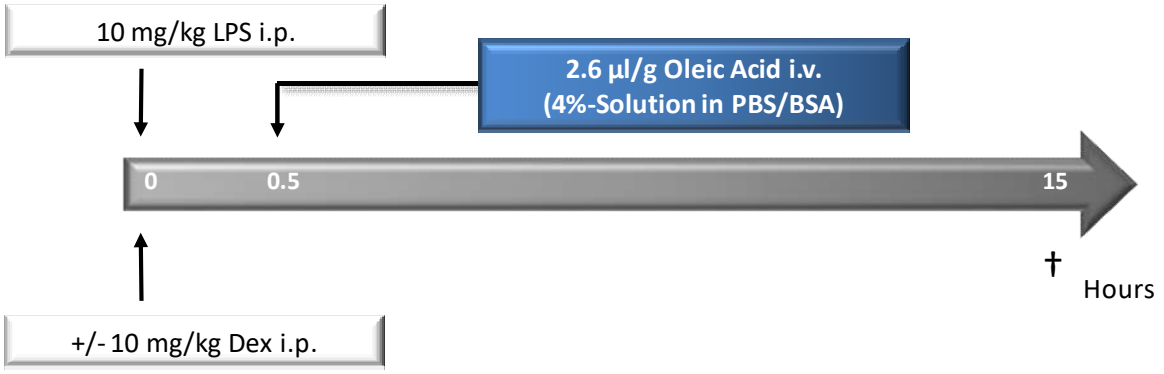

Figure 9: Induction of ALI. Mice were treated with LPS i.p., with or without i.p. Dex. Thirty minutes later, OA was i.v. injected. Mice were sacrificed 15 hours later.

3.2.6 Sample Collection

3.2.6.1 Isolation of Bronchoalveolar Lavage Fluid Cells

The thoracic cavity was opened and a venous catheter was inserted into the trachea. The catheter was fixed with a thread and the needle removed. A syringe containing 1 ml ice cold PBS/BSA was attached to the catheter. Bronchoalveolar lavage fluid (BALF) was collected by infusing the lung gently with the PBS/BSA. This washing step was repeated until a total volume of approximately 3 ml BALF was collected. The samples were centrifuged at 350 x g at 4°C for 7 min. The supernatant was discarded and the cell pellet was resuspended in 1 ml PBS. To remove erythrocytes, 6 ml TAC buffer were added to the cell suspension and samples were incubated at RT for 12 min. The reaction was stopped by adding 8 ml PBS/BSA. Then, BALF samples were centrifuged, the supernatant removed and the cell pellet resuspended in the reflux. The total volume of BALF samples was determined by using pipettes. Depending on the expected cell number, an adequate volume of the cell suspension was diluted in trypan blue to distinguish between living cells and apoptotic ones. BALF cells were counted with a Neubauer hemocytometer.

3.2.6.2 Serum

Blood samples were obtained by cardiac puncture and left for coagulation at RT for 2 hours. Subsequently, the samples were centrifuged at V_{max} for 30 min. The serum was removed and stored at -20°C before it was used for ELISA.

3.2.7 Isolation of AECs

AECs were isolated using previously described protocols by Corti and Gereke with several modifications (**fig. 10**) (Corti et al., 1996; Gereke et al., 2012).

As for the isolation of the BALF, the thoracic cavity was opened and a venous catheter was inserted into the trachea (**see 3.2.6.1**). A lavage of the lungs was performed using 800 µl PBS supplemented with 15 mM EDTA to remove infiltrating cells including macrophages. Lungs were perfused via the right heart ventricle with 15 ml PBS to remove the remaining blood. Afterwards, lungs were filled with 2 ml pre-warmed (37°C) dispase (50 U/ml) and then allowed to collapse naturally. This was followed by infusing the lungs slowly with 1 ml pre-warmed (45°C) low-melt agarose. Subsequently, lungs were immediately covered with crushed ice for 2 min to let the agarose solidify. This was done to stiffen the lung tissue as low melt agarose provides a positive alveolar pressure to maintain the inflated state (Sanderson, 2011). The lungs were removed from the thoracic cavity and transferred to a round bottom culture tube with additional 2 ml dispase. Lungs were incubated at RT for 45 min. Then, the digested lungs were placed in a 60 mm tissue culture dish and were carefully minced with the help of a scissor. Seven ml DMEM were added together with 100 µl DNase I (10 mg/ml) to the lung tissue. The culture dish was placed on a shaker at RT for 10 min.

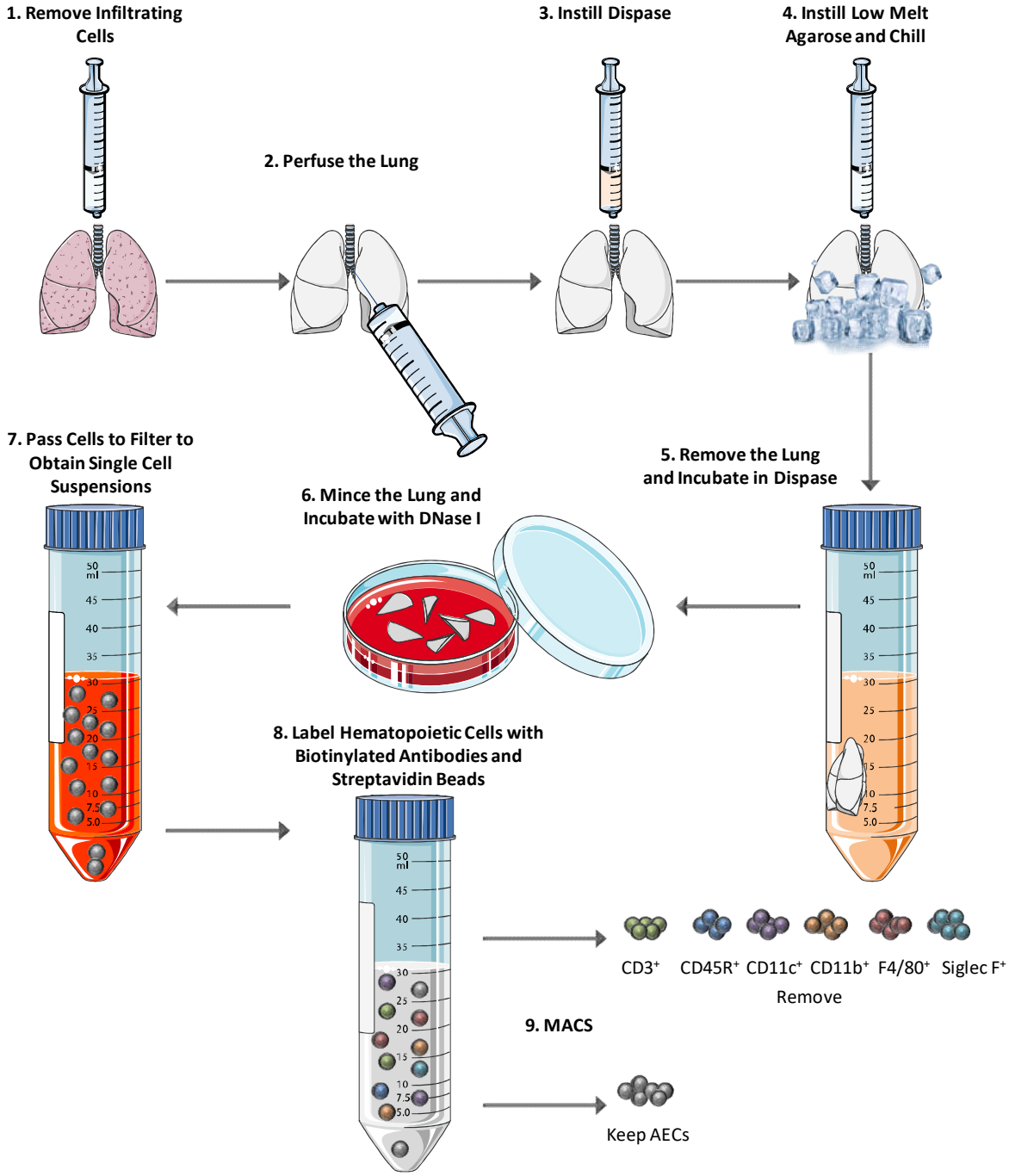

Figure 10: Scheme of AEC isolation. Lungs were lavaged to remove infiltrating cells followed by perfusion to remove remaining blood. Lung tissue was enzymatically digested with dispase together with low melt agarose. Lungs were minced and treated with DNase I. Afterwards, the lung tissue was serially passed through filters to obtain single cell suspensions. Hematopoietic cells were magnetically labeled and removed by MACS to obtain AECs by negative selection.

The resulting cell suspension was serially passed through 100 µm and 40 µm cell strainers and extensively washed with DMEM to prevent loss of cells. The filtered cell suspensions were centrifuged at 130 x g and 4°C for 12 min. Cells were treated with TAC buffer to achieve erythrocyte lysis (**see 3.2.6.1**) and centrifuged again. The cell pellet was

resuspended in 1 ml DMEM and cell numbers were determined with the help of a Neubauer hemocytometer. Fc blockage was performed by adding 100 µl TruStain fcX (anti-CD16/CD32) to the cells for incubation at 4°C for 15 min. This step was necessary to minimize unspecific binding of FcR-expressing cells including myeloid cells. Afterwards, cells were washed in MACS buffer and centrifuged at 300 x g and 4°C for 7 min. The cell pellet was resuspended and labeled with 10 µl per 1 x 10^7 cells biotinylated antibody-cocktail plus 40 µl MACS buffer at 4°C for 20 min. The biotinylated antibody-cocktail includes a mixture of anti-mouse CD3, anti-mouse CD45R, anti-mouse CD11b, anti-mouse CD11c, anti-mouse F4/80 and anti-mouse Siglec F antibodies to deplete all remaining cells of the hematopoietic lineage. Following a washing step with MACS buffer, cells were resuspended in 10 µl per 1 x 10^7 cells streptavidin microbeads together with 90 µl MACS buffer and incubated at 4°C for 15 min. Cells were washed again and the resulting cell pellet was resuspended in 500 µl MACS buffer. Magnetic separation was performed using the autoMACS program DEPLETE S to remove all unwanted cells. The remaining $CD3^-$ $CD45R^-CD11b^-CD11c^-F4/80^-Siglec\ F^-$ cells were considered to be mainly AECs (although they contained other cells of non-hematopoietic origin as well). Following MACS, the negative selected cell fraction was washed in MACS buffer and cells were ready to be used for different purposes.

3.2.8 Isolation of Peritoneal Macrophages

Mice were injected i.p. with 1 ml 4% thioglycolate solution to attract macrophages into the peritoneal cavity. Four days later, mice were sacrificed and a small incision was made along the midline of the abdominal wall. Peritoneal exudate cells were obtained by rinsing the peritoneal cavity several times with PBS/BSA with the help of a pasteur pipette. The collected peritoneal lavage was centrifuged at 328 x g and 4°C for 6 min. The resulting cell pellet was resuspended in 1 ml $DMEM^{++}$ and cell numbers were determined. To obtain monolayers of peritoneal macrophages, cells were seeded in 100 mm cell culture dishes at a concentration of 1 x 10^6 cells per ml and cultured with 10 ml $DMEM^{++}$. Macrophages were allowed to adhere at 37°C for 1 hour. To remove non-adherent cells, the medium was aspirated and the dishes were extensively washed with PBS. Peritoneal macrophages were detached with 2 ml PBS supplemented with 2 mM EDTA at 37°C for 30

min. Afterwards, cells were washed and cell numbers determined. Peritoneal macrophages were then ready to use.

3.2.9 ELISA

3.2.9.1 Anti-OVA Antibody Isotype ELISA

The levels of different isotypes of anti-OVA antibodies in serum samples of mice with AAI were determined by ELISA (Michel et al., 2013). To this end, 96-well flat bottom plates were coated with 50 µg/ml OVA dissolved in coating buffer. Plates were incubated at 4°C overnight. Thereafter, plates were washed four times with PBS-Tween. Wells were blocked with assay diluent at RT with shaking for 1 hour. This was done to prevent unspecific binding of the reactants and thus to minimize the background. Plates were washed again with PBS-Tween and serum samples were diluted depending on the Ig isotype. For the detection of the IgG1 isotype, samples were diluted 1:200.000, for the IgG2a isotype 1:2500 and for the IgE isotype 1:100 in assay diluent. To improve IgE detection, protein G plus agarose was added to the respective wells for 1 hour incubation at RT on a shaker to remove IgG antibodies. After three additional washing steps, diluted serum samples were added to the plates and were incubated at 4°C overnight. Plates were washed and HRP-conjugated anti-IgG1, anti-IgG2a, or anti-IgE antibodies were added to the respective wells at a 1:1000 dilution for 1 hour incubation at RT with shaking. Finally, plates were washed five times with soaking for 30 sec between each step. TMB substrate solution was added to each well and incubated at RT in the dark until the color developed. The color reaction was stopped by adding stop solution to the wells. The absorbance was determined at 450 nm and 570 nm with a spectrophotometer.

3.2.9.2 IL-6 ELISA

Secretion of IL-6 was quantified in serum samples of mice with ALI. The mouse IL-6 ELISA kit was used according to the manufacturer's instructions. Flat bottom plates were coated with IL-6 capture antibody in coating buffer at 4°C overnight. Afterwards, plates were washed four times with PBS-Tween and blocked with assay diluent at RT with shaking for 1 hour. Plates were washed and diluted serum samples, as well as IL-6 standards were

added to the respective wells. Samples were incubated at RT on a shaker for 2 hours. In all cases, serum samples were diluted 1:1.000 in assay diluent. Following washing, avidin-HRP solution was added to each well for 30 min incubation at RT with shaking. As described before, wells were washed five times and TMB substrate solution was added. Finally, the color reaction was stopped with stop solution and the absorbance measured at 450 nm and 570 nm.

3.2.10 Flow Cytometry

In order to investigate the cellular composition of the BALF, samples were analyzed by fluorescence activated cell sorting (FACS). Prior to each analysis, antibodies were titrated using either BALF cells or splenocytes to determine optimal working dilutions for each antibody-fluorochrome conjugate. Compensation for spectral overlaps was done when multi-color immunofluorescence staining was performed. This was achieved by using cells that had been stained with a single antibody solution. Compensation was automatically performed by the FACS Diva software.

After preparation of BALF samples, 1 x 10^5 up to 1 x 10^6 cells were resuspended in 200 µl FACS buffer and transferred to FACS tubes. Unspecific antibody binding was inhibited by Fc blockage (**see 3.2.7**). To this end, cells were treated with 20 µl TruStain fcX for at 4°C for 15 min. Afterwards, cells were stained with 20 µl of an antibody-cocktail and incubated at 4°C in the dark for 20 min. Following antibody staining, BALF cells were washed with FACS buffer and centrifuged at 450 x g and 4°C for 5 min. The supernatant was removed and the cell pellet was resuspended in the reflux by vortexing. Data were acquired on the BD FACS Canto II flow cytometer and analyzed using FlowJo software.

3.2.10.1 Gating Strategy for BALF Cells

BALF cells were stained for the surface markers Siglec F, F4/80, CD11b, GR-1, CD4 and CD3 (for AAI experiments) or CD8 instead (for ALI experiments).

First, live and apoptotic cells were separated on the basis of their size and granularity using their forward and sideward scatter (FSC-A and SSC-A). Doublets were eliminated to detect disproportions between cell size and cell signal. Therefore, cells were scaled for the area against height with FSC-A against FSC-H. Amongst the live cell population,

leukocytes subsets (eosinophils, macrophages, monocytes, neutrophils and $CD4^+$ or $CD8^+$ T cells) were identified by plotting different antibody markers against each other in three different dot-plots (**fig. 11**).

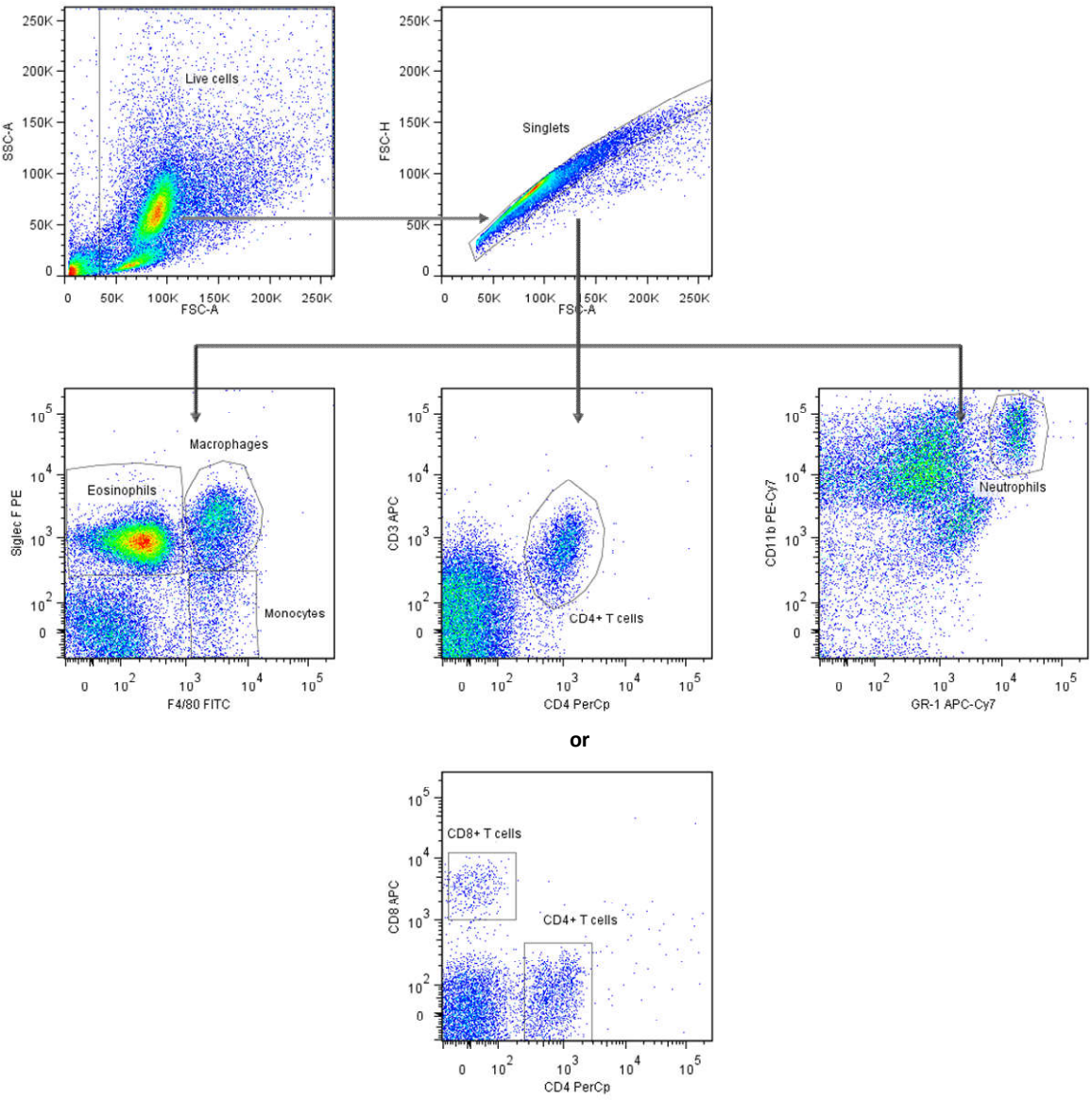

Figure 11: Gating strategy for BALF samples. Representive dot plots showing gating of live cells, singlets and distinct cell populations such as eosinophils, macrophages, monocytes, neutrophils and $CD4^+$ T cells, as well as $CD8^+$ T cells for ALI samples.

3.2.10.2 Lysotracker Staining

Lysotracker Green DND-26 has been shown to be a marker for AT-II cells (Van der Velden et al., 2013). It is a fluorescent dye that stains acidic cell compartments, especially lamellar bodies exclusively found in AT-II cells. After cell surface staining with antibodies, MACS-sorted cells were washed with DMEM and centrifuged at 300 x g and 4°C for 7 min. Afterwards, cells were pelleted in 1 ml of 50 mM Lysotracker diluted in DMEM and incubated at 37°C in the dark for 45 min. Finally, cells were washed again in DMEM and then ready for flow cytometric analysis.

3.2.11 Hemalum and Eosin Staining of Lung Tissue

For the preparation of lung samples, a venous catheter was placed into the trachea and 1 ml 4% Roti Histofix was injected into the lungs. Subsequently, whole lungs were excised and placed in 6-well culture plates with additional 3 ml Roti Histofix. After 24 hours fixation at RT, Roti Histofix was replaced by PBS and lungs were kept at 4°C before use.
Fixed lungs were placed in tissue cassettes and further processed by using an automatic tissue processor. Tissue dehydration was achieved using increasing concentrations of ethanol followed by clearance with xylene, and finished by incubating the tissue with paraffin wax.

Tissue Processing

1 h	50% Ethanol		
1 h	70% Ethanol		
2 h	80% Ethanol		Dehydration
3 h	96% Ethanol		
3 h	99% Ethanol		
2 h	Xylene	→	Clearance
4 h	Paraffin	→	Paraffinization

Finally, lungs were embedded in paraffin blocks using tissue embedding system. Lungs were cut at 5 µm thickness and the sections were adhered to microscope slides using a

water bath at 37°C. Microscope slides were dried overnight at the same temperature. Lung sections were deparaffinized with xylene and rehydrated through a series of descending ethanol concentrations followed by one short washing step with H_2O. For nuclear staining, lung sections were incubated with hemalum solution which was followed by bluing under running tap water. Afterwards, lung sections were incubated with eosin solution to stain the cytoplasm. Slides were shortly washed with H_2O and dehydrated again with increasing concentrations of ethanol followed by clearance with xylene.

Hemalum and Eosin Staining

30 min	Xylene	→	Deparaffinization
4 min	99% Ethanol	}	Rehydration
4 min	96% Ethanol		
4 min	70% Ethanol		
1 min	H_2O		
10 min	Hemalum Solution	}	Staining of Nuclei and Cytoplasm
10 min	Running Tap Water		
5 min	Eosin Solution		
1 min	H_2O		
4 min	70% Ethanol	}	Dehydration
4 min	96% Ethanol		
4 min	99% Ethanol		
30 min	Xylene	→	Clearance

Microscope slides were mounted in Entellan and analyzed microscopically.

3.2.12 RNA Isolation

3.2.12.1 RNA Isolation from Lungs

RNA isolation from lungs was carried out using the RNeasy Plus Universal kit according to the manufacturer's instructions. Lungs were homogenized in 900 µl Qiazol using the tissue homogenizer Ultra Turrax T18. The lung homogenates were transferred to new tubes and incubated at RT for 5 min. To minimize contamination with genomic DNA, 100 µl gDNA Eliminator solution were added to samples that were vortexed for 15 sec. Afterwards, 180 µl were added and samples were vortexed again for 15 sec and incubated at RT for 3 min. Homogenates were centrifuged at V_{max} and 4°C for 15 min. The aqueous supernatant was transferred to new tubes and mixed with the same volume of 70% ethanol. Half of this mixture was loaded onto RNeasy Mini Spin columns which were placed in collection tubes. Samples were centrifuged at V_{max} and 20°C for 20 sec. The flow-through was discarded and depending on the sample volume, this step was repeated. Thereafter, 700 µl RWT buffer were added to the columns and samples were centrifuged at 8.000 x g for 20 sec. The flow-through was discarded again and 500 µl RPE-buffer were added to the samples and centrifuged at 8.000 x g for 2 min. Afterwards, columns were dried by spinning down the tubes for 1 min. Columns were placed in new tubes and 35 µl RNase-free water were directly loaded to the column membrane. RNA was collected by centrifugation at 8.000 x g for 1 min. The eluate was kept and the whole step was repeated to increase the RNA yield. Isolated lung RNA was used immediately or stored at -20°C.

3.2.12.2 RNA Isolation from AECs

RNA isolation from MACS-sorted AECs was performed using the Quick RNA MiniPrep kit according to the manufacturer's instructions. After sorting, AEC samples were centrifuged at 300 x g and 4°C for 7 min. Cells were lysed with 600 µl RNA Lysis buffer and centrifuged at 10.000 x g and 20°C for 1 min to clear the lysate. To minimize the amount of genomic DNA, the supernatant was transferred to Spin-Away filters in collection tubes and centrifuged at 10.000 x g for 1 min. The eluate was kept and mixed with the same volume

of 99.8% ethanol. Half of this mixture was loaded to Zymo-Spin III G columns in collection tubes and spun down for 30 sec at 10.000 x g. The flow-through was discarded and the columns were loaded with the rest of the sample for additional centrifugation. Afterwards, 800 µl RNA Prep buffer were added to the columns and samples were centrifuged again. The flow-through was removed again and 700 µl RNA Wash buffer were loaded to the columns. Samples were centrifuged for 30 sec. The washing step was repeated with 400 µl RNA Wash buffer for 2 min centrifugation to ensure complete removal of the wash buffer. The columns were placed in new collection tubes and 30 µl DNase/RNase-free water were directly loaded to the column membrane. RNA was eluted by centrifugation at V_{max} for 30 sec. Isolated RNA was used immediately or stored at -20°C.

The concentration of the isolated RNA was determined using a Nanodrop 2000 photometer. In addition, the quality of the isolated RNA was assessed by agarose gel electrophoresis (**see 3.2.2**). To this end, 1 µg RNA were loaded together with orange G loading dye on a 1% gel. Intact RNA should appear as two sharp bands representing the 18s and 28s rRNA.

3.2.13 Synthesis of cDNA

RNA samples from lungs and AECs were reversely transcribed into complementary DNA (cDNA) using the iScript cDNA Synthesis kit according to the manufacturer's instructions.

Standard Reaction

1 µg	RNA Template
0.25 µl	Reverse Transcriptase
4 µl	5x iScript Reaction Mix
16 µl	Nuclease-Free Water

Samples were incubated in the reaction mix at 25°C for 5 min, followed by 30 min at 42°C. The reaction was stopped by incubation at 85°C for 5 min. Successful cDNA synthesis was verified by performing a PCR reaction with PfuS polymerase (**see 3.2.2**) using amplification of hypoxanthine phosphoribosyl transferase (HPRT), a housekeeping gene.

The PCR product was visualized on a 1.5% agarose gel (**see 3.2.2**). The amplified PCR product should appear as one sharp band.

3.2.14 Quantitative Real-Time PCR

The mRNA expression levels of several genes were determined via qRT-PCR. To this end, cDNA was analyzed using the real-time PCR system 7500.

Standard Reaction

1 µl	cDNA
0.5 µl	Primermix
12.5 µl	SYBR-Green Powermix
11 µl	H_2O

Real-Time PCR Protocol

2 min	50°C	→	Preheating
10 min	95°C	→	Initial Denaturation and Enzyme Activation
15 sec	95°C	}	50 Cycles Amplification
1 min	60°C	}	
15 sec	95°C	→	Denaturation of DNA
1 min	60°C	→	Hybridization
15 sec	95°C	→	Test of the Melting Curve
15 sec	60°C	→	Final Elongation of the Amplicon

Normalization of target gene expression is necessary to compensate for intra- and interkinetic qRT-PCR variations occurring during the PCR run. Therefore, all gene expression levels were normalized to an invariant endogenous control, e.g. HPRT, which is a housekeeping gene that is equally expressed in all cells of an organism under normal and pathophysiological conditions. Data analysis was performed using the ΔΔCT method.

3.2.15 Next Generation Sequencing

Transcriptome profiling of AECs was performed in collaboration with Dr. Gabriela Salinas-Riester at the Microarray and Deep-Sequencing facility of the University Medical Center in Göttingen.

Total RNA was isolated from MACS-sorted AECs using the Trizol method (Invitrogen, Carlsbad, CA, USA) according to the manufacturer's instructions and treated with DNase I to remove contamination with genomic DNA. RNA quality was determined using the 2100 bioanalyzer (Agilent Technologies, Santa Clara, CA; USA). Library preparation for RNA-seq was performed using the TruSeq RNA sample preparation kit (ID RS-122-2002; Illumina, San Diego, CA, USA) according to the manufacturer's instructions. Size range and purity of final cDNA libraries were assessed using the 2100 bioanalyzer. Libraries were captured on a flow cell (Illumina, San Diego, CA, USA) for cluster generation and subsequently amplified and sequenced on the HiSeq 2000 (Illumina, San Diego, CA, USA) deep sequencing system. Single read sequencing with 50 bp was conducted with 17.5 to 35 million reads per sample. Sequence images were transformed to bcl-files with the BaseCaller software (Illumina, San Diego, CA, USA) and demultiplexed to fastq-files with CASAVA software (version 1.8.2; Illumina, San Diego, CA, USA). Sequences were aligned to the murine reference genome sequence (UCSC genome mm10) using Bowtie2 software (version 2.1.0) (Langmead and Salzberg, 2012). The reads were counted to each gene to the reference gene annotation using HTSeq (version 0.5.4.p3; Anders et al., 2015). Data was preprocessed and analyzed in the R/Bioconductor software (version 3.0.2/2.13; Huber et al., 2015) loading DESeq (Anders and Huber, 2010), gplots (Warnes, 2016) and biomaRt (Durinck et al., 2009) packages. Genes were filtered exceeding more than 20 counts for at least one sample, which was followed by normalization, estimation of dispersions and testing for differentially expressed genes. This was based on a test assuming that negative binomial data distribution was computed via DESeq (version 1.14.0). Candidate genes were filtered to a minimum of two times fold change and FDR-corrected p-value < 0.05. Regarding the functional association, the candidate genes were analyzed for gene ontology enrichment via GoSeq (version 1.4.0; Young et al., 2010).

3.2.16 Protein Extraction from Lungs

Lungs were homogenized in 500 µl protein lysis buffer using the tissue homogenizer Ultra Turrax T18. The resulting lung homogenate was incubated on ice for 1 hour and subsequently centrifuged at V_{max} and 4°C for 20 min. The supernatant containing the protein lysate was transferred to new tubes and stored at -20°C.
Total protein was measured with the Nanodrop 2000 photometer. The protein concentration was determined using Bradford reagent and calculated with the help of a BSA standard curve.

3.2.17 Western Blot

Samples were diluted to 15 µg/ml in Ripa buffer and boiled together with 10 µl Laemmli buffer for 5 min at 95°C. Proteins were separated by SDS-PAGE using a 10% stacking and running gel for 1 hour at 20 mA. A protein marker was added to the gel to identify the size of the protein bands. Afterwards, the gel was placed on a nitrocellulose membrane between two Whatman papers that were wetted with blotting buffer before. Protein transfer was performed using the semi-dry method for 1 hour at 16 Volt. Subsequently, proteins on the membrane were blocked with blocking solution for 1 hour at RT with shaking. The membrane was washed with PBS-Tween three times for 5 min. After washing, the membrane was incubated with the primary antibody overnight at 4°C with shaking. Unbound antibodies were removed by three washing steps with PBS-Tween. Then, the HRP-conjugated secondary antibody was added to the membrane. Following 1 hour incubation at RT, the nitrocellulose membrane was washed again three times with PBS-Tween. Proteins were detected by chemiluminiscence by adding 2 ml western blot developing solution to the membrane. The bands were visualized using the Chemocam imager.

3.2.18 Statistical Analyses

Statistical evaluation was achieved using GraphPad Prism 5 software and Microsoft Office Excel 2007 and 2010. The unpaired, two-tailed t-test was chosen to compare two groups. Results were depicted as mean ± standard error of the mean (SEM) and a *p*-value < 0.05 was considered to indicate statistical significance: $p < 0.05$ (*), $p \leq 0.01$ (**), $p \leq 0.001$ (***) and $p \leq 0.0001$ (****). Outlying sample exclusion was performed using Grubb's test with $\alpha = 5\%$.

4. Results

4.1 GC-Treatment in a Murine Model of AAI Requires an Intact GR-Dimerization Interface

In the treatment of various diseases, the anti-inflammatory effects of GCs rely either on the transactivating or on the transrepressing mechanisms of the GR. Though, it is unclear which mechanism is more important in mediating these beneficial effects.

An AAI was induced in GR^{dim} mice to dissect the GR mechanisms in the treatment of asthma. GR^{dim} mice carry a point mutation that impairs GR-dimerization and subsequently the transactivating mode of action. At the same time, the transrepressing mechanism is still intact allowing interaction with pro-inflammatory transcription factors. Previous findings indicated that dimerization was required for the treatment of AAI (unpublished data). To confirm these findings, GR^{dim} mice and wild type (GR^{wt}) mice were sensitized to OVA along with the adjuvant alum by i.p. injections on four consecutive weeks. Thereafter, allergen exposure was performed by intranasal instillation of OVA to elicit the allergic inflammation in the airways. At the same time, part of the mice received i.p. injections with Dex which represents systemic GC-treatment. Control groups were administered PBS and alum by i.p. injections and PBS only by intranasal instillation.

4.1.1 OVA-specific Antibody Production Is Increased after AAI Induction

As mentioned before, CSR is an important feature of AAI in asthma. Following allergen sensitization, B cells undergo CSR to produce IgE antibodies in response to T_H2 cell-secreted IL-4 and IL-13. To prove the efficiency of the OVA-immunization protocol, Ig isotype class-switch was analyzed in serum samples of GR^{wt} and GR^{dim} mice. Levels of OVA-specific IgE and IgG1 antibodies (characteristic for a T_H2 response) and T_H1-specific IgG2a antibodies were determined by ELISA.

In comparison to control groups, levels of OVA-specific IgG1 and IgE isotypes were significantly increased in both genotypes following the induction of AAI (**fig. 12 A and B**). The same could also be observed for IgG2a (**fig. 12 C**). Regardless of the isotype, Dex-treatment did not influence the OVA-induced Ig production (**fig. 12 A-C**) as differences

were not significant. Moreover, no clear differences in the Ig levels were found between GR^{wt} and GR^{dim} mice. Thus, immunization with OVA led to the AAI-characteristic Ig isotype class-switch with elevated levels of IgG1 and IgE in both genotypes.

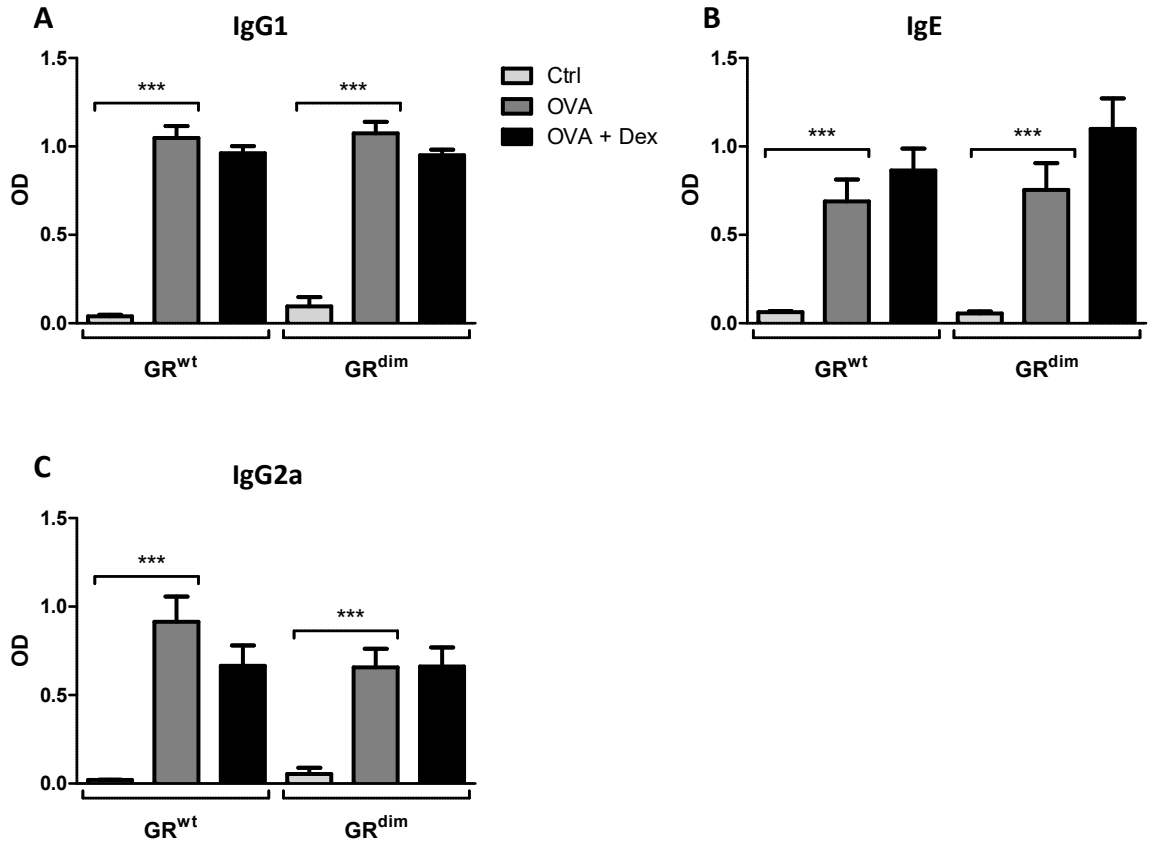

Figure 12: OVA-specific antibody production in GR^{wt} and GR^{dim} mice. For the detection of allergen-induced Ig isotype class-switch IgG1 (A), IgE (B) and IgG2a (C) levels were determined with the respective antibodies by ELISA. Serum samples were taken by cardiac puncture two days after the last allergen challenge step from control groups (Ctrl), OVA-immunized groups (OVA) and additionally Dex-treated groups (OVA + Dex). Ig levels were determined spectrophotometrically and are depicted as optical density (OD). Data are presented as mean values ± SEM (GR^{wt}: IgG1 n = 13-17, IgE n = 7-9 and IgG2a n = 9-10; GR^{dim}: IgG1 n = 14-17, IgE n = 7-9 and IgG2a n = 8-11; each group). Statistical significances were determined using unpaired, two-tailed t-test (*: $p < 0.05$; **: $p \leq 0.01$;***: $p \leq 0.001$).

4.1.2 GC-Treatment Does Not Abolish Pulmonary Infiltrates in GR^{dim} Mice with AAI

To specifically analyze the AAI in the lungs of GR^{wt} and GR^{dim} mice, quantitative analysis of pulmonary infiltrates was performed. Bronchoalveolar lavage (BAL) was performed to obtain the airway infiltrating cells. For investigating the cellular composition of the BALF samples, cell numbers were determined and cells were stained with distinct cell surface markers for flow cytometry.

In contrast to control animals, a significant increase of inflammatory cells could be observed in both genotypes (**fig. 13 A**). This inflammatory influx was dominated by eosinophils (60%; *data not shown*) which mimics the characteristic eosinophilia of AAI in asthma (**fig. 13 C**).

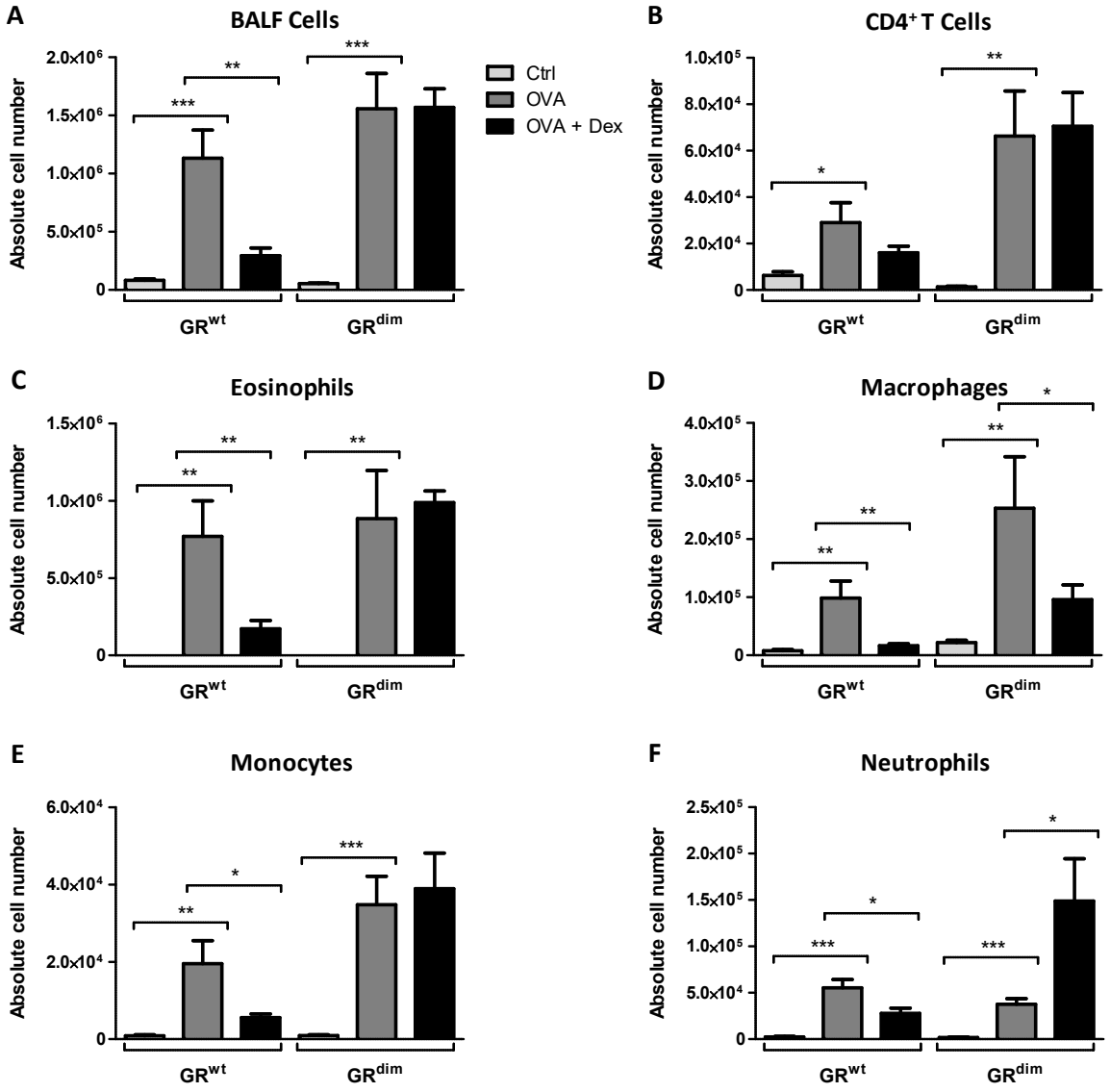

Figure 13: Quantitative analysis of pulmonary infiltrates from GR^{wt} and GR^{dim} mice. Following immunization and challenge with OVA, lungs were extensively lavaged to obtain infiltrating inflammatory cells. BALF samples were taken from control groups (Ctrl), OVA-immunized groups (OVA) and additionally Dex-treated groups (OVA + Dex). Absolute cell numbers were determined for total BALF cells (A), $CD4^+$ T cells (B), eosinophils (C), macrophages (D), monocytes (E) and neutrophils (F). BALF cells were stained with respective cell surface markers and analyzed by flow cytometry. Data are presented as mean values ± SEM (GR^{wt}: n = 10-13; GR^{dim}: n = 8-12; each group). Statistical significances were determined using unpaired, two-tailed t-test (*: $p < 0.05$; **: $p \leq 0.01$;***: $p \leq 0.001$).

Other cell types including macrophages, $CD4^+$ T cells, neutrophils and monocytes contributed a minor part to this cellular influx (**fig. 13 B, D, E and F**). The overall cell numbers in the BALF samples of OVA-sensitized GR^{dim} mice were slightly higher in comparison to GR^{wt} mice, but this difference was not significant.

When Dex-treatment was applied in GR^{wt} mice, cell numbers were significantly reduced in BALF samples. This was in conjunction with significant decreases in eosinophil, macrophage, monocyte and neutrophil numbers. $CD4^+$ T cell numbers were also reduced although this was not significant.

Interestingly, Dex did not have any effect on BALF cell numbers in GR^{dim} mice as numbers remained unaltered in comparison to OVA-sensitized mice without Dex-treatment (**fig. 13 A**). This was due to unchanged cell numbers of eosinophils, $CD4^+$ T cells and monocytes (**fig. 13 B, C and E**). Neutrophils numbers were increased following Dex-treatment whereas macrophages were the only cell type that showed reduced cell numbers (**fig. 13 D and F**). These data indicate that GC-treatment is not effective in GR^{dim} mice to abolish the inflammatory cell influx in the allergic airways.

4.1.3 Dex-Treatment Has No Effect on Airway Remodeling in GR^{dim} Mice

AAI is not only characterized by massive infiltration of inflammatory cells, but also by structural changes of the airways which is also known as airway remodeling. To this end, histological analyses of lung sections from GR^{wt} and GR^{dim} mice were performed. Following the induction of AAI, lungs were embedded in paraffin and sections were stained with hemalum and eosin (H & E) (**fig. 14 A and B**).

In healthy animals, the alveolar compartment was free of inflammatory cellular infiltrates. At the same time, bronchioles of GR^{wt} and GR^{dim} mice showed the characteristic round shape with no signs of structural changes (**fig. 14 A and B**). In line with the previous findings, large numbers of infiltrating cells could be observed in the alveolar tissue of mice of both genotypes following induction of AAI. This was accompanied by airway remodeling which was shown by bronchoconstriction. In addition, goblet cell hyperplasia could be seen together with large amounts of mucus inside the constricted bronchioles (**fig. 14 A and B**). Dex-treatment resulted in a remarkable reduction of the inflammatory cell influx and reversed airway remodeling in GR^{wt} mice (**fig. 14 A**). However, Dex did not

have any effect in GR^{dim} mice as airway remodeling and cell influx were still present (**fig. 14 B**).

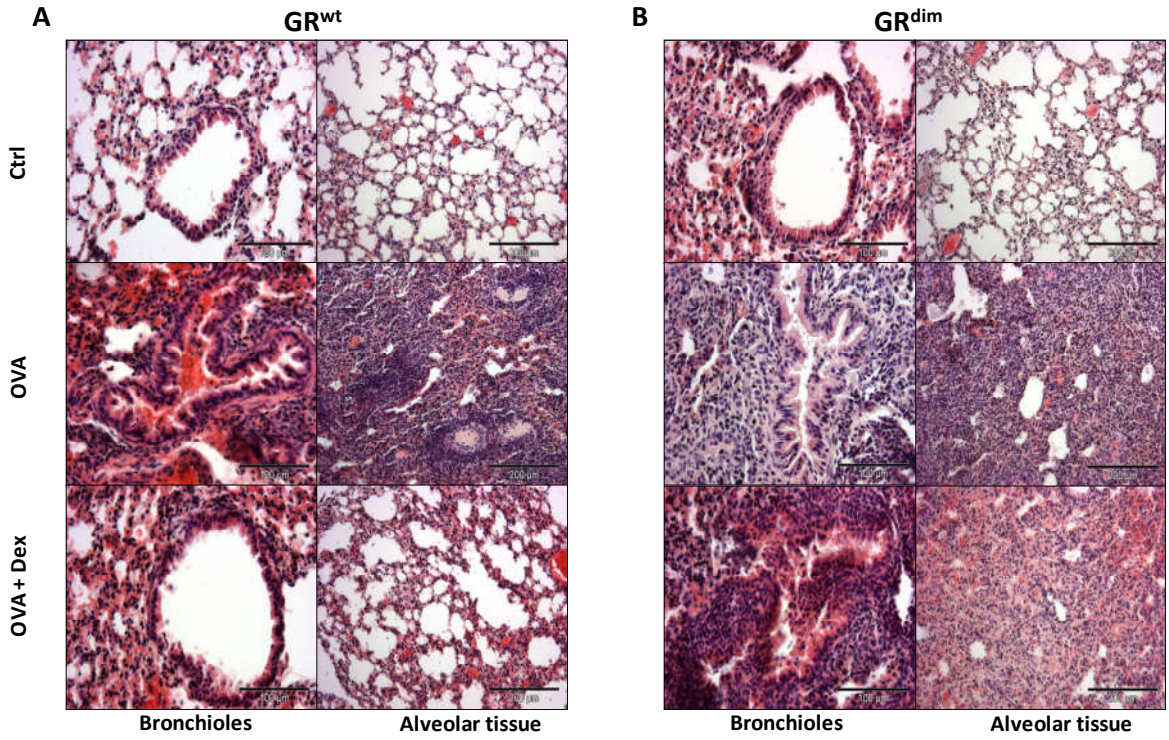

Figure 14: Histological analysis of lung tissue from GR^{wt} and GR^{dim} mice. Following induction of AAI, lungs were taken from control groups (Ctrl), OVA-immunized groups (OVA) and additionally Dex-treated groups (OVA + Dex). Lungs were embedded in paraffin, sectioned and stained with H & E. Structural and cellular changes within the lung were analyzed, in particular in bronchioles and alveolar tissue. Each section is representative for each condition and genotype (GR^{wt}: n = 3-4; GR^{dim}: n = 2-4; each group). The size bars correspond to 100 µm for bronchioles (20 x magnification) and 200 µm for alveolar tissue (10 x magnification).

Taken together, GR^{dim} mice are completely refractory to GC-treatment in AAI which correlates to the previous findings (unpublished data). These data indicate that GR-dimerization is substantial to exhibit the beneficial effects in the treatment of AAI.

4.2 Isolation and Purification of AECs from Murine Lungs

Besides the GC mechanism, it is important to identify target cells relevant for GC-treatment of asthma. Previous findings revealed that the lung itself and pulmonary structural cells have to be the target rather than the infiltrating immune cells (unpublished data). Thus, AECs have been proposed to be potential targets of the GC-treatment due to their crucial role in the immune responses of the lung.

To specifically examine AECs, a protocol for the isolation and purification needed to be established. The previously published protocols (Corti et al., 1996; Gereke et al., 2012) were used with slight modifications. Lung tissue was enzymatically digested with dispase which has been shown to specifically dissociate AECs from the organ (Corti et al., 1996). Dispase-treated lung cells were magnetically labeled with an antibody-cocktail to remove contaminating leukocytes including T cells, B cells and myeloid cells by MACS. Unlabeled cells should represent the AEC positive cell fraction.

Dispase treatment of lung tissue alone yielded in 32 million cells that were subsequently sorted by MACS (**table 16**). After elimination of leukocytes, 6 million cells were obtained per lung. The viability of these isolated cells was around 92% which was assessed by trypan blue staining.

Cell Counts Before MACS	Cell Counts After MACS	Cell Viability
31.94 Million Cells/Lung	6.33 Million Cells/Lung	92.4% of Live Cells
± 4.92	± 0.28	± 1.21 %

Table 16: Statistics of AEC isolation protocol. (Data ± SEM; n = 18)

The purity of the MACS-sorted cells was tested by flow cytometry using the standard epithelial cell marker EpCAM together with the AT-II cell marker lysotracker green DND-26 (Van der Velden et al., 2013).

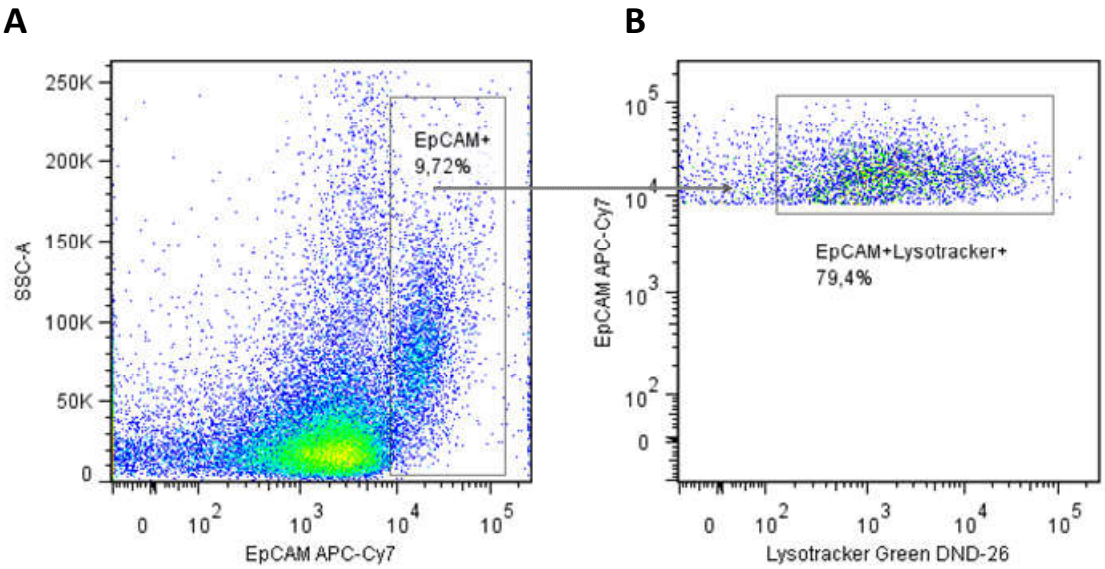

Figure 15: Purity of isolated AECs. MACS-sorted AECs were stained with the epithelial cell marker EpCAM together with the AT-II cell marker lysotracker for flow cytometry to assess the purity.

Only 10% of the sorted cells were indeed epithelial cells (**fig. 15 A**). This means that only 0.6 million AECs were present in the sorted lung cells. The majority of the epithelial population was AT-II cells as 79% of all $EpCAM^+$ cells were positive for lysotracker (**fig. 15 B**). It is unclear which other cell types are included in the MACS-sorted cell mixture. While no markers for other structural lung cells were included, it might be that fibroblasts, endothelial cells or airway smooth muscle cells were the remaining cells.

Thus, this protocol for isolation of primary AECs from murine lungs could not yield in a pure population. It rather results in a heterogeneous population of lung parenchymal cells (LPCs).

4.3 Transcriptome Analysis of LPCs from GR^{dim} Mice

Dimerization of the GR was required for the therapeutic efficacy in murine AAI. Moreover, AECs were proposed to be potential GC-targets. To assess a potential link, transcriptome analysis was performed with LPCs from GR^{wt} and GR^{dim} mice as the employed protocol did not result in a pure population of AECs. LPCs were isolated following the induction of AAI and additional Dex-treatment. Transcriptome analysis allows the identification of novel candidate genes that are differentially regulated in the different experimental settings of both genotypes. RNA-seq was performed by the TAL-facility of the University Medical Center in Göttingen.

Results of the transcriptome profiling were visualized with a heatmap showing the 50 most differentially regulated candidate genes (**fig. 16**). These candidate genes were hierarchically clustered across the different samples. Validity of the analysis could be confirmed by similar expression patterns between the biological replicates of each experimental condition.

In line with the previous findings, expression patterns of Dex-treated groups were substantially different between GR^{wt} and GR^{dim} mice. In both genotypes different genes were either up- or downregulated in LPCs following Dex-treatment. In addition, Dex-treated GR^{wt} mice showed different gene expression patterns in comparison to untreated GR^{wt} mice. The same could also be observed for both experimental conditions in GR^{dim} mice. Moreover, LPCs showed different expression patterns of both genotypes during AAI itself, even without additional Dex-treatment. Several candidate genes were chosen for further analysis including activating- transcription factor (ATF)-6, integrin α E (ITGAE), elastase neutrophil-expressed (ELANE) and CD163.

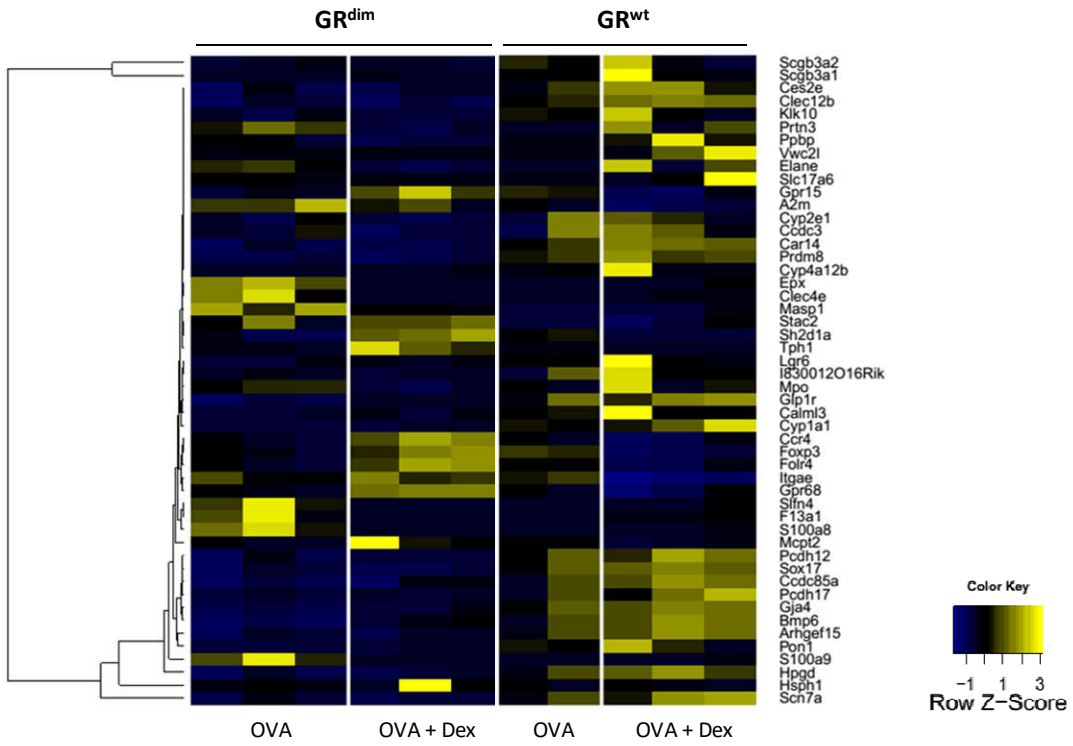

Figure 16: Transcriptome profiling of LPCs from GR^{wt} and GR^{dim} mice in AAI and following Dex-treatment.
Heatmap displaying hierarchical clustering of the top 50 differentially regulated candidate genes in LPCs from GR^{wt} and GR^{dim} mice after the induction of AAI (OVA) and subsequent Dex-treatment (OVA + Dex). Each row shows the relative expression level for a single gene whereas each column shows the expression pattern of a single sample. Expression levels are indicated in the Z-score and are plotted in a yellow-blue color scale. Color intensity represents the relative gene expression levels that are either higher (yellow) or lower (blue) than the median expression across all samples. Biological replicates were used for each condition (GR^{wt}: n = 2-3; GR^{dim}: n = 3; each group).

Taken together, RNA-seq analysis identified different transcriptomes in LPCs of GR^{wt} and GR^{dim} mice. Impaired GR-dimerization and transactivation resulted in a distinct expression pattern after Dex-treatment. These data once more highlighted the importance of GR-dimerization in efficient treatment of AAI as well as drew the attention to the pulmonary structural cells as potential target sites.

4.4 Impaired GR-Dimerization Interface Disrupts GC-Mediated Repression of Inflammatory Genes in AAI

4.4.1 GC-Treatment Is Not Effective in Repressing Inflammatory Gene Expression in LPCs of GR^{dim} Mice

In contrast to the wild type situation, an impaired GR-dimerization interface resulted in a different transcriptome profile in LPCs following GC-treatment. For the verification of the RNA-seq analysis, qRT-PCR was performed with LPCs from GR^{wt} and GR^{dim} mice. Following induction of AAI and selective treatment with Dex, LPCs were isolated from both genotypes. RNA was isolated, reversely transcribed into cDNA and processed to qRT-PCR analysis. Various genes were analyzed for differential mRNA expression levels. IL-5 and IL-13 are T_H2-specific cytokines that help to maintain the allergic inflammation in asthma (Holgate, 2011a; Verstraelen et al., 2008). IL-33, MCP-1 and RANTES are all known to be secreted by AECs and are also associated to asthma pathogenesis (Fehrenbach, 2001; Holgate, 2012a; Kato and Schleimer, 2007). Occludin and claudin 5 are components of tight junctions that are required for epithelial integrity (Arora and Kale, 2013; Holgate, 2007). Along with these asthma- and AEC-related genes, several candidate genes were analyzed that had been shown to be differentially expressed in LPCs of wild type and mutant mice. ITGAE also known as CD103 is an integrin that mediates the migration of lymphocytes into epithelial tissues (Smyth et al., 2007). CD163 is a scavenger receptor which is mainly known as marker for monocytes and macrophages (Onofre et al., 2009). ATF-6 is a transcription factor for unfolded protein responses and has been linked to asthma pathogenesis (Miller et al., 2012). ELANE is known as neutrophil elastase that mediates airway damage (Chua, 2006).

AAI led to significant increases of IL-5, IL-13, IL-33, MCP-1 and RANTES mRNA expression in LPCs of both GR^{wt} and GR^{dim} mice (**fig. 17 A-E**). Subsequent Dex-treatment markedly repressed this induction in LPCs of GR^{wt} mice (**fig. 17 A-E**). In contrast, inflammatory gene expression was even enhanced in LPCs following Dex-treatment in GR^{dim} mice (**fig. 17 A-E**). This effect was significant for IL-33 and MCP-1 (**fig. 17 C and D**).

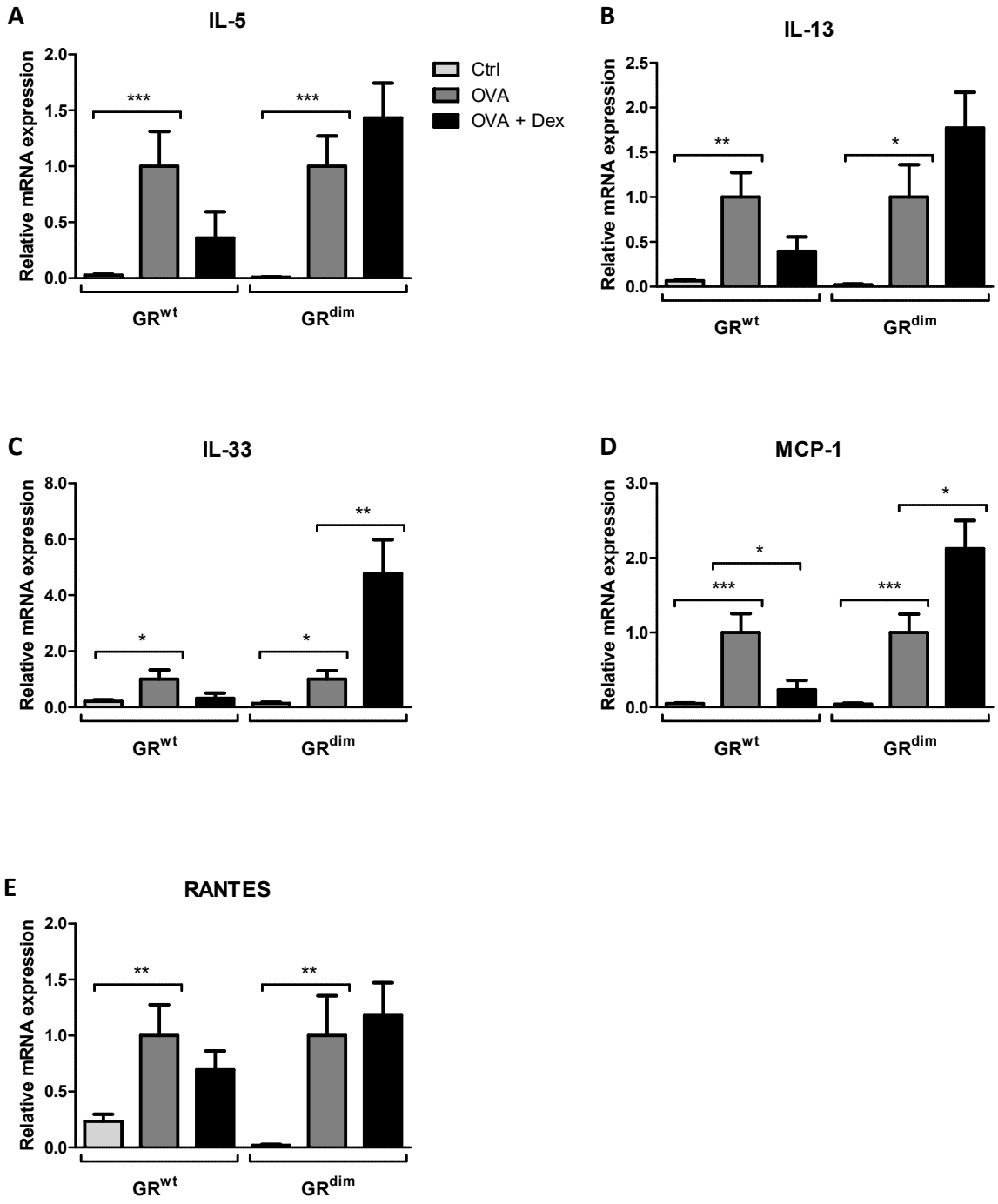

Figure 17: GC-effects on inflammatory gene expression in LPCs of GR^{wt} and GR^{dim} mice. AAI was induced by immunization with OVA together with the adjuvant alum, followed by intranasal challenge with the same antigen (OVA). Part of the mice was treated with Dex (OVA + Dex). Control mice received PBS with alum or PBS alone (Ctrl). LPCs were isolated by enzymatic digestion of lung tissue with dispase and subsequent removal of immune cells by MACS. RNA was isolated and analyzed by qRT-PCR for expression of IL-5 (A), IL-13 (B), IL-33 (C), MCP-1 (D) and RANTES (E). Relative quantities were normalized with respect to the mRNA expression levels in the OVA-groups of the respective genotype (fold change = 1). HPRT was used as endogenous control. All values are depicted as mean ± SEM (GR^{wt}: n = 5-11; GR^{dim}: n = 5-11; each group). Statistical significances were determined using unpaired, two-tailed t-test (*: $p < 0.05$; **: $p \leq 0.01$;***: $p \leq 0.001$).

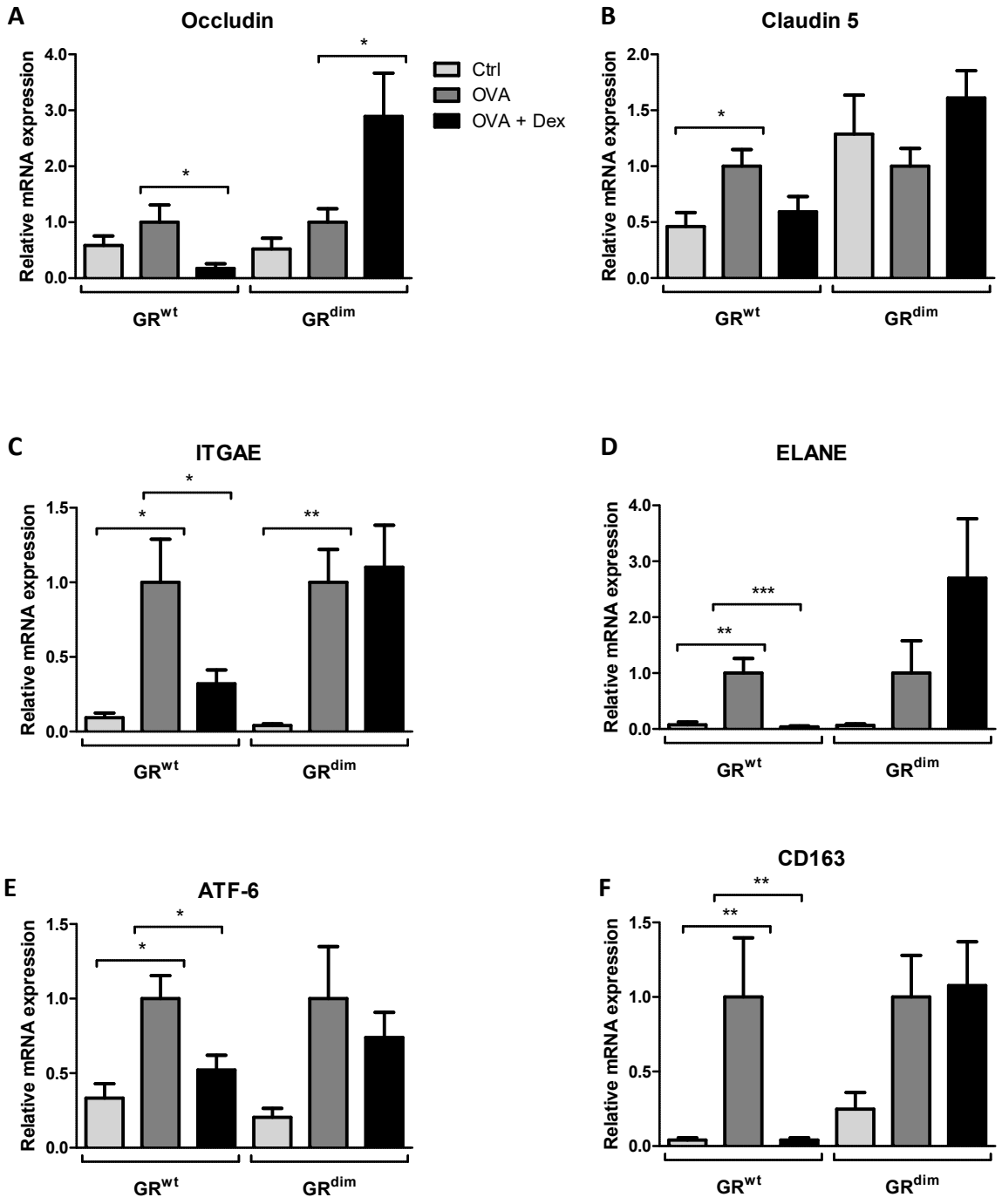

Figure 18: GC-effects on tight junction and candidate gene expression in LPCs of GR^{wt} and GR^{dim} mice.

AAI was induced by immunization with OVA together with the adjuvant alum, followed by intranasal challenge with the same antigen (OVA). Part of the mice was treated with Dex (OVA + Dex). Control mice received PBS with alum or PBS alone (Ctrl). LPCs were isolated by enzymatic digestion of lung tissue with dispase and subsequent removal of immune cells by MACS. RNA was isolated and analyzed by qRT-PCR for expression of occludin (A), claudin 5 (B), ITGAE (C), ELANE (D), ATF-6 (E) and CD163 (F). Relative quantities were normalized with respect to the mRNA expression levels in the OVA-groups of the respective genotype (fold change = 1). HPRT was used as endogenous control. All values are depicted as mean ± SEM (GR^{wt}: n = 5-11; GR^{dim}: n = 5-11; each group). Statistical significances were determined using unpaired, two-tailed t-test (*: $p < 0.05$; **: $p \leq 0.01$;***: $p \leq 0.001$).

Furthermore, AAI also led to remarkable increases of occludin, claudin 5, ITGAE, ELANE, ATF-6 and CD163 expression in GR^{wt} mice which was dampend by Dex-treatment (**fig. 18 A-F**). LPCs of GR^{dim} mice showed induction of occludin, ITGAE, ELANE, ATF-6 and CD163 when AAI was induced (**fig. 18 A, C, D, E and F**). GC-treatment with Dex enhanced the increased expression of occludin and ELANE whereas levels of ITGAE and CD163 remained unaltered (**fig. 18 A, C, D and F**). In contrast, a slight decrease of ATF-6 expression could be observed in GR^{dim} mice after treatment although this effect was not significant (**fig. 18 E**). In case of claudin 5, no clear alterations could be found in LPCs of mutant mice (**fig. 18 B**). Thus, qRT-PCR analyses of LPCs from both mouse strains revealed different expression levels of the analyzed genes. Expression of several examined genes was not diminished by Dex-treatment in GR^{dim} mice and in some cases expression was even increased.

4.4.2 Inflammatory Gene Expression in Lungs of GR^{dim} Mice Is Not Abolished by Dex-Treatment

LPCs contain AECs among other cells and represent only a small proportion of the whole lung. Therefore, qRT-PCR was performed to obtain an overview of how the impaired dimerization interface affects the GC-responsiveness and inflammatory gene expression in the whole organ. After induction of AAI and Dex-treatment, infiltrating immune cells were removed by lavage from the lungs. RNA was isolated from homogenized lung tissue, reversely transcribed and analyzed by qRT-PCR.

In line with qRT-PCR analysis of LPCs, remarkable increases of IL-5, IL-13, IL-33, MCP-1 and RANTES mRNA expression were found in the lungs of GR^{wt} and GR^{dim} mice with AAI (**fig. 19 A-E**). At the same time, Dex abolished these increases in GR^{wt} mice (**fig. 19 A-E**). In addition, enhanced levels of IL-5, IL-33 and RANTES in lungs of Dex-treated GR^{dim} mice correlated with the LPC data (**fig. 19 A, C and E**). MCP-1 expression levels remained unaltered in mutant mice following GC-treatment (**fig. 19 D**). IL-13 mRNA expression was slightly decreased whereas this effect was not significant (**fig. 19 B**).

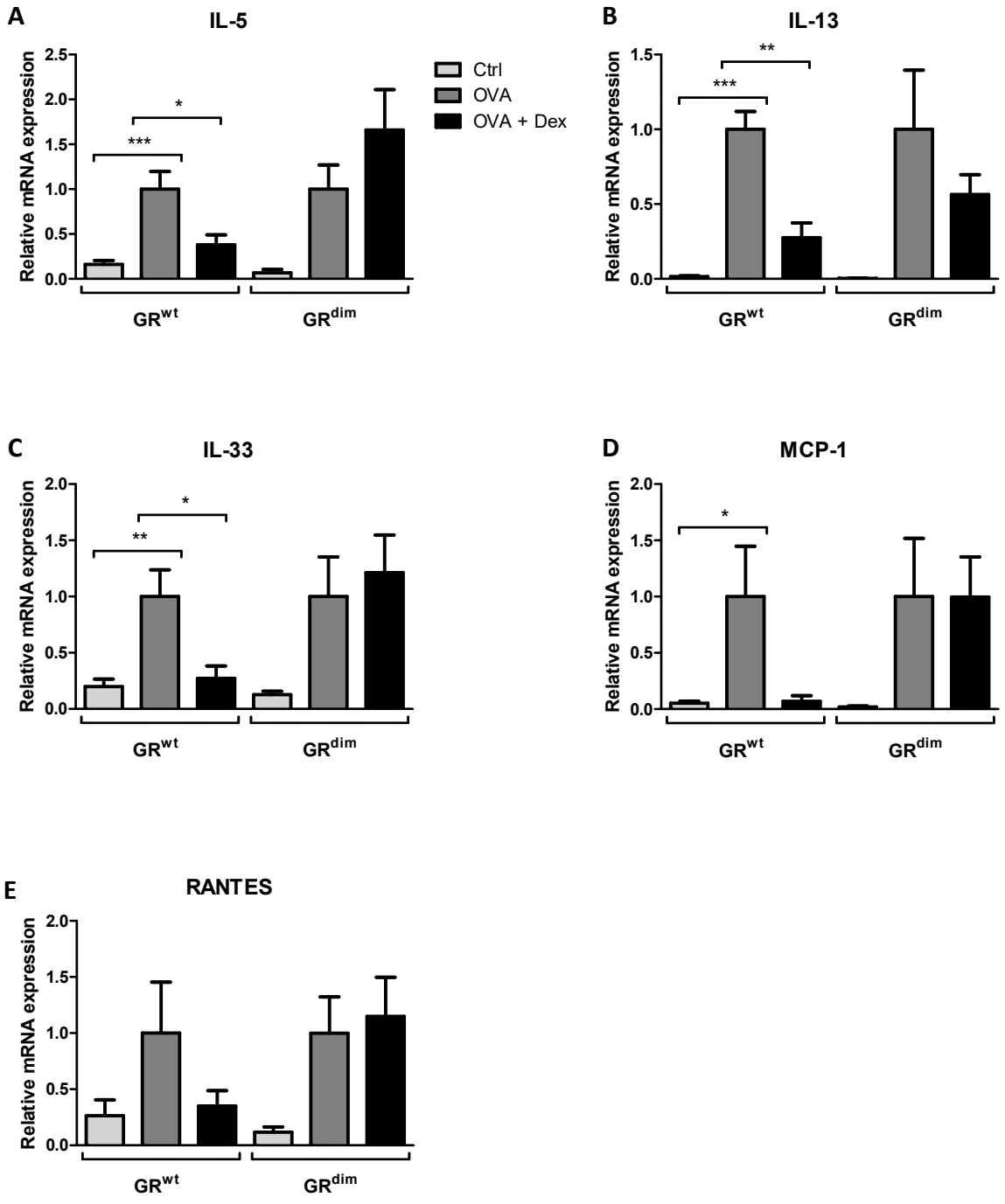

Figure 19: GC-effects on inflammatory gene expression in lungs of GR^{wt} and GR^{dim} mice. AAI was induced by immunization with OVA together with the adjuvant alum, followed by intranasal challenge with the same antigen (OVA). Part of the mice was treated with Dex (OVA + Dex). Control mice received PBS with alum or PBS alone (Ctrl). Lungs were extensively lavaged to remove infiltrating immune cells. RNA was isolated and analyzed by qRT-PCR for expression of IL-5 (A), IL-13 (B), IL-33 (C), MCP-1 (D) and RANTES (E). Relative quantities were normalized with respect to the mRNA expression levels in the OVA-groups of the respective genotype (fold change = 1). HPRT was used as endogenous control. All values are depicted as mean ± SEM (GR^{wt}: n = 4-8; GR^{dim}: n = 3-11; each group). Statistical significances were determined using unpaired, two-tailed t-test (*: $p < 0.05$; **: $p \leq 0.01$;***: $p \leq 0.001$).

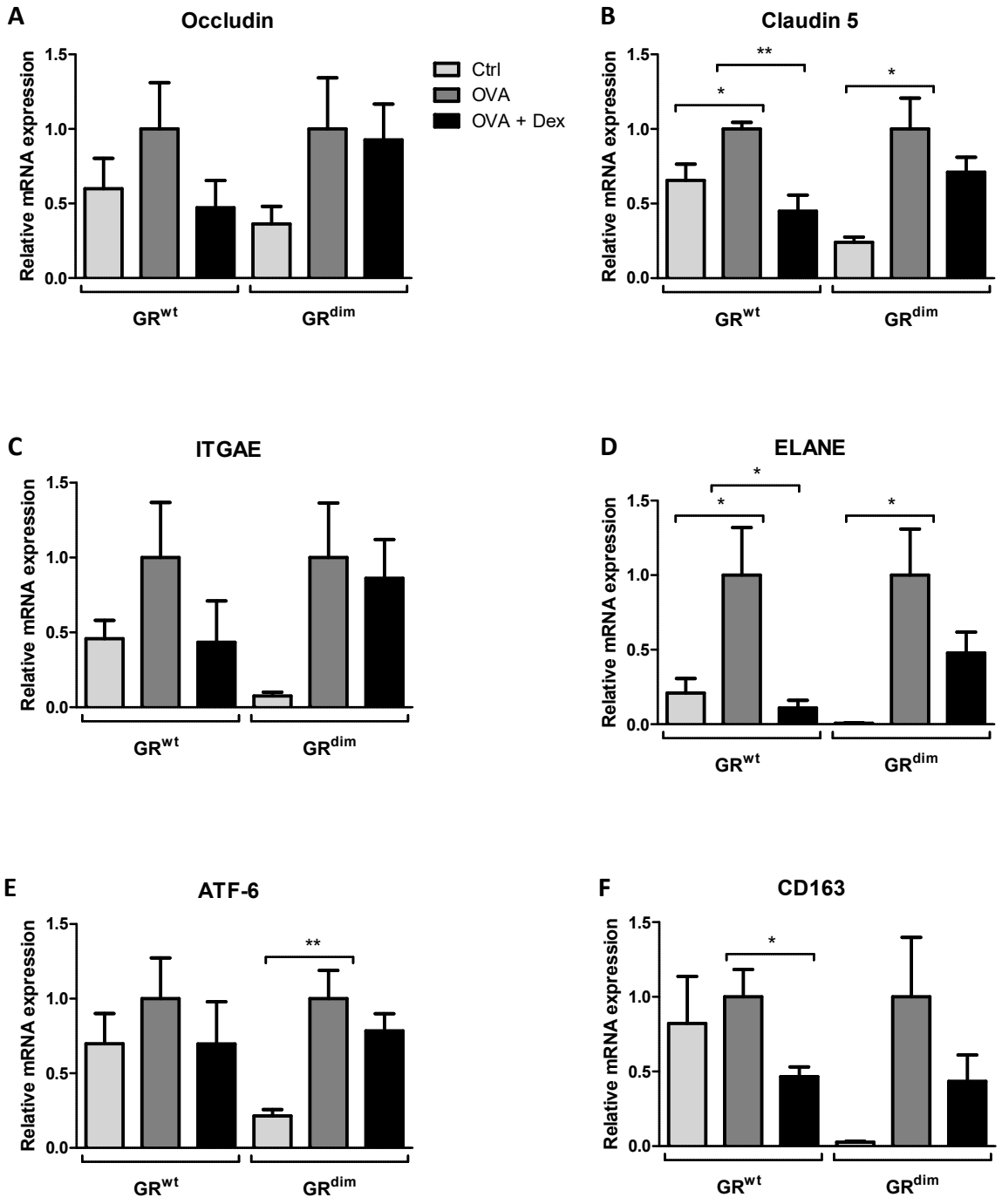

Figure 20: GC-effects on tight junction and candidate gene expression in lungs of GR^{wt} and GR^{dim} mice.

AAI was induced by immunization with OVA together with the adjuvant alum, followed by intranasal challenge with the same antigen (OVA). Part of the mice was treated with Dex (OVA + Dex). Control mice received PBS with alum or PBS alone (Ctrl). Lungs were extensively lavaged to remove infiltrating immune cells. RNA was isolated and analyzed by qRT-PCR for expression of occludin (A), claudin 5 (B), ITGAE (C), ELANE (D), ATF-6 (E) and CD163 (F). Relative quantities were normalized with respect to the mRNA expression levels in the OVA-groups of the respective genotype (fold change = 1). HPRT was used as endogenous control. All values are depicted as mean ± SEM (GR^{wt}: n = 4-8; GR^{dim}: n = 3-11; each group). Statistical significances were determined using unpaired, two-tailed t-test (*: $p < 0.05$; **: $p \leq 0.01$;***: $p \leq 0.001$).

In lung samples of both mouse strains, also increases of occludin, claudin 5, ITGAE, ELANE, ATF-6 and CD163 mRNA expression could be observed after induction of AAI (**fig. 20 A-F**). Dex repressed these genes in lungs of GR^{wt} mice. Although slight decreases of these analyzed genes were observed in the lungs of Dex-treated GR^{dim} mice, this effect was not significant.

Taken together, qRT-PCR analysis using LPCs and lungs from GR^{wt} and GR^{dim} mice revealed differential expression of the analyzed asthma- and AEC-related genes as well as the novel candidate genes. Although statistical significances were not always achieved, clear tendencies were obtained. The findings of differential gene expression correlated with the different transcriptome profiles that had been identified by RNA-seq. The impaired GR-dimerization interface deteriorated the GC-responsiveness in AAI, as Dex-treatment failed to abolish the inflammatory gene expression. These observations were more distinct in LPCs than in lung samples. Thus, GCs mediate their beneficial effects in AAI by the transactivating mechanism that is potentially linked to LPCs and especially to AECs.

4.5 AECs Are Important Targets of GCs in the Treatment of Murine AAI

As mentioned before, previous findings drew the attention to structural cells of the lung as potential GC-targets. Immune cells were found to be dispensable for GC-treatment of AAI. AECs were hypothesized to be important targets because of their crucial functions in the immune responses of the lung. They drive the immune responses by the secretion of a plethora of anti- and pro-inflammatory mediators. This mediates the differentiation and recruitment of various immune cells (Kato and Schleimer, 2007; Schleimer et al., 2007).
Isolation and purification of AECs resulted in a heterogeneous population of LPCs which presumably also include other structural cells of the lung. Transcriptome profiling and subsequent qRT-PCR analysis of LPCs and lungs from GR^{wt} and GR^{dim} mice revealed different expression patterns of inflammatory genes following Dex-treatment of AAI. These effects were found to be more distinct in LPCs than in the whole organ. This highlighted an important link to GC-targets in AECs.

4.5.1 Inducible GR Inactivation in AT-II Cells of GR^{spc} Mice

To specifically analyze the role of AECs in the GC-treatment of AAI, GR^{spc} mice were employed. These mice are GR-deficient specifically in AT-II cells in a temporally defined manner. The tissue specific knock-out was achieved by using an inducible Cre/loxP recombination system. Recombination was induced by application of tamoxifen.

Prior to the induction of AAI, successful ablation of the GR needed to be assessed. Proteins were isolated from homogenized lung samples of wild type (GR^{flox}) and GR^{spc} mice for western blot analysis. On protein level, no differences in GR expression were observed between the lungs of both genotypes (**fig. 21 A**).

In addition, GR mRNA expression levels were determined by qRT-PCR analysis in lung samples of both mouse strains. In comparison to GR^{flox} mice, GR expression was reduced to 86% in the lungs of GR^{spc} mice (**fig. 21 B**). It is estimated that the AT-II cell population represents approximately 15% of the total lung cells (Mason, 2006). Therefore, a reduction in the GR expression of 14% correlates with the number of AT-II cells in the total lung.

Thus, tamoxifen treatment presumably led to a successful knock-out of the GR in AT-II cells of GR^{spc} mice which could be shown on mRNA level, but not on protein level.

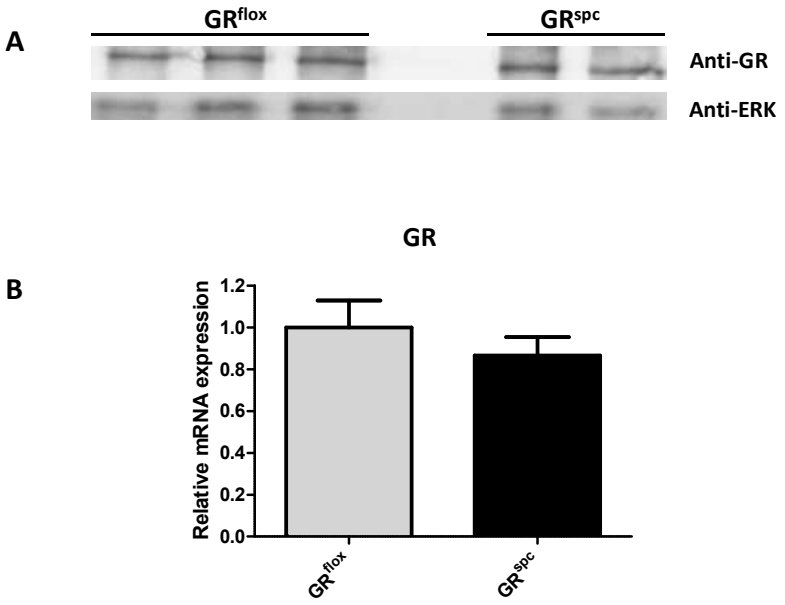

Figure 21: GR expression in lungs of GR^{spc} mice after induction of recombination. GR^{spc} mice are GR-deficient specifically in AT-II cells in a temporally defined manner. The knock-out was achieved by application of tamoxifen. GR protein levels were compared in lung homogenates of GR^{flox} and GR^{spc} mice by western blot analysis. ERK served as loading control (A). GR mRNA expression was analyzed in lung samples of both mouse strains. RNA was isolated from homogenized lungs, reversely transcribed into cDNA and analyzed by qRT-PCR. Relative quantities were normalized with respect to the mRNA expression levels in lungs of GR^{flox} mice (fold change = 1). HPRT was used as endogenous control. All values are depicted as mean ± SEM (GR^{flox}: n = 15; GR^{spc}: n = 14) (B).

4.5.2 AAI Leads to an Increase of OVA-Specific Antibodies in GR^{spc} Mice

AAI was induced in GR^{flox} and GR^{spc} mice by immunization and challenge with OVA with selective Dex-treatment. Prior to and in between the immunization period, mice were treated with tamoxifen for the induction of recombination.

Efficient immunization with OVA was assessed by ELISA. OVA-specific Ig isotype class-switch was tested in serum samples of both genotypes. To this end, IgG1, IgE and IgG2a levels were determined. Irrespective of the genotype, induction of AAI led to significant increases of all Ig isotype levels in serum (**fig. 22 A-C**). In comparison to AAI, additional Dex-treatment did not significantly alter Ig levels in the serum of GR^{flox} and GR^{spc} mice (**fig. 22 A-C**). Thus, elevated levels of IgG1, IgE and IgG2a revealed efficient immunization with OVA in both genotypes.

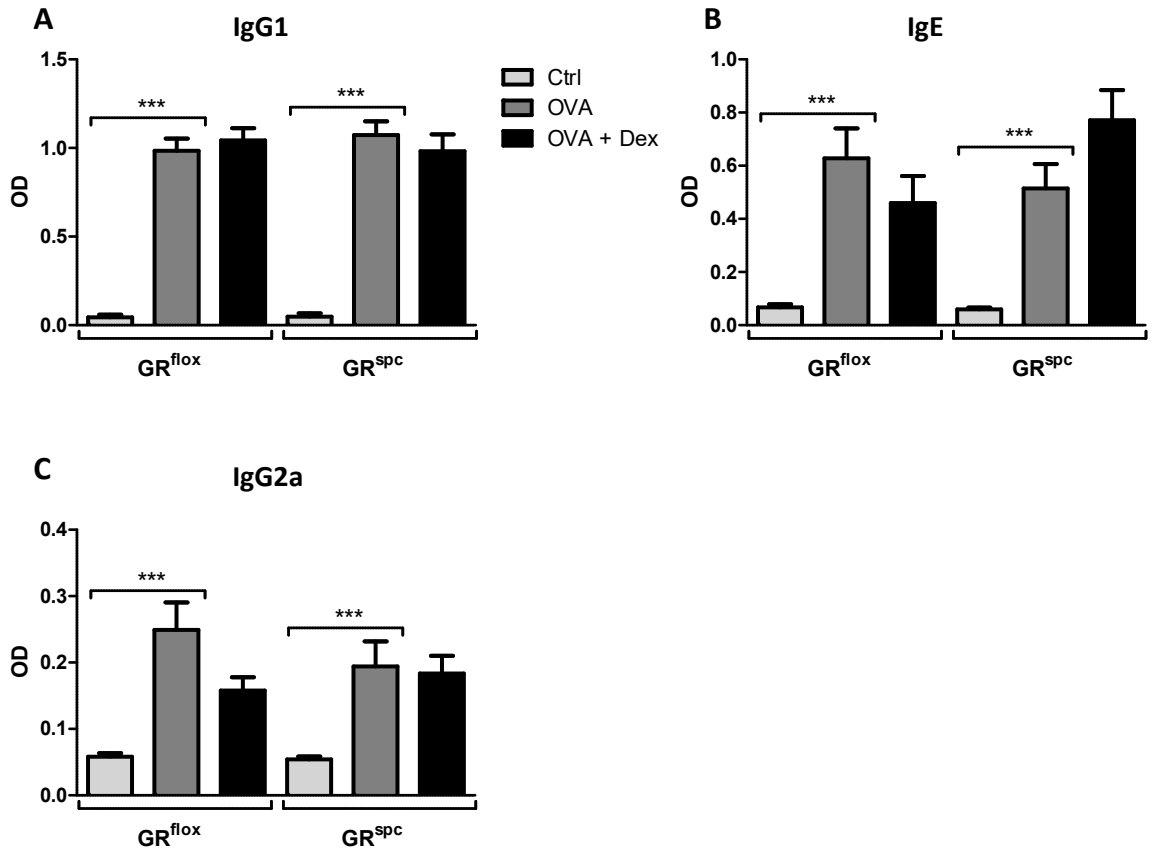

Figure 22: OVA-specific antibody production in GR^{flox} and GR^{spc} mice. For the detection of allergen-induced Ig isotype class-switch IgG1 (A), IgE (B) and IgG2a (C) levels were determined with the respective antibodies by ELISA. Serum samples were taken by cardiac puncture two days after the last allergen challenge step from control groups (Ctrl), OVA-immunized groups (OVA) and additionally Dex-treated groups (OVA + Dex). Ig levels were determined spectrophotometrically and are depicted as optical density (OD). Data are presented as mean values ± SEM (GR^{flox}: IgG1 n = 11-13, IgE n = 10-12 and IgG2a n = 13-15; GR^{spc}: IgG1 n = 12-13, IgE n = 11-12 and IgG2a n = 15; each group). Statistical significances were determined using unpaired, two-tailed t-test (*: $p < 0.05$; **: $p \leq 0.01$;***: $p \leq 0.001$).

4.5.3 Dex Partially Represses Pulmonary Infiltrates in GR^{spc} Mice

Pulmonary infiltrates were analyzed with regard to the impact of the GR knock-out in AT-II cells on the GC-efficacy in AAI. After induction of AAI, lungs were extensively lavaged to obtain infiltrating immune cells. BALF cells were counted and stained with different cell surface markers for flow cytometry.

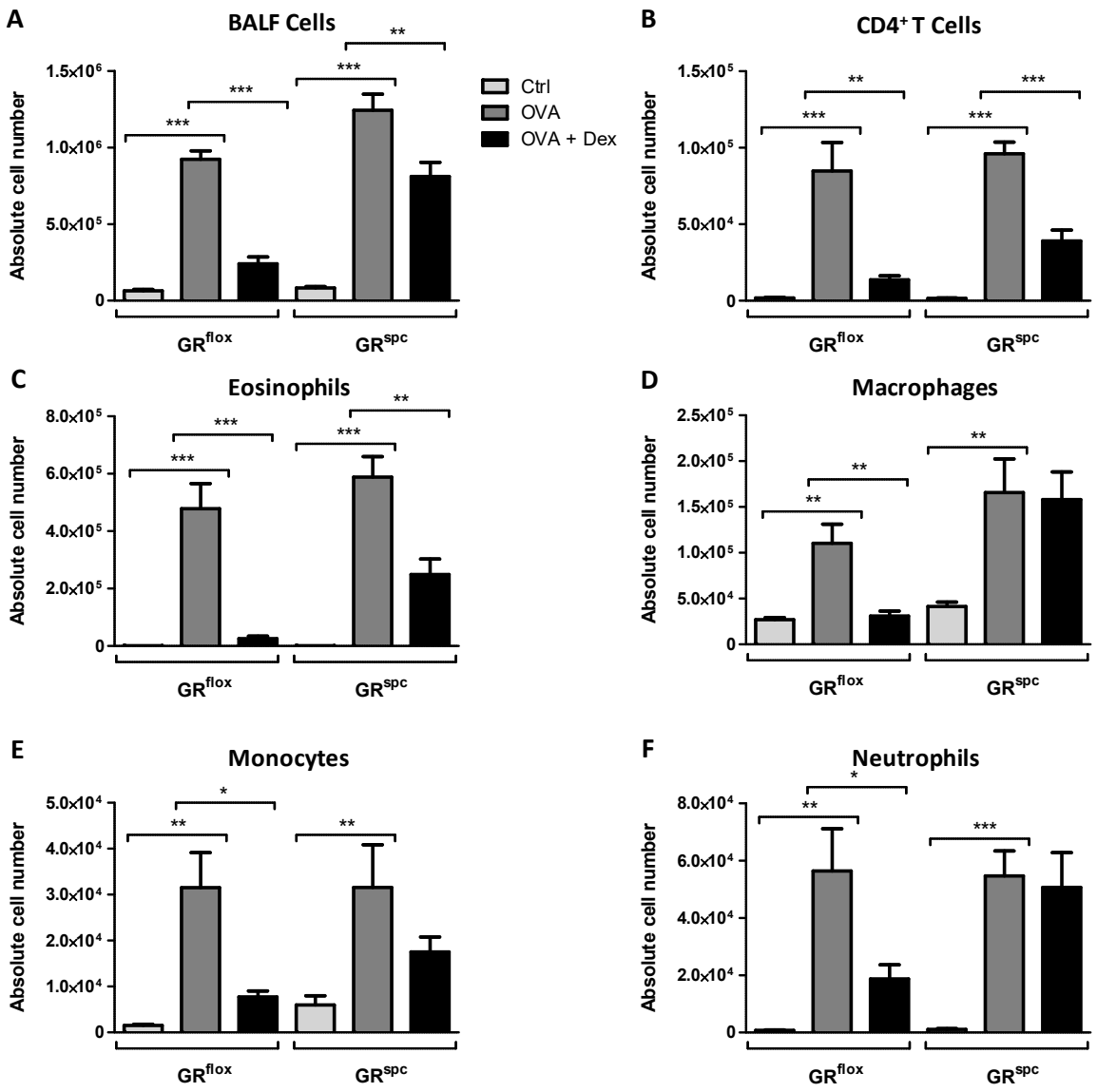

Figure 23: Quantitative analysis of pulmonary infiltrates from GR^{flox} and GR^{spc} mice. Following immunization and challenge with OVA, lungs were extensively lavaged to obtain infiltrating inflammatory cells. BALF samples were taken from control groups (Ctrl), OVA-immunized groups (OVA) and additionally Dex-treated groups (OVA + Dex). Absolute cell numbers were determined for total BALF cells (A), $CD4^+$ T cells (B), eosinophils (C), macrophages (D), monocytes (E) and neutrophils (F). BALF cells were stained with respective cell surface markers and analyzed by flow cytometry. Data are presented as mean values ± SEM (GR^{flox}: n = 7-13; GR^{spc}: n = 10-14; each group). Statistical significances were determined using unpaired, two-tailed t-test (*: $p < 0.05$; **: $p \leq 0.01$;***: $p \leq 0.001$).

Induction of AAI resulted in significant increases of inflammatory cells in the airways of GR^{flox} and GR^{spc} mice (**fig. 23 A**). The inflammatory cell influx was dominated by eosinophils. Elevated numbers of $CD4^+$ T cells, macrophages, monocytes and neutrophils contributed to this increase (**fig. 23 B-F**). Additional Dex-treatment in GR^{flox} mice led to a significant reduction of absolute BALF cell numbers (**fig. 23 A**). Eosinophilia was significantly repressed along with reduced numbers of $CD4^+$ T cells, macrophages, monocytes and neutrophils (**fig. 23 B-F**).

Decreased numbers of infiltrating cells could be observed in the airways of GR^{spc} mice following GC-treatment (**fig. 23 A**). Although numbers of eosinophils, $CD4^+$ T cells and monocytes were reduced, AAI could not completely be abolished (**fig. 23 B, C and E**). Despite reduced eosinophil numbers, eosinophilia was still present in the airways of mutant mice as 30% of all BALF cells were still eosinophils (*data not shown*). In addition, macrophage and neutrophil cell numbers remained unaltered (**fig. 23 D and F**).

Thus, GC-treatment was not able to completely abolish the AAI in GR^{spc} mice highlighting AT-II cells as potential GC-targets.

4.5.4 Dex Cannot Completely Reverse Airway Remodeling in GR^{spc} Mice

Furthermore, histological analysis of lung tissue from GR^{flox} and GR^{spc} mice was performed to visualize airway remodeling. Lungs were isolated following induction of AAI and Dex-treatment, embedded in paraffin and sections were stained with H & E for microscopical analysis.

In contrast to control animals, AAI led to a massive influx of inflammatory cells in the alveolar compartment of both mouse strains which correlated to the flow cytometry data. AAI also induced airway remodeling which was revealed by bronchoconstriction. Mucus hypersecretion and goblet cell hyperplasia were associated with the constricted bronchioles (**fig. 24 A and B**). Dex-treatment completely reversed these structural changes in the airways of GR^{flox} mice (**fig. 24 A**). At the same time, treatment was not able to completely clear the inflammation in the airways of GR^{spc} mice. Numbers of infiltrating cells were slightly reduced in the alveolar compartment and bronchioles were still constricted (**fig. 24 B**).

Thus, Dex was not able to completely reverse airway remodeling in lungs of GR^{spc} mice.

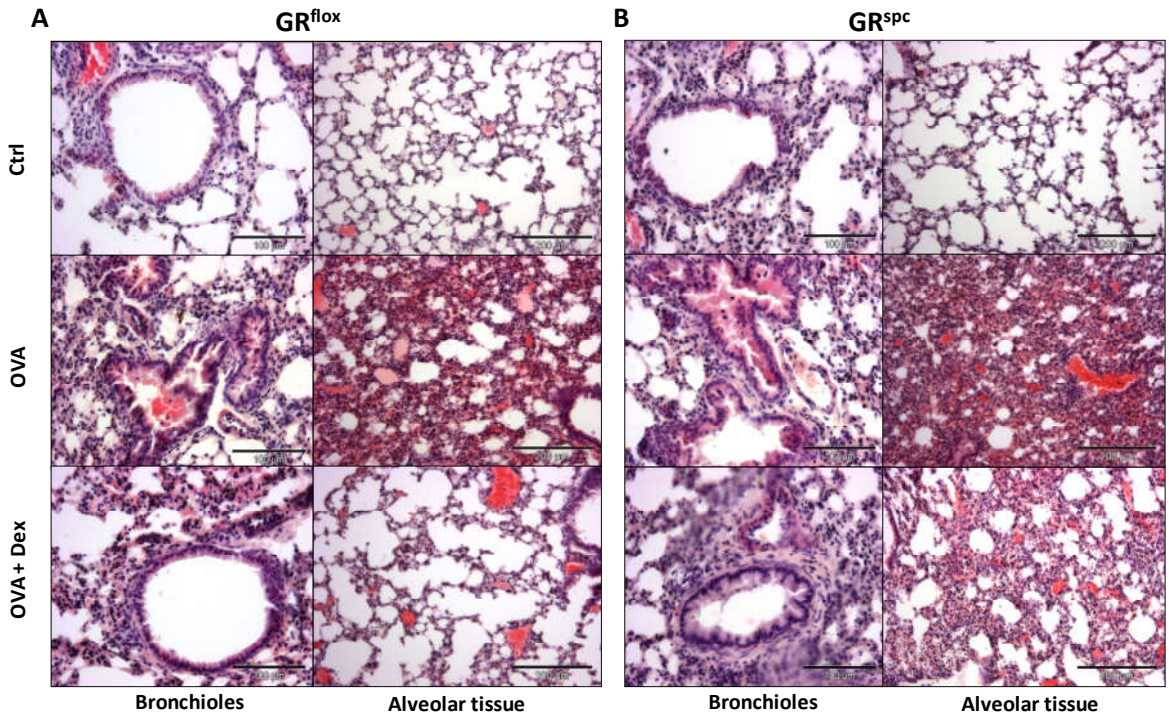

Figure 24: Histological analysis of lung tissue from GR^{flox} and GR^{spc} mice. Following induction of AAI, lungs were taken from control groups (Ctrl), OVA-immunized groups (OVA) and additionally Dex-treated groups (OVA + Dex). Lungs were embedded in paraffin, sectioned and stained with H & E. Structural and cellular changes within the lung were analyzed, in particular in bronchioles and alveolar tissue. Each section is representative for each condition and genotype (GR^{flox}: n = 1-2; GR^{spc}: n = 1-2; each group). The size bars correspond to 100 µm for bronchioles (20 x magnification) and 200 µm for alveolar tissue (10 x magnification).

4.5.5 Inflammatory Gene Expression in LPCs of GR^{spc} Mice Is Partially Repressed by Dex

To further analyze the role of AT-II cells in the GC-treatment of AAI, qRT-PCR was performed with LPC samples from GR^{flox} and GR^{spc} mice. Following induction of AAI with subsequent Dex-treatment, LPCs were isolated from lung tissue by enzymatic digestion and removal of leukocytes by MACS. T_H2-specific cytokines IL-5 and IL-13 were analyzed together with IL-33, MCP-1 and RANTES that are secreted by AECs. In addition, tight junction proteins occludin and claudin 5, as well as the novel candidate genes ITGAE, ELANE, ATF-6 and CD163 were analyzed.

AAI induced increased mRNA expression levels of IL-5, IL-13, IL-33, MCP-1 and RANTES in LPC samples of GR^{flox} and GR^{spc} mice (**fig. 25 A-E**). Dex-treatment reversed these increased expression levels in GR^{flox} mice (**fig. 25 A-E**). In mutant mice, an enhancement of the increased mRNA expression could be observed for IL-5, IL-13 and MCP-1 after treatment with Dex (**fig. 25 A, B and D**). Levels of IL-33 and RANTES were slightly decreased although this was not significant (**fig. 25 C and E**).

Upon AAI induction, elevated expression levels were also found for occludin, claudin 5, ITGAE, ELANE, ATF-6 and CD163 in LPCs of both genotypes (**fig. 26 A-F**). Levels of occludin, ITGAE, ELANE and ATF-6 were found to be markedly reduced in LPCs of GR^{flox} mice following GC-treatment (**fig. 26 A, C, D and E**). A reduction of mRNA expression levels for the same genes could be observed in GR^{spc} mice. Noteworthy, the reduction of occludin, ITGAE, ELANE and ATF-6 expression was not as strong as in GR^{flox} mice (**fig. 26 A, C, D and E**). In both genotypes, no effect on CD163 and claudin 5 expression were found after Dex-treatment (**fig. 26 B and F**).

Thus, Dex-treatment could not completely repress the AAI-induced inflammatory gene expression in LPC samples of GR^{spc} mice.

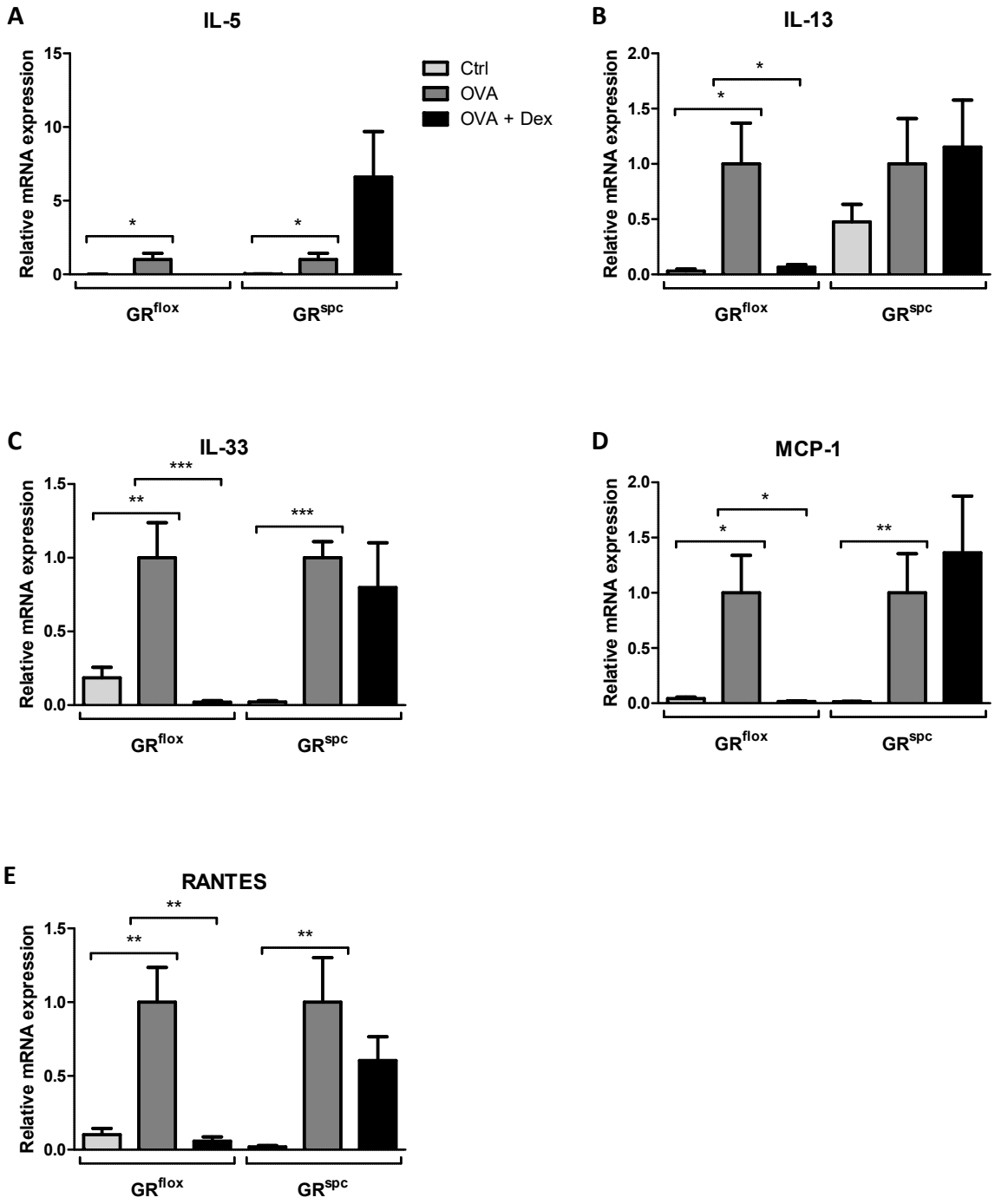

Figure 25: GC-effects on inflammatory gene expression in LPCs of GR^{flox} and GR^{spc} mice. AAI was induced by immunization with OVA together with the adjuvant alum, followed by intranasal challenge with the same antigen (OVA). Part of the mice was treated with Dex (OVA + Dex). Control mice received PBS with alum or PBS alone (Ctrl). LPCs were isolated by enzymatic digestion of lung tissue with dispase and subsequent removal of immune cells by MACS. RNA was isolated and analyzed by qRT-PCR for expression of IL-5 (A), IL-13 (B), IL-33 (C), MCP-1 (D) and RANTES (E). Relative quantities were normalized with respect to the mRNA expression levels in the OVA-groups of the respective genotype (fold change = 1). HPRT was used as endogenous control. All values are depicted as mean ± SEM (GR^{flox}: n = 4-8; GR^{spc}: n = 4-9; each group). Statistical significances were determined using unpaired, two-tailed t-test (*: $p < 0.05$; **: $p \leq 0.01$;***: $p \leq 0.001$).

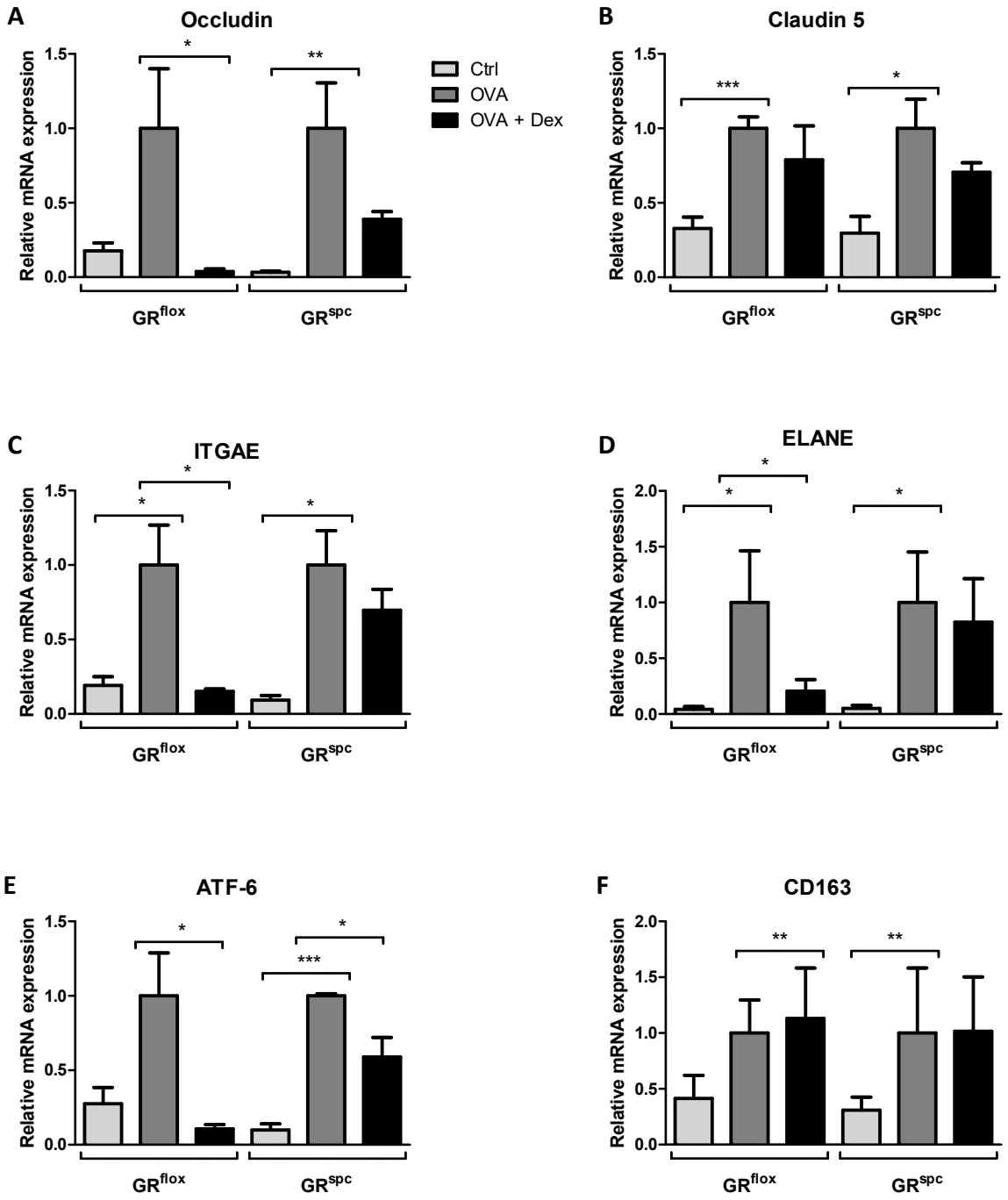

Figure 26: GC-effects on tight junction and candidate gene expression in LPCs of GR^{flox} and GR^{spc} mice.

AAI was induced by immunization with OVA together with the adjuvant alum, followed by intranasal challenge with the same antigen (OVA). Part of the mice was treated with Dex (OVA + Dex). Control mice received PBS with alum or PBS alone (Ctrl). LPCs were isolated by enzymatic digestion of lung tissue with dispase and subsequent removal of immune cells by MACS. RNA was isolated and analyzed by qRT-PCR for expression of occludin (A), claudin 5 (B), ITGAE (C), ELANE (D), ATF-6 (E) and CD163 (F).Relative quantities were normalized with respect to the mRNA expression levels in the OVA-groups of the respective genotype (fold change = 1). HPRT was used as endogenous control. All values are depicted as mean ± SEM (GR^{flox}: n = 4-8; GR^{spc}: n = 4-9; each group). Statistical significances were determined using unpaired, two-tailed t-test (*: $p < 0.05$; **: $p \leq 0.01$;***: $p \leq 0.001$).

4.5.6 Dex-Treatment Cannot Completely Abolish the Inflammatory Gene Expression in the Lungs of GR^{spc} Mice

In addition to LPCs, mRNA expression levels of the same genes were analyzed in the whole organ. RNA was isolated from lungs of both genotypes after induction of AAI and additional Dex-treatment, reversely transcribed into cDNA and processed to qRT-PCR analysis.

In line with the qRT-PCR analysis of LPCs, expression of IL-5, IL-13, IL-33, MCP-1 and RANTES were highly increased in lungs of GR^{flox} and GR^{spc} mice (**fig. 27 A, C, D and E**). This increase could be significantly reduced in the lungs of GR^{flox} mice by Dex-treatment (**fig. 27 A, C, D and E**). IL-5, IL-13 and RANTES levels were slightly reduced in GR^{spc} mice following Dex-treatment whereas this reduction was not significant and not as strong as in GR^{flox} mice (**fig. 27 A, B and E**). Expression of IL-33 was unaltered in comparison to AAI and MCP-1 expression was even enhanced upon Dex-treatment (**fig. 27 C and D**).

Moreover, occludin, claudin 5, ITGAE, ELANE, ATF-6 and CD163 were all significantly increased in lungs of GR^{flox} mice with AAI. This increase could be significantly reversed by additional Dex-treatment (**fig. 28 A-F**). In the lungs of mutant mice, occludin, ITGAE, ELANE, ATF-6 and CD163 expression levels were also found to be strongly increased in AAI (**fig. 28 A, C, D, E and F**). Upon Dex-treatment, mRNA expression of occludin and ITGAE was slightly decreased in lungs of GR^{spc} mice but this effect was not significant (**fig. 28 A and C**). In contrast, a slight enhancement of elevated ELANE and ATF-6 expression were found (**fig. 28 D and E**). Dex did not have any impact on CD163 mRNA expression (**fig. 28 F**). No clear alterations were found for the claudin 5 expression in the lungs of GR^{spc} mice (**fig. 28 B**).

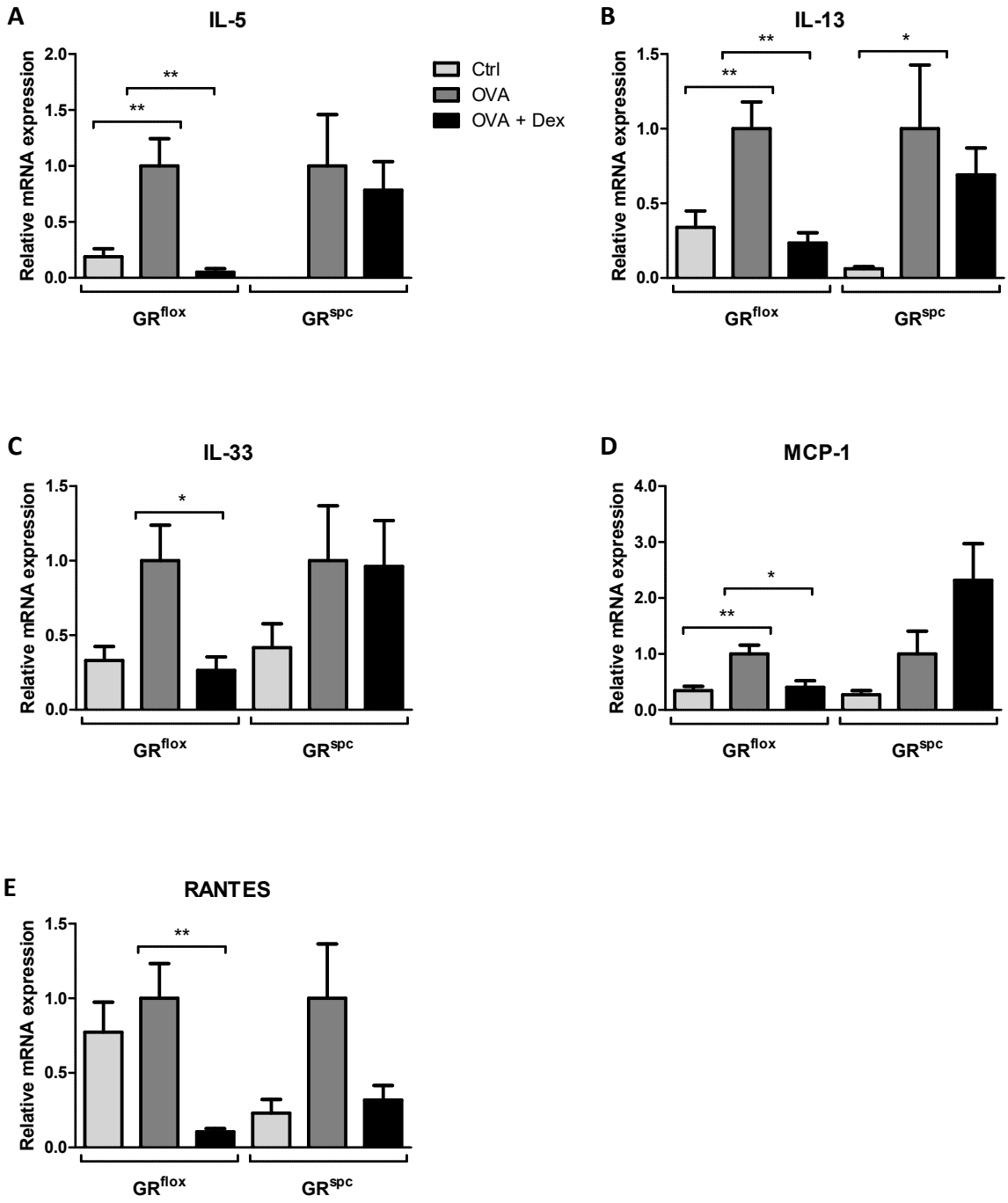

Figure 27: GC-effects on inflammatory gene expression in lungs of GR^{flox} and GR^{spc} mice. AAI was induced by immunization with OVA together with the adjuvant alum, followed by intranasal challenge with the same antigen (OVA). Part of the mice was treated with Dex (OVA + Dex). Control mice received PBS with alum or PBS alone (Ctrl). Lungs were extensively lavaged to remove infiltrating immune cells. RNA was isolated and analyzed by qRT-PCR for expression of IL-5 (A), IL-13 (B), IL-33 (C), MCP-1 (D) and RANTES (E). Relative quantities were normalized with respect to the mRNA expression levels in the OVA-groups of the respective genotype (fold change = 1). HPRT was used as endogenous control. All values are depicted as mean ± SEM (GR^{flox}: n = 4-11; GR^{spc}: n = 5-13; each group). Statistical significances were determined using unpaired, two-tailed t-test (*: $p < 0.05$; **: $p \leq 0.01$;***: $p \leq 0.001$).

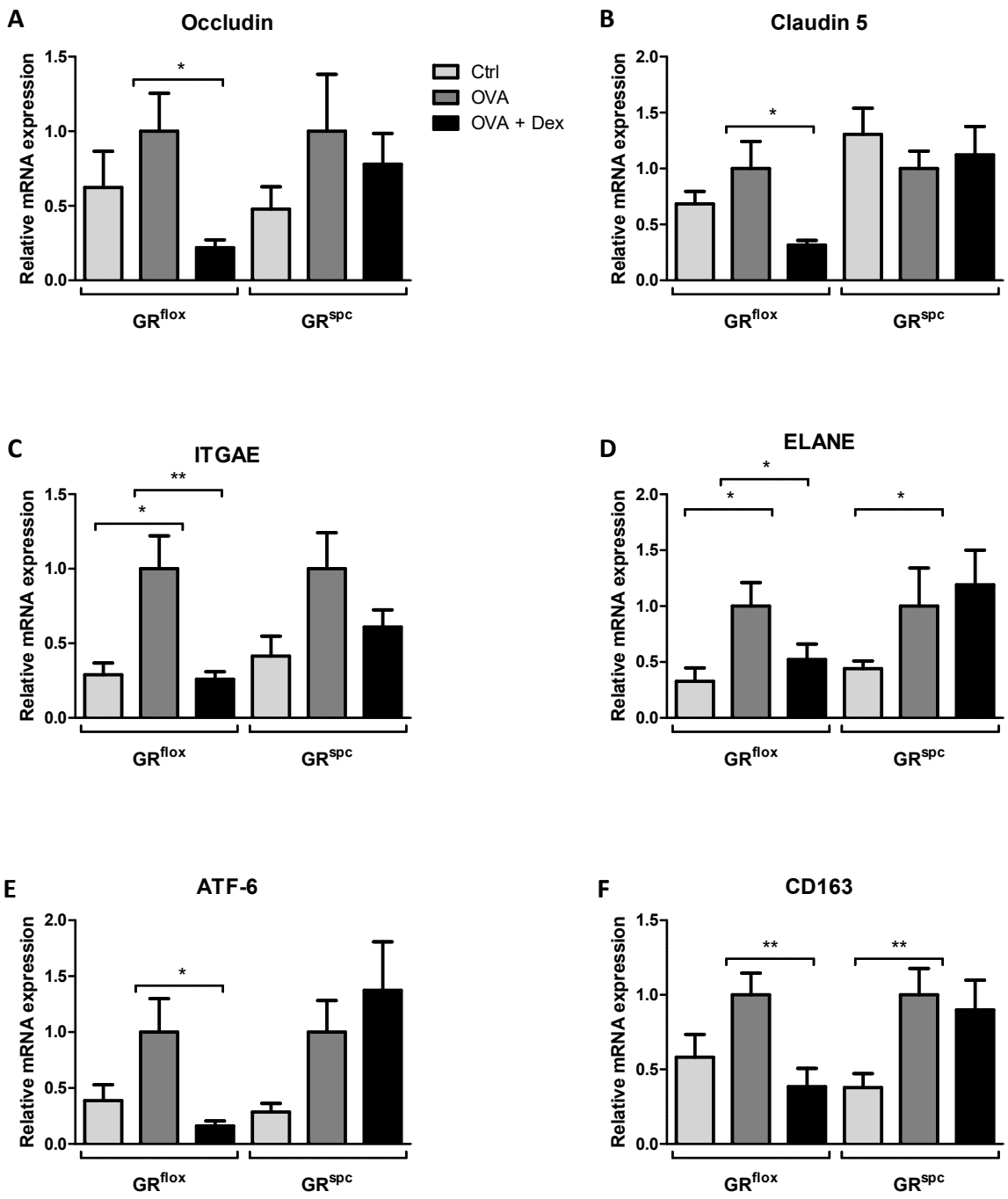

Figure 28: GC-effects on tight junction and candidate gene expression in lungs of GR^{flox} and GR^{spc} mice.

AAI was induced by immunization with OVA together with the adjuvant alum, followed by intranasal challenge with the same antigen (OVA). Part of the mice was treated with Dex (OVA + Dex). Control mice received PBS with alum or PBS alone (Ctrl). Lungs were extensively lavaged to remove infiltrating immune cells. RNA was isolated and analyzed by qRT-PCR for expression of occludin (A), claudin 5 (B), ITGAE (C), ELANE (D), ATF-6 (E) and CD163 (F). Relative quantities were normalized with respect to the mRNA expression levels in the OVA-groups of the respective genotype (fold change = 1). HPRT was used as endogenous control. All values are depicted as mean ± SEM (GR^{flox}: n = 4-11; GR^{spc}: n = 5-13; each group). Statistical significances were determined using unpaired, two-tailed t-test (*: $p < 0.05$; **: $p \leq 0.01$;***: $p \leq 0.001$).

Inflammatory gene expression analysis with qRT-PCR in LPC and lung samples of GR^{spc} mice revealed that the allergic inflammation could not be completely abolished by GC-treatment. Nevertheless, Dex did not have any impact on the AAI-induced expression of some analyzed genes or even led to an enhancement of mRNA expression of other analyzed genes.

Taken together, GC-treatment of AAI in GR^{spc} mice was not able to completely clear the inflammatory responses in the airways. However, AT-II cells were shown to be important targets for the GC-efficacy in AAI. Hence, AT-II cells might not seem to be the only GC-targets as other structural cells of the lung endothelial cells or airway smooth muscle cells might serve as target as well. Differential expression of the analyzed genes correlated to the GR^{dim} findings providing a link between GC mechanism and target site.

4.6 AECs Do Not Mediate the GC-Efficacy in ALI

AECs and in particular AT-II cells could be identified as important targets for the GC-treatment of murine AAI. As GCs have also been used in the treatment of ALI, AECs could be important targets in this disease as well. To analyze the role of AT-II cells as potential GC-targets, ALI was induced in GR^{flox} and GR^{spc} mice. To this end, mice were injected i.p. with LPS to induce a systemic inflammatory response. Along with LPS, mice were additionally injected i.v. with OA that specifically triggers lung injury. Part of the mice was also treated with Dex by i.p. injections representing systemic GC-treatment.

4.6.1 Pulmonary Infiltrates Are Reduced in the Lungs of GR^{spc} Mice by Dex-Treatment of ALI

Pulmonary infiltrates from GR^{flox} and GR^{spc} mice were analyzed by flow cytometry to evaluate the GC-efficacy in murine ALI. After induction of ALI, BALF cells were obtained by extensively lavaging the lung. Cell numbers were determined and BALF cells were stained with distinct cell surface markers for flow cytometric analysis.

In both mouse strains, elevated numbers of inflammatory cells were found after induction of AAI (**fig. 29 A**). This increased influx was dominated by neutrophils and also macrophages to a minor degree which is characteristic for ALI (**fig. 29 D and F**). Moreover, numbers of $CD4^+$ T cells, $CD8^+$ T cells, monocytes and eosinophils were markedly increased (**fig. 29 B, C, E and G**). Dex-treatment repressed this increase of inflammatory cells in the airways of GR^{flox} mice and also in GR^{spc} mice (**fig. 29 A**). Numbers of all analyzed cell types were strongly reduced to a similar extent in both mouse strains (**fig. 29 B-G**).

Thus, GC-treatment with Dex effectively repressed the inflammatory cell influx in the airways of GR^{spc} mice as similar to GR^{wt} mice.

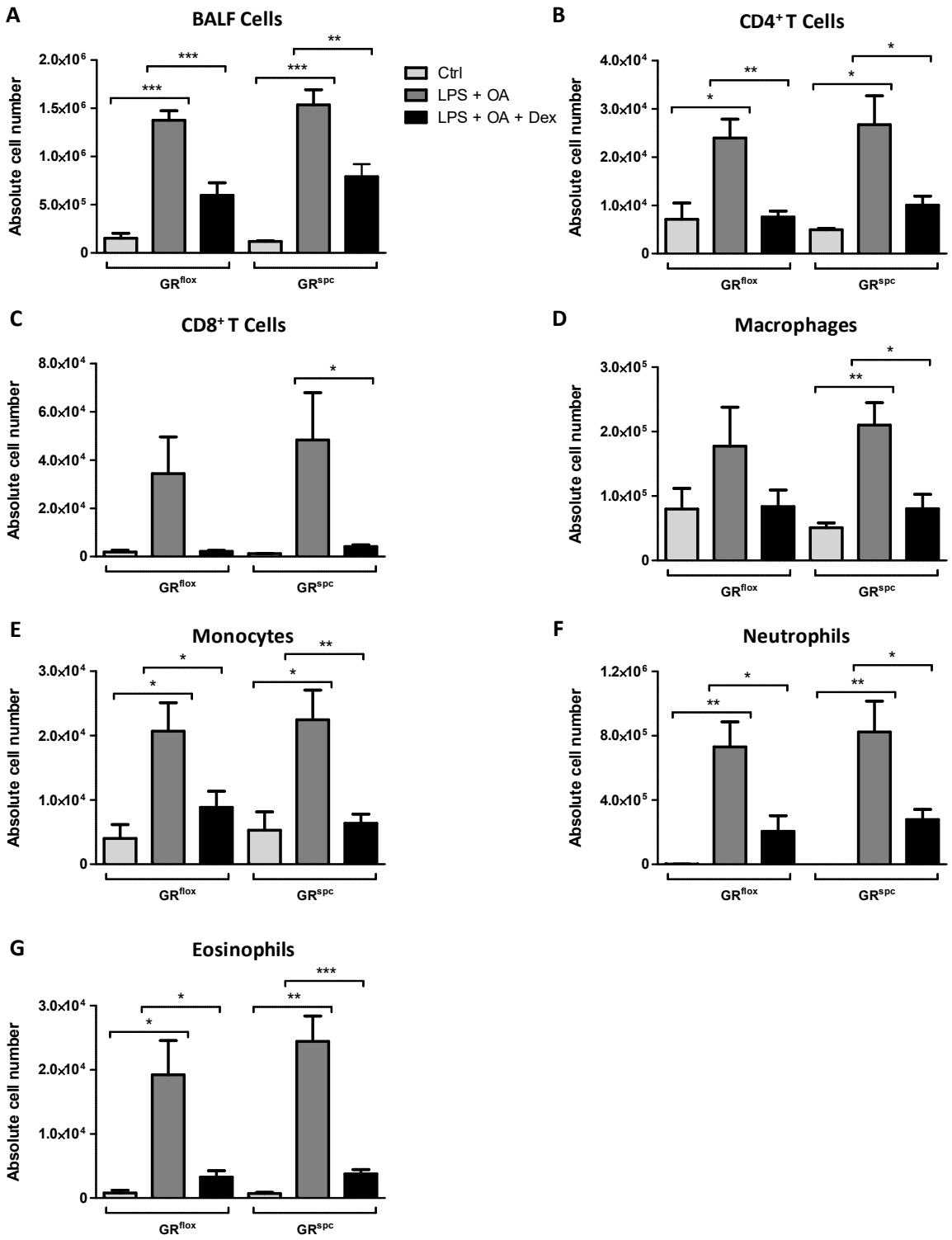

Figure 29: Quantitative analysis of pulmonary infiltrates from GR^{flox} and GR^{spc} mice with ALI. Following induction of ALI with LPS and OA, lungs were extensively lavaged to remove infiltrating inflammatory cells. BALF samples were taken from control groups (Ctrl), LPS- and OA-treated groups (LPS + OA) and additionally Dex-treated groups (LPS + OA + Dex). Absolute cell numbers were determined for total BALF cells (A), CD4$^+$ T cells (B), CD8$^+$ T cells (C), macrophages (D), monocytes (E), neutrophils (F) and eosinophils (G). BALF cells were stained with respective cell surface markers and analyzed by flow cytometry. Data are presented as mean values ± SEM (GR^{flox}: n = 5-8; GR^{spc}: n = 4-8; each group). Statistical significances were determined using unpaired, two-tailed t-test (*: $p < 0.05$; **: $p \leq 0.01$;***: $p \leq 0.001$).

4.6.2 GCs Suppress IL-6 Levels in Serum of GR^{spc} Mice

Furthermore, IL-6 levels were determined in serum of GR^{flox} and GR^{spc} mice following induction of ALI and subsequent Dex-treatment. IL-6 is a pro-inflammatory cytokine that is mainly secreted by alveolar macrophages in response to lung injury (Johnson and Matthay, 2010).

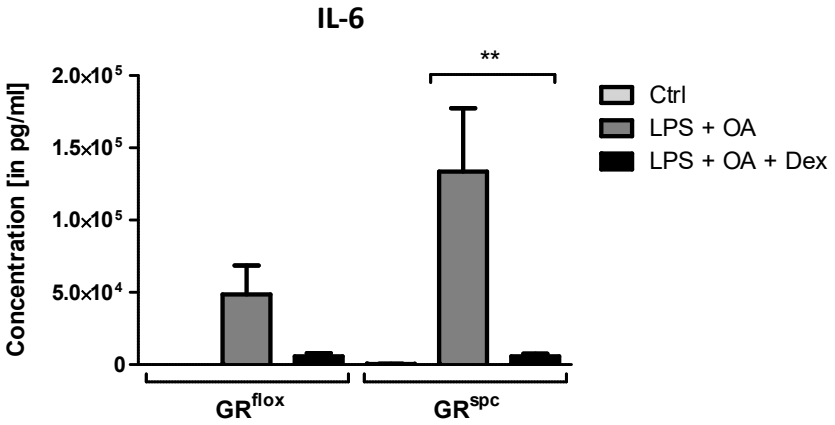

Figure 30: IL-6 levels in serum of GR^{flox} and GR^{spc} mice. Concentrations of IL-6 were determined by ELISA with respective antibodies. Serum samples were taken by cardiac puncture 15 hours after the induction of ALI from control groups (Ctrl), LPS- and OA-treated groups (LPS + OA) and additionally Dex-treated groups (LPS + OA + Dex). IL-6 concentrations were determined spectrophotometrically and are depicted as pg/ml. Data are presented as mean values ± SEM (GR^{flox}: n = 6-9; GR^{spc}: n = 6-10). Statistical significances were determined using unpaired, two-tailed t-test (*: $p < 0.05$; **: $p \leq 0.01$;***: $p \leq 0.001$).

Induction of ALI resulted in elevated IL-6 levels in serum of both genotypes (**fig. 30**). These elevated levels were reduced by Dex-treatment in GR^{flox} mice. In GR^{spc} mice, Dex led to a significant decrease of the IL-6 concentration in serum (**fig. 30**).
Thus, GC-treatment effectively suppressed IL-6 levels in serum samples of both mouse strains.

4.6.3 Dex Reduces Leukocyte Infiltration in the Alveolar Tissue of GR^{spc} Mice

Histological analysis of alveolar tissue was performed to visualize the inflammatory responses in the injured airways. In contrast to healthy lungs, AAI resulted in a strong influx of inflammatory cells in the alveolar tissue of GR^{flox} and GR^{spc} mice (**fig. 31 A and B**).

Dex-treatment abolished this influx as the alveolar compartment was comparable to that of control groups. This beneficial effect was the same in both genotypes (**fig. 31 A and B**). Thus, Dex was able to reduce the leukocyte infiltration in the alveolar tissue of GR^{spc} mice as effective as in GR^{wt} mice.

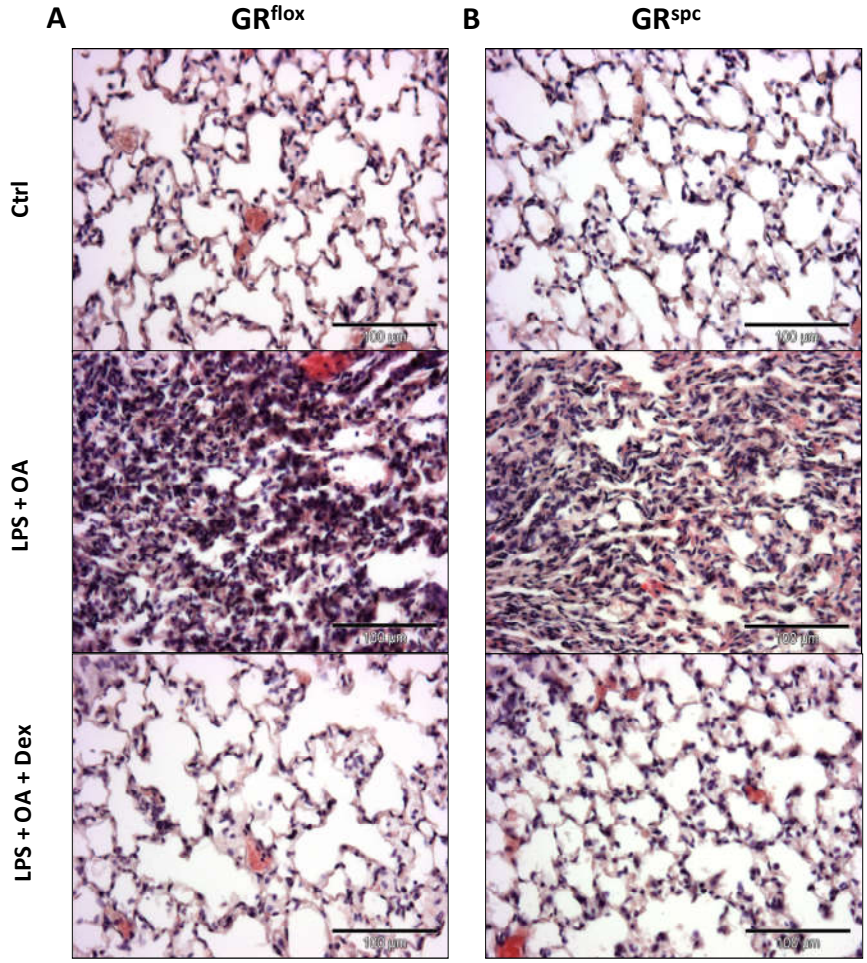

Figure 31: Histological analysis of alveolar tissue from GR^{flox} and GR^{spc} mice. Following induction of ALI, lungs were taken from control groups (Ctrl), LPS- and OA-treated groups (LPS + OA) and additionally Dex-treated groups (LPS + OA + Dex). Lungs were embedded in paraffin, sectioned and stained with H & E. Structural and cellular changes within the lung were analyzed in the alveolar compartment. Each section is representative for each condition and genotype (GR^{flox}: n = 2; GR^{spc}: n = 2; each group). The size bars correspond to 100 µm (20 x magnification).

4.6.4 GR-Deletion in AT-II Cells Does Not Affect the GR-Dependent Gene Regulation in the Treatment of ALI

In addition, qRT-PCR analysis was performed with lung samples from GR^{flox} and GR^{spc} mice. After induction of AAI, lungs were homogenized for RNA isolation and analyzed for

inflammatory gene expression by qRT-PCR. IL-1β, MCP-1 and iNOS are all pro-inflammatory molecules which are expressed by inflammatory cells in response to ALI. Enhanced expression of these molecules is associated with the pathogenesis of ALI (Butt et al., 2016; Johnson and Matthay, 2010).

As expected, all analyzed genes showed increased mRNA expression levels after treatment with LPS and OA in both mouse strains (**fig. 32 A-C**). Increased inflammatory gene expression was efficiently suppressed by Dex-treatment to the same extent in GR^{flox} and GR^{spc} mice. All analyzed genes showed reduced mRNA expression levels (**fig. 32 A-C**). Thus, the GR-deletion in AT-II cells had no influence on the GR-dependent gene regulation in the treatment of ALI as the expression of the analyzed genes was effectively repressed by Dex-treatment.

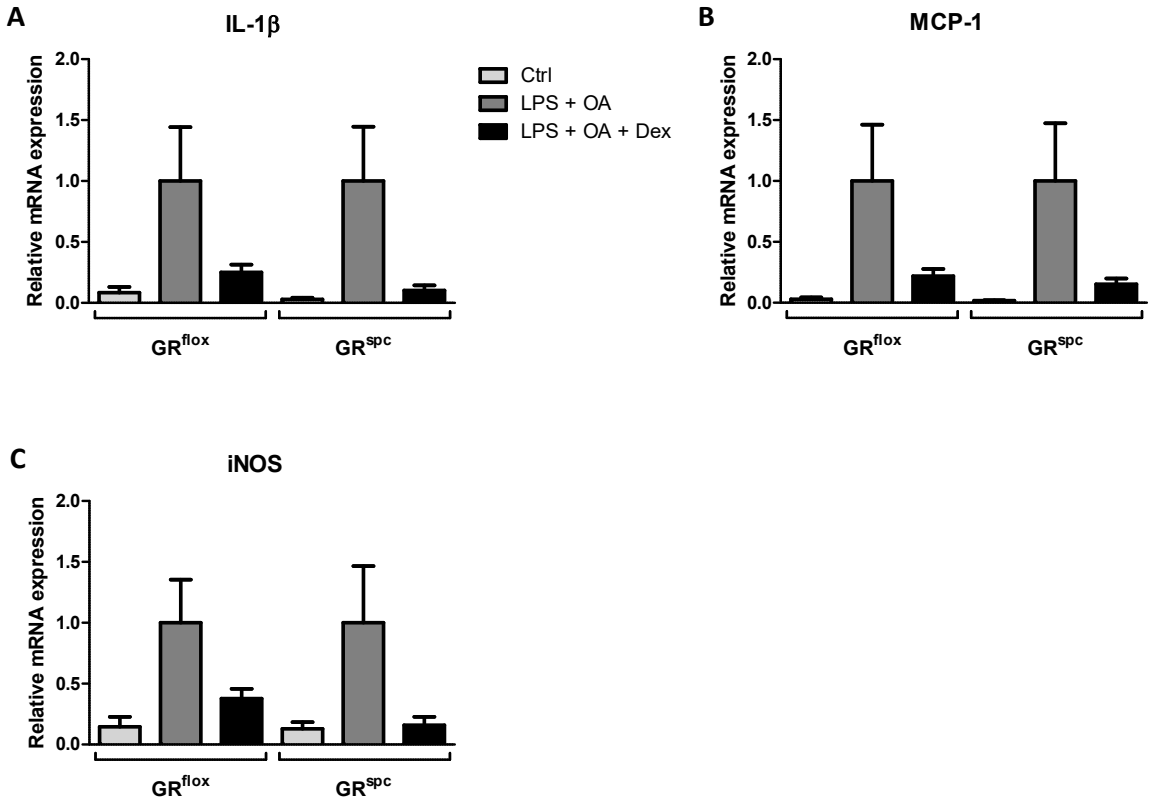

Figure 32: GC-effects on ALI-induced inflammatory gene expression in lungs of GR^{flox} and GR^{spc} mice.

ALI was induced by combined treatment of LPS and OA (LPS + OA). Part of the mice was treated with Dex (LPS + OA + Dex). Control mice received PBS alone (Ctrl). Lungs were extensively lavaged to remove infiltrating immune cells. RNA was isolated and analyzed by qRT-PCR for expression of IL-1β (A), MCP-1 (B) and iNOS (C). Relative quantities were normalized with respect to the mRNA expression levels in the ALI groups of the respective genotype (fold change = 1). HPRT was used as endogenous control. All values are depicted as mean ± SEM (GR^{flox}: n = 4-8; GR^{spc}: n = 3-8; each group). Statistical significances were determined using unpaired, two-tailed t-test (*: $p < 0.05$; **: $p \leq 0.01$;***: $p \leq 0.001$).

Taken together, GR^{spc} mice completely responded to GC-treatment of ALI. In contrast to AAI, AT-II cells are not required for effective GC-treatment of ALI.

4.7 Targeted Delivery of GCs in Inflammatory Lung Diseases Using Inorganic-Organic Hybrid Nanoparticles

In recent years, nanoparticles have been of major interest because they can easily serve for the diagnosis and treatment of various diseases. As carrier for different drugs, nanoparticles allow target site-directed drug delivery. This novel therapeutic system can potentially prevent the development of severe side effects that develop after systemic and also topic administration of drugs. These side effects are also a limiting factor for the use of GCs in the treatment of various inflammatory disorders like asthma. Recently developed betamethasone nanoparticles (BNPs) have been shown to suppress the production of pro-inflammatory cytokines (Heck et al., 2015). These inorganic-organic hybrid nanoparticles have been synthesized by precipitating cationic zirconiumoxide together with the anionic GC betamethasonephosphate (BMP) and the fluorescent dye flavinmononucleotide (FMN) in aqueous solution (Heck et al., 2015; Roming et al., 2010). These BNPs have a hydrodynamic diameter of 30-40 nm and show green fluorescence (Heck et al., 2015). Studies with a murine model of multiple sclerosis revealed the efficacy of BNPs, which were as potent as systemic GCs in improving disease symptoms and suppressing inflammation (unpublished data).

4.7.1 BNPs-SPC Are Not Effective in the Treatment of AAI

AT-II cells have been shown to be important targets in the GC-treatment of murine AAI. To specifically deliver BNPs to AT-II cells, nanoparticles were conjugated with an anti-SPC antibody; designated as BNPs-SPC (collaboration with Prof. Dr. Claus Feldmann, Karlsruhe Institute of Technology). AAI was induced in wild type mice by immunization and challenge with OVA. Mice were treated with Dex systemically by i.p. injections. BNPs and BNPs-SPC (20 µl of 4.4 µmol/ml) were applied topically by intranasal instillation following allergen challenge. Pulmonary infiltrates were analyzed by flow cytometry to evaluate the BNP-SPC efficacy in the treatment of AAI in comparison to systemic Dex-application. BALF

cell numbers were determined and distinct cell surface markers were used for flow cytometric analysis of inflammatory cells. As observed before, AAI induced a significant increase of inflammatory cells in the allergic airways which could be significantly reduced by Dex-treatment (**fig. 33 A**). In line with this, eosinophilia in the allergic airways was repressed by Dex (**fig. 33 B**). BNPs did not have any impact on the increased BALF cell numbers and eosinophilia (**fig. 33 A and B**). Unfortunately, BNPs-SPC even enhanced the increase in cell numbers which could also be observed for eosinophils (**fig. 33 A and B**).

OVA-specific Ig isotype class-switch was assessed in serum samples by ELISA to prove the immunization efficiency. Immunization with OVA was successful as levels of IgG1 were increased (**fig. 33 C**). Neither Dex, nor BNPs and BNPs-SPC had any impact on the elevated IgG1 levels (**fig. 33 C**).

Thus, BNPs-SPC were not able to suppress AAI as similar to Dex. The same could be observed for BNPs. Targeted delivery of GCs to AT-II cells by using these nanoparticles seemed to have failed.

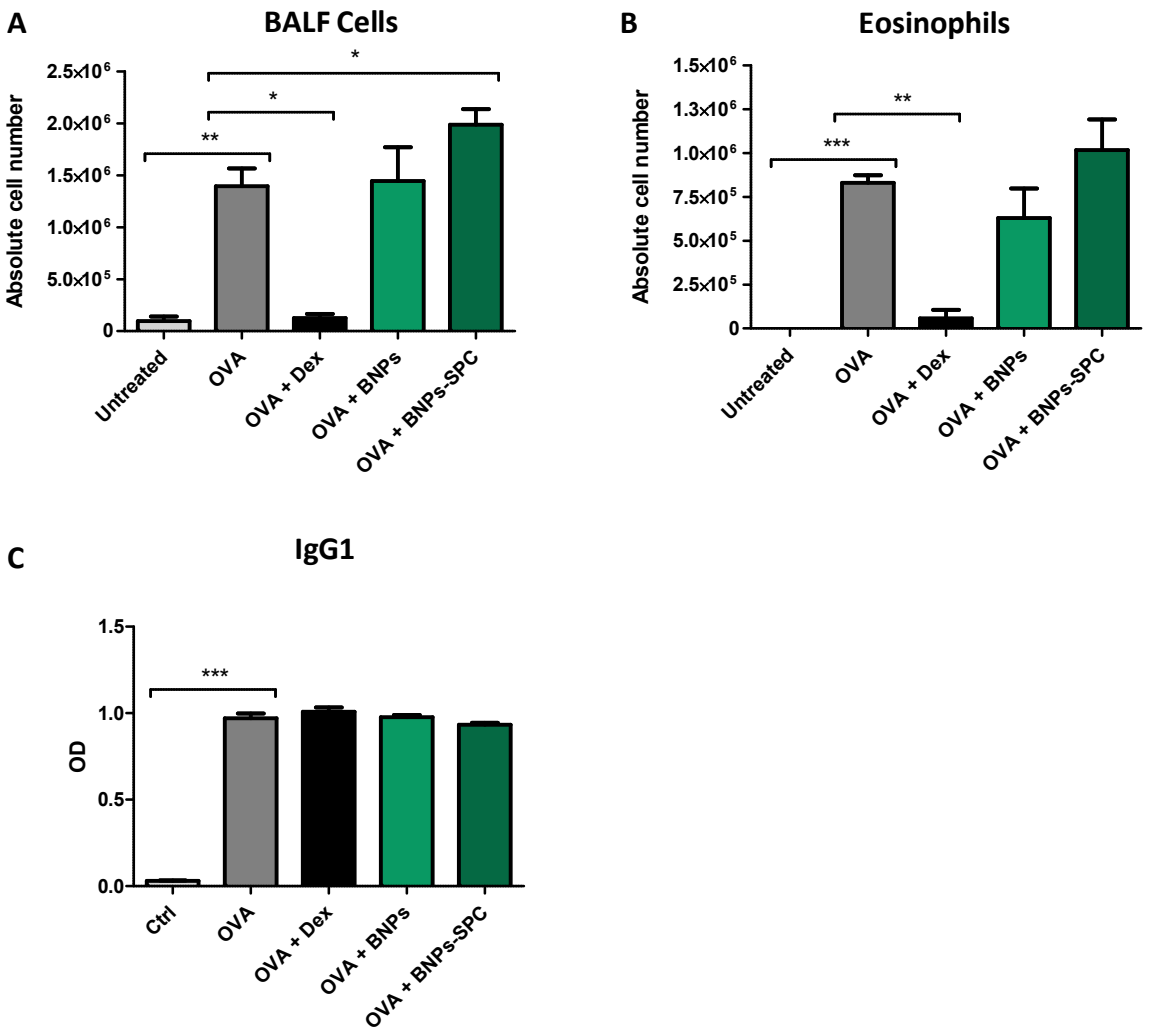

Figure 33: BNPs-SPC in the treatment of AAI. Mice were immunized with OVA and the adjuvant alum which was followed by intranasal challenge with the same antigen to elicit the AAI (OVA). Part of the mice was additionally treated with Dex (OVA + Dex) whereas others were intranasally treated either with BNPs (OVA + BNPs) or with BNPs-SPC (OVA + BNPs-SPC). Control mice were treated with PBS and alum or with PBS alone (Ctrl). BALF-cells were obtained by extensively lavaging the lung to obtain infiltrating cells. Cell numbers were determined and BALF-cells were stained with distinct cell surface markers for flow cytometric analysis. Absolute cell numbers of total BALF cells (A) and eosinophils (B) are shown (n = 2-5; each group). OVA-specific Ig isotype class-switch was determined in serum samples by ELISA with respective antibodies. IgG1 levels were determined spectrophotometrically and are depicted as optical density (OD) (n = 2-5; each group). Data are presented as mean values ± SEM. Statistical significances were determined using unpaired, two-tailed t-test (*: $p < 0.05$; **: $p \leq 0.01$;***: $p \leq 0.001$).

4.7.2 BNP-SPC Uptake Is Not AT-II Cell-Specific

BNPs-SPC aim to specifically target AT-II cells for GC delivery in AAI. To test this specificity, nanoparticle uptake was analyzed in LPCs in comparison to peritoneal macrophages. LPCs were isolated from lungs by enzymatic digestion and subsequent removal of immune cells by MACS. LPCs were treated with increasing concentrations of BNPs and BNPs-SPC and cultured for 24 hours. To obtain macrophages, mice were treated with thioglycolate to attract macrophages to the peritoneal cavity. Four days later, the peritoneal cavity was extensively lavaged to obtain the peritoneal macrophages. Like LPCs, macrophages were treated with different nanoparticle concentrations for 24 hours.

Nanoparticle uptake was assessed by flow cytometry using the mean fluorescence intensity (MFI) of FMN as measure. In case of LPCs, the uptake was analyzed in $EpCAM^+$ cells.

LPCs showed an increase of green fluorescence that correlated with the increasing concentrations of both BNPs and BNPs-SPC (**fig. 34 A and B**). Uptake of BNPs-SPC seemed to be more efficient than that of BNPs as MFI values were higher in LPCs (**fig. 34 A and B**). BNP uptake could also be observed for peritoneal macrophages with higher MFI values depending on higher concentrations (**fig. 34 C**). BNPs-SPC were also internalized by macrophages (**fig. 34 D**). Uptake of both nanoparticle types occurred similarly as MFI values were comparable (**fig. 34 C and D**). In comparison to peritoneal macrophages, nanoparticles seemed to have a higher uptake in LPCs as MFI values were much higher (**fig. 34 A-D**).

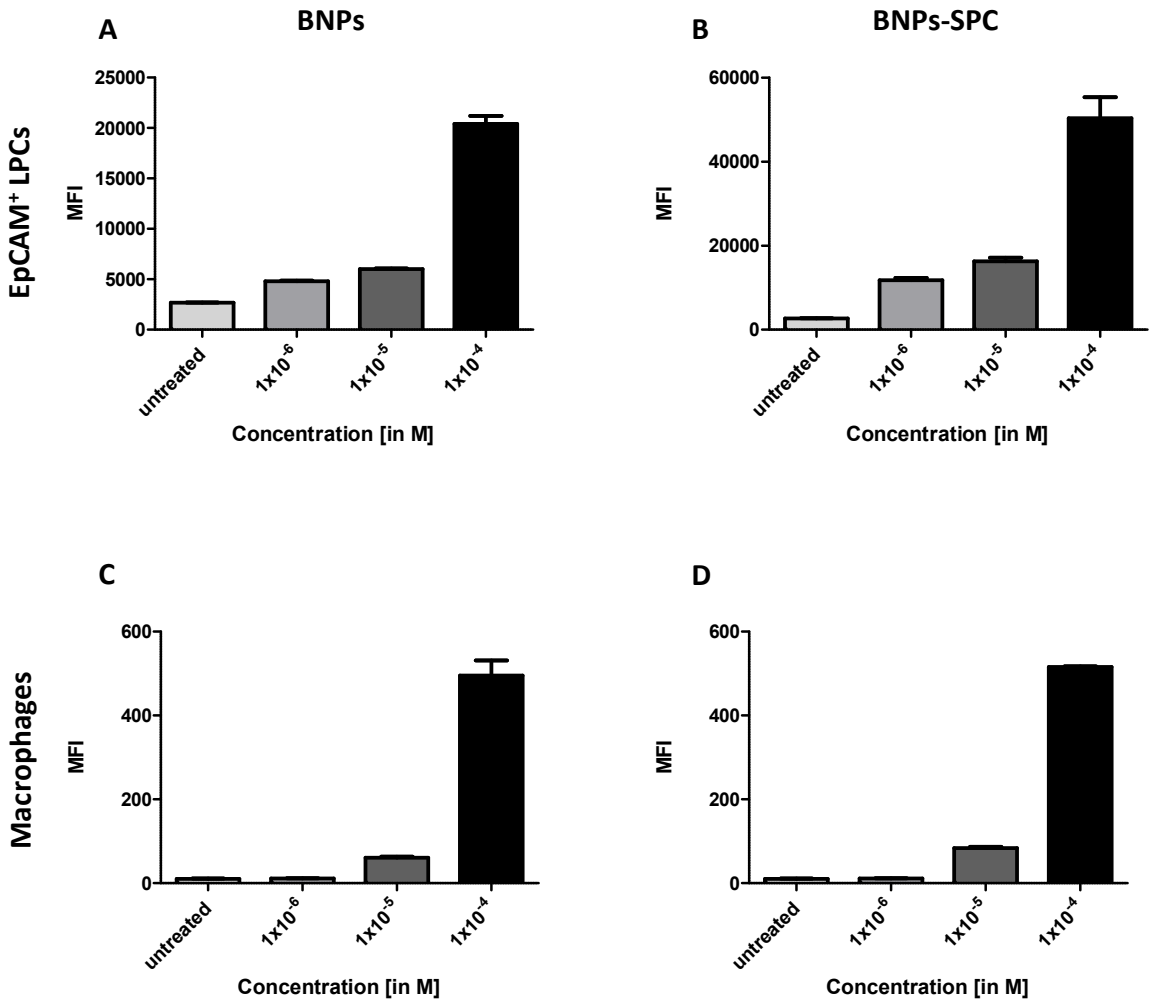

Figure 34: Nanoparticle uptake in LPCs and peritoneal macrophages. LPCs were isolated by enzymatic digestion of lung tissue followed by removal of immune cells by MACS. To obtain peritoneal macrophages, mice were treated with thioglycolate. After 4 days, the peritoneal cavity was extensively lavaged to remove the peritoneal macrophages. LPCs and macrophages were treated with increasing concentrations of BNPs (A and C) or BNPs-SPC (B and D) and cultured for 24 hours. Nanoparticle uptake was analyzed by flow cytometry and measured as MFI of the green nanoparticle fluorescence. In case of LPCs, $EpCAM^+$ cells were analyzed to specifically examine the uptake in AECs. Data are presented as mean ± SEM (LPCs: n = 2; macrophages: n = 2; each group).

Thus, this uptake analysis revealed that BNPs-SPC were not able to specifically target AT-II cells. Macrophages were also able to take up these nanoparticles despite the presence of the specific antibody.

4.7.3 BNPs Are Not Effective in the Treatment of ALI

Furthermore, the efficacy of BNPs was investigated in the treatment of ALI. Wild type mice were injected with LPS and OA to induce ALI which was followed by additional treatment either with Dex i.p. or BNPs intranasally. Control mice were treated with PBS only. Pulmonary infiltrates were analyzed by flow cytometry using BALF cells. As expected, Dex significantly reduced increased BALF cell numbers in the injured airways (**fig. 35 A**). Likewise, Dex reduced the ALI-characteristic neutrophilia (**fig. 35 B**). In line with the AAI findings, BNPs were not able to reduce the number of inflammatory cells. Neutrophil numbers were even slightly enhanced after mice with ALI were treated with BNPs.

In line with the increased local inflammatory cell recruitment, systemic IL-6 levels were elevated as well following the induction of ALI (**fig. 35 C**). Dex significantly decreased IL-6 production whereas BNPs had no effect on the concentration in serum (**fig. 35 C**).

Thus, BNPs were not effective in the treatment of ALI as inflammatory responses were not suppressed.

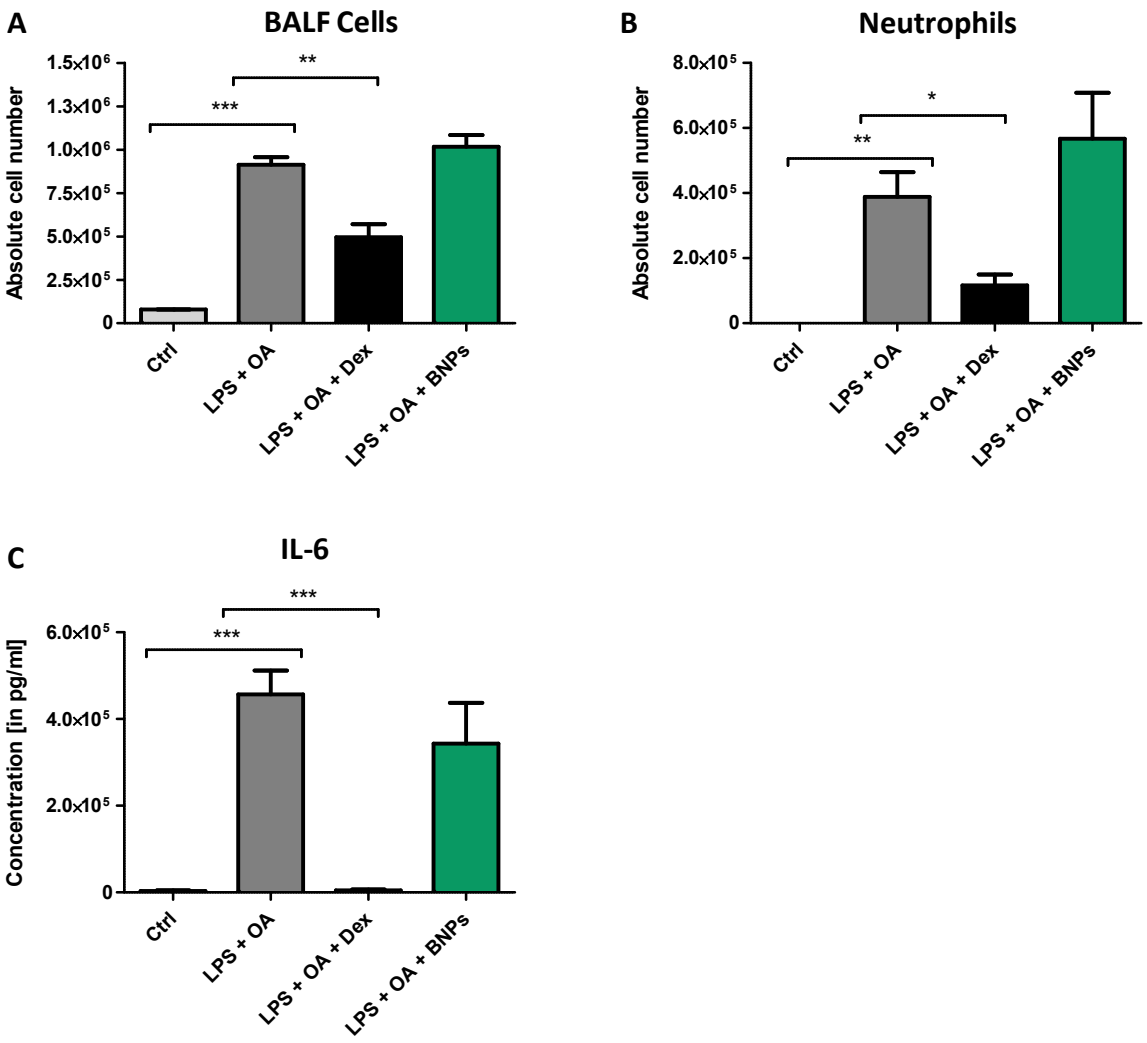

Figure 35: BNPs in the treatment of ALI. Mice were treated with LPS and OA to induce ALI (LPS + OA). Part of the mice was treated i.p. with Dex (LPS + OA + Dex) whereas others were intranasally treated with BNPs (LPS + OA + BNPs). Control animals were injected with PBS only (Ctrl). BALF cells were obtained by extensively lavaging the lungs to remove the infiltrating immune cells. Cell numbers were determined and distinct cells surface markers were used for flow cytometric analysis. Absolute cell numbers of total BALF cells (A) and eosinophils (B) are shown (n = 4-6; each group). IL-6 levels were determined in serum samples. Serum was obtained by cardiac puncturing and IL-6 concentrations were determined by ELISA with respective antibodies. Concentrations are depicted as pg/ml (n = 5-6; each group). Data are presented as mean values ± SEM. Statistical significances were determined using unpaired, two-tailed t-test (*: $p < 0.05$; **: $p \leq 0.01$;***: $p \leq 0.001$).

Taken together, target site-directed delivery of GCs using BNPs or BNPs-SPC failed in the treatment of both AAI and ALI. Therefore, these nanoparticles are no promising tool in optimizing GC-treatment in these inflammatory lung diseases.

5. Discussion

For decades, GCs have been successfully employed in the treatment of multiple diseases such as asthma, rheumatoid arthritis and multiple sclerosis. They are powerful drugs because they efficiently suppress inflammatory responses and therefore improve disease symptoms. They have also been popular because of their broad availability and cost-effectiveness. Beneficial effects are mediated by various mechanisms of the GR. Inflammatory gene expression is regulated by GCs mainly through transactivating and transrepressing mechanisms of the GR, but also include other genomic actions (Barnes, 2011b; Rhen and Cidlowski, 2005). In addition, GCs are also known to exert non-genomic effects for instance on the PI3K-pathway (Rhen and Cidlowski, 2005). Nonetheless, it is unknown how and to which extent these mechanisms contribute to the therapeutic efficacy. Unfortunately, the use of GCs is limited by the development of severe side effects such as osteoporosis, growth retardation and drug resistance (Dahl, 2006; Rhen and Cidlowski, 2005; Stahn and Buttgereit, 2008). Adverse effects are mainly due to the ubiquitous expression of the GR throughout the human body. Systemically and also topically applied GCs are known to enter the systemic circulation where they can affect organs that are not associated with the underlying disease (Dahl, 2006; Rhen and Cidlowski, 2005). Moreover, GC-treatment is also limited by the occurrence of resistance in selected patients (Barnes, 2013; Kadmiel and Cidlowski, 2013). With regard to these limiting factors, a better understanding of the different GC mechanisms is substantial to improve GC-treatment. Tolerability and specificity of GC-treatment need to be optimized.

5.1 Therapeutic Efficacy of GCs in AAI Requires an Intact GR-Dimerization Interface

Asthma is a major global health problem as millions of people are affected worldwide. It is characterized by chronic lung inflammation that is associated with bronchoconstriction and airway remodeling. Patients suffer from symptoms such as wheezing, shortness of breath and AHR which considerably impairs the quality of life. Until today, asthma treatment remains challenging in terms of disease endotypes that only respond to distinct therapeutic agents. Nevertheless, the majority of asthma patients respond well to treatment with GCs. In combination with or without β_2-agonists, GCs achieve long-term

control of asthma symptoms. However, it is unclear which GC mechanism is relevant for exerting the beneficial effects in the treatment of asthma. To address this question, GR^{dim} mice were used to study the GC-treatment of murine AAI. GR^{dim} mice carry the point mutation A458T in the DBD of the GR which impairs its dimerization capability. This mutation mainly affects the transactivating mode of GR action whereas transrepression of pro-inflammatory transcription factors is still possible (Reichardt et al., 1998). Since mice do not develop asthma naturally, an AAI was induced which is a hallmark of human asthma (Kips et al., 2003; Nials and Uddin, 2008). Mice were sensitized to OVA, which was administered together with the adjuvant alum thus mounting a T_H2-specfic immune response. To specifically elicit the allergic inflammation in the airways, mice were challenged intranasally with OVA. Dex was applied by i.p. injections to mimic systemic GC-treatment as performed in patients with severe asthma. Albeit relying on the immunization with an artificial antigen, the applied OVA-model recapitulates many although not all features of human asthma and is therefore a suitable model to study its mechanisms (Bates et al., 2009; Kips et al., 2003; Shin et al., 2009).

Allergen induced CSR is an important feature of AAI in asthma. After allergen exposure, T_H2 cells secrete a plethora of cytokines including IL-4 and IL-13 that are responsible to induce CSR in B cells. Consequently, allergic inflammation is associated with elevated IgE levels (Bloemen et al., 2007; Gould and Sutton, 2008; Holgate, 2012a). Following the induction of AAI, OVA-induced Ig class-switch was assessed in serum samples of GR^{wt} and GR^{dim} mice to prove whether immunization was efficient. Irrespective of the genotype, OVA-induced AAI led to elevated levels of IgE, but also of IgG1 and IgG2a. This is in line with clinical studies demonstrating that asthma patients also have increased levels of allergen-specific IgGs (Williams et al., 2012b). Thus, immunization with OVA was successful in both mouse strains.

Dex, however, had no influence on the elevated Ig levels. This could be due to the short treatment duration as well as due to the time point sampling occurred, as it is known that GCs are able to interfere with CSR in B cells (Benko et al., 2014; Jabara et al., 2001).

Similar to human asthma, OVA-induced AAI is characterized by a massive influx of inflammatory cells in the allergic airways, which occured in GR^{wt} and GR^{dim} mice. Airway infiltration was dominated by eosinophils which is characteristic for AAI in asthma. GC-treatment significantly diminished inflammatory cell numbers in GR^{wt} mice. In contrast,

Dex did not have any impact on the overall cell numbers in the allergic airways of GR^{dim} mice. Similarly, eosinophilia was still present and neutrophil numbers were even increased.

In addition to leukocyte infiltration, airway remodeling, bronchoconstriction, mucus hypersecretion and goblet cell hyperplasia were observed in lungs of both mouse strains. These alterations were completely resolved in GR^{wt} mice after treatment with Dex. The opposite could be observed for lungs of GR^{dim} mice, which were refractory to GC-treatment. These findings correlated with the flow cytometric analysis of pulmonary infiltrates, and indicated that an intact GR-dimerization interface was essential to exert the beneficial effects of GCs in murine AAI. The transactivating mechanism of the GR thus appears to be more relevant than the transrepressing mechanism.

Interestingly, GR^{dim} mice are not only refractory to GC-treatment in AAI but also in other disease models. For instance, Dex failed to resolve inflammatory responses in murine models for rheumatoid arthritis, atopic dermatitis, sepsis and ALI (Baschant et al., 2011; Kleiman et al., 2012; Tuckermann et al., 2007; Vandevyver et al., 2012; Vettorazzi et al., 2015).

In the past, the transactivating mode of action was associated with the development of the GC-mediated adverse effects. Recent findings, however, revealed that GR-dimerization was not required for the induction of osteoporosis, a complication of long-term GC-therapy (Rauch et al., 2010). Therefore, the development of novel therapeutic approaches, that selectively target the GR-dimerization, might help to avoid adverse effects.

5.2 AECs Are Important Targets in the GC-Treatment of AAI

In addition to the mechanistic basis of GC-action, it is crucial to identify the target cells of GCs in the treatment of asthma. Previous studies had demonstrated that immune cells were dispensable for the efficacy of GCs in the treatment of murine AAI. Dex-treatment completely abolished inflammatory responses in mice that were GR-deficient specifically in T cells, B cells, DCs and myeloid cells (unpublished data). Furthermore, bone marrow chimeras were created with GR^{wt} and GR^{dim} mice. The A458T mutation is ubiquitously present in all cell types of GR^{dim} mice and consequently also affects all cells of the

hematopoietic lineage. To confirm that immune cells were indeed dispensable in the treatment of AAI, bone marrow of GR^{dim} mice was transplanted into irradiated GR^{wt} mice and vice versa. Surprisingly, GR^{wt} mice with a hematopoietic system of GR^{dim} origin responded normally to Dex-treatment of AAI. At the same time, GR^{dim} mice with hematopoietic cells from GR^{wt} mice were refractory to the treatment with Dex (unpublished data). These findings indicated that the lung itself with its structural cells is most likely the target of GC-treatment, rather than immune cells.

It was hypothesized that AECs might be the targets being responsible for the efficacy of GCs in murine AAI due to their crucial role in maintaining the immune responses in the lung.

To test this assumption, a protocol for the isolation and purification of AECs was established based on the enzymatic digestion of lung tissue followed by removal of hematopoietic cells. However, it turned out that only a minor part of these cells was indeed epithelial cells. Although for practical reasons no markers for other structural cells of the lung could be included, the isolated cells presumably also include fibroblasts, airway smooth muscle cells, endothelial cells and mesenchymal cells. Thus unfortunately, isolation of AECs resulted in a heterogeneous population of LPCs rather than in a single uniform cell population.

Despite the problem that the employed protocol did not result in a pure population of AECs, transcriptome profiling was performed with the resulting LPCs from GR^{wt} and GR^{dim} mice following the induction of AAI and additional Dex-treatment. RNA-seq analysis allows the identification of novel candidate genes that are differentially expressed upon Dex-treatment of AAI and thus helps to obtain a better insight into the transcriptional regulation by GCs. Furthermore, a potential link between the mechanism and target cells of GCs, in particular AECs, should be assessed. The analysis revealed different transcriptome profiles in LPC samples of GR^{wt} and GR^{dim} mice following Dex-treatment. Numerous differentially expressed genes were identified such as ATF-6, CD163, ELANE and ITGAE which were chosen for further analysis. In line with the bone marrow chimera analysis, these data suggested a crucial role of AECs and other pulmonary structural cells in the efficacy of GCs in AAI that is presumably linked to the transactivation of target genes.

It is against this background that GR^{spc} mice were used to particularly examine the role of AT-II cells in the treatment of AAI. These mice are GR-deficient specifically in AT-II cells in a temporally defined manner. A tamoxifen-inducible Cre/loxP recombination system was used to prevent potential changes in lung morphology because the GC-GR interaction is essential in embryonic development and organogenesis. These changes could be indeed observed in conventional GR^{spc} mice with a constant knock-out. Alveolar walls were increased in thickness resulting in close apposition of endothelial and epithelial layers (Habermehl et al., 2011).

Inducible GR^{spc} mice were treated with tamoxifen for GR ablation in AT-II cells. The knock-out was assessed on protein level and mRNA level. Western blot analysis could not reveal a reduced GR expression in the lungs of mutant mice, but qRT-PCR analysis showed a moderately reduced GR mRNA expression. This result was not unexpected as whole lungs were analyzed and GR expression therefore cannot be completely abolished. Namely, AT-II cells only represent a small proportion of total lung cells and other lung cells still express the GR. The total percentage of AT-II cells in the lung is 15% which correlates with the detected reduction (Mason, 2006). Thus, it is likely that tamoxifen treatment successfully induced gene recombination in GR^{spc} mice.

AAI was induced in GR^{spc} mice with OVA to examine the impact of GR-deficient AT-II cells on the GC-efficacy. Both mouse strains showed elevated levels of IgG1, IgE and IgG2a and Dex had no effect on these levels. Nevertheless, the elevated Ig levels revealed that immunization with OVA had been efficient in GR^{spc} mice. Similar to the findings obtained with GR^{dim} mice, flow cytometric and histological analysis revealed a significant increase of pulmonary infiltrates in the allergic airways of GR^{flox} and GR^{spc} mice which was characterized by eosinophilia. Dex-treatment efficiently reduced the immune cell influx in GR^{flox} mice as expected. Although infiltration was also reduced in GR^{spc} mice, Dex-treatment was not as effective as in GR^{flox} mice. Furthermore, macrophage and neutrophil numbers were unaltered and eosinophilia was not completely abolished in GR^{spc} mice.

Histological analysis of the lung from both mouse strains provided a comparable picture. AAI led to the same structural changes in of GR^{flox} and GR^{spc} mice with bronchoconstriction and mucus hypersecretion. These changes were completely resolved in GR^{flox} mice, but only partially in GR^{spc} mice. Taken together, these findings remarkably demonstrated that AT-II cells contribute to the GC-efficacy in the treatment of murine AAI

because disease symptoms could not be completely repressed by Dex. At the same time, partial repression was still observed in mutant mice since other structural cells of the lung such as airway smooth muscle cells and endothelial cells presumably contribute to the GC-efficacy as well. Remarkably, AAI is the first disease model in which GCs do not target immune cells. In other disease models of multiple sclerosis, rheumatoid arthritis, graft-versus-host disease or contact allergy, either T cells or myeloid cells had been the target for effective GC-treatment (Baschant et al., 2011; Theiss-Suennemann et al., 2015; Tuckermann et al., 2007; Wüst et al., 2008).

The finding that AT-II cells are targets of GC-treatment in asthma is supported by a study dealing with the GR distribution in the lungs of healthy and asthmatic individuals. Highest GR expression was found in alveolar walls while no differences were detected in the analyzed groups (Adcock et al., 1996). This increased GR expression might hint at AT-II cells as target site of GC-action in the treatment of asthma.

Noteworthy, the importance of AECs in the development of asthma is well established. In recent years, it has become evident that asthma is a disease of the airway epithelium (Holgate, 2007, 2011b; Wang et al., 2008). The development of asthma relies on the altered or damaged epithelial barrier function rather than on the allergic pathways alone (Holgate, 2011b). Several GWAS identified numerous candidate genes such as PCDH1 or ORMDL3 that were not only associated with a higher risk for the development of asthma, but were also associated with the airway epithelium. The airway epithelium of genetically susceptible individuals is more prone to inflammatory insults like viral infections which triggers ongoing inflammatory responses that eventually give rise to asthma (Holgate, 2011b).

All in all, it appears that AECs are valuable targets for the development of novel therapeutic approaches in asthma. Target site-directed delivery of GCs to AECs would potentiate the efficacy and would also reduce the development of adverse effects.

5.3 Inflammatory Genes Are Regulated by the Transactivating GR Mechanism in AECs

GR^{dim} mice were refractory to GC-treatment of AAI indicating that an intact dimerization interface was crucial for exerting the therapeutic efficacy. At the same time, AECs were also shown to be required for the GC-efficacy. Thus, mechanism and target site of GC-action in murine AAI were elucidated which might both be linked in the transcriptional control of GC-target genes in AECs.

To address this issue, lungs and LPCs were isolated from GR^{dim}, GR^{spc} and wild type mice following the induction of AAI and selective Dex-treatment, and various inflammatory genes were analyzed concerning differential mRNA expression by qRT-PCR.

One hallmark of asthma is the secretion of the T_H2-specific cytokines IL-5 and IL-13 that maintain the allergic inflammation in the airways (Bloemen et al., 2007). IL-5 is crucial for the maturation, recruitment and survival of eosinophils (Finkelman et al., 2010; Williams et al., 2012a). Increased levels of IL-13 are linked to CSR in B cells, mucus hypersecretion and to AHR (Corren, 2013; Finkelman et al., 2010; Williams et al., 2012a). In asthma therapy, GCs suppress these cytokines via the transrepressing mode of action (Barnes, 2011b). As expected, AAI induced a remarkable increase of IL-5 and IL-13 mRNA expression in lungs and LPCs of all analyzed mouse strains. Dex-treatment efficiently reduced these increased cytokine levels in wild type mice, an effect that could not be observed in both mutant mouse strains. It was unexpected that Dex could not repress these T_H2 cytokines in GR^{dim} mice although transrepression was still possible. T_H2 cells and their cytokines are regulated by the transcription factors STAT6 and GATA3 which are targets for the GC-mediated transrepression (Barnes, 1998, 2011b; Ho et al., 2009; Shen and Stavnezer, 1998). In this model, however, transactivation seems to be more important to modulate T_H2 cell function. This might be mediated by GILZ which is an important transcriptional regulator of GCs (Vandevyver et al., 2013). GILZ is a target of GC-mediated transactivation and its induction is inhibited in GR^{dim} mice (Rauch et al., 2010). GILZ is able to inhibit both DNA binding and transcriptional activation of various transcription factors (Stellato, 2007; Vandevyver et al., 2013). Interaction between GILZ and STAT6 as well as GATA3 has been reported to modulate T_H2 cell functions (Ronchetti et al., 2015). Thus, GCs regulate T_H2 cells and their cytokines in parallel by transactivation

and transrepression although the results obtained in the asthma model at hand suggest that activation of GILZ is possibly the more important mechanism. Alternatively, the way how GCs repress these cytokines depends on the specific cell type.

Since IL-5 and IL-13 mRNA expression was not repressed by Dex-treatment in GR^{spc} mice, AT-II cells could also be an important source of these cytokines in AAI which has not been reported before.

AECs are a prominent source of IL-33, MCP-1 and RANTES that are all secreted in response to inflammatory stimuli (Fehrenbach, 2001; Makrinioti et al., 2014; Stellato, 2007). IL-33 is expressed at higher levels in asthmatic lungs and induces robust T_H2 cell-specific immune responses, eosinophilic inflammation and AHR (Kabata et al., 2013; Makrinioti et al., 2014; Nabe et al., 2015). Increased levels of MCP-1 and RANTES are found in asthma patients. Both chemokines provoke mast cell activation and mediate the recruitment of other immune cells into the allergic airways (Alam et al., 1996; Conti and DiGioacchino, 2001; Holgate et al., 1997). All three genes have been shown to be repressed by treatment with GCs (Nabe et al., 2015; Stellato, 2007). Analyzed lungs and LPCs of all mouse strains were characterized by increased levels of IL-33, MCP-1 and RANTES. As expected, treatment with Dex could abolish this increased mRNA expression in wild type mice. In contrast, GC-treatment failed to diminish the elevated levels in GR^{dim} and GR^{spc} mice. As for the analyzed T_H2 cytokines, expression of MCP-1 and RANTES has been suggested to be regulated by transrepression although the experiments at hand suggest that GR-dimerization was essential for suppression (Barnes, 2001). Of note, the relative contribution of these cytokines and chemokines produced by AECs in response to AAI in comparison to T_H2 cells, ILC2 cells and other immune cells is not known.

In addition to the analyzed pro-inflammatory cytokines and chemokines, expression of the tight junction proteins occludin and claudin 5 was investigated in lung and LPC samples. The epithelial integrity is impaired in asthma patients making them highly susceptible to infections and other inflammatory insults (Cummins, 2012; Davies, 2014; Soini, 2011). Several *in vitro* studies demonstrated that GCs increase the expression of these tight junction proteins by transactivation thereby improving the epithelial barrier function (Felinski et al., 2008; Förster et al., 2005; Kielgast et al., 2016). Contrariwise, mRNA expression of occludin and claudin 5 was increased following induction of AAI. Treatment with Dex led to a reduction of these elevated levels in wild type mice. Again

AAI-induced expression could not be repressed in mutant mouse strains although this result was not always clear. Transcriptional control of these tight junction proteins is difficult to evaluate as the *in vivo* findings in AAI were opposed to the reported *in vitro* studies. Thus, it is not clear whether GC mechanisms mediate the transcriptional control of tight junction proteins and whether AECs can directly control the epithelial integrity by production of tight junction proteins.

Transcriptome profiling of LPCs from GR^{dim} mice has identified many novel candidate genes such as ITGAE, ELANE, ATF-6 and CD163 that were chosen for further qRT-PCR analysis. ITGAE is an integrin mediating cell-cell or cell-ECM interactions. It is highly expressed by DCs and T cells on mucosal sites and binds to E-cadherin on epithelial cells (Annacker et al., 2005; Smyth et al., 2007). Several studies suggested an involvement in the development of asthma (Bernatchez et al., 2015; Nakano et al., 2012). ELANE is mainly secreted by neutrophils and causes major tissue damage by mediating the recruitment of further immune cells to the site of inflammation (Koga et al., 2013; Sandhaus and Turino, 2013). Furthermore, it contributes to the development of AAI and AHR in asthma as well (Koga et al., 2013; McGarvey et al., 2002; Nadel et al., 1999). ATF-6 is a transcription factor that is involved in protein folding processes (Hsu and Turvey, 2013). The asthma candidate gene ORMDL3, which is expressed by AECs, regulates the activation of this transcription factor. Therefore, ATF-6 expression is also associated with asthma pathogenesis (Hsu and Turvey, 2013; Miller et al., 2012, 2014).

Expression of ITGAE, ELANE and ATF-6 was increased in analyzed lung and LPC samples after AAI was induced. Subsequent GC-treatment with Dex repressed the expression of these candidate genes in wild type mice but was not effective in GR^{dim} and GR^{spc} mice.

These findings indicate that the three genes are promising candidates contributing to the resolution of AAI by GCs in AECs requiring an intact GR-dimerization interface.

The scavenger receptor CD163 is mainly known to be a marker for alternatively activated monocytes and macrophages (Onofre et al., 2009). CD163-expressing macrophages have an anti-inflammatory function and CD163 is a well-known target of GR transactivation. In addition, asthma is associated with differential expression of this receptor (van de Garde et al., 2014; Kowal, 2004; Kowal et al., 2014). CD163 mRNA expression was induced during AAI in lung tissue and LPCs of all mouse strains. Dex abolished the increased CD163 expression in wild type mice whereas treatment was ineffective in both mutant mouse

strains. Thus, CD163 presumably exerts a different and pro-inflammatory role when expressed by AECs compared to when it is expressed by macrophages.

This finding demonstrates that the novel candidate genes including CD163 might in fact be important targets for effective GC-treatment of AAI. Nevertheless, the exact function and role of these genes in the pathogenesis of AAI and GC-therapy need to be further investigated.

Taken together, GR^{dim} and GR^{spc} mice behaved similarly with regard to the transcriptional control of all analyzed genes. In contrast to wild type mice, GCs were not able to suppress the AAI-induced gene expression in both mutant mouse strains. This was independent of the analyzed type of sample as most genes showed similar expression patterns in lungs and LPCs. Noteworthy, transcriptional control of GC-target genes in AAI is not only mediated by the transactivation but also by other mechanisms of GCs. It has already been reported that transcriptional control of a subset of GC-target genes can be maintained in the presence of the A458T mutation (Frijters et al., 2010; Lim et al., 2015). Furthermore, AECs were implicated to be a more prominent source of cytokines and other inflammatory mediators than previously expected.

In conclusion, these data revealed a novel mechanism of GC-therapy of AAI mainly being dependent on the GR-transactivation of GC-responsive genes in AECs.

5.4 AECs Are Dispensable for the GC-Treatment of ALI

In the treatment of AAI, AECs have been shown to be important targets of GCs. Since GCs are also used in the treatment of other inflammatory lung diseases, it is not known whether AECs might be generally required for therapeutic efficacy.

ALI is an inflammatory insult to the lung which can be caused either directly or indirectly by e.g. sepsis, trauma or gastric aspiration. It is a common condition in critically ill patients with high morbidity and mortality. The disease is characterized by acute onset with massive pulmonary influx of leukocytes, hypoxia and edema (Saguil and Fargo, 2012). GC-treatment of ALI is still under debate, because its efficacy is unclear. Nevertheless, numerous clinical trials are investigating the use of GCs in ALI (Meduri et al., 2016; Zhang et al., 2015). So far, a beneficial role in the early phase of the disease has been revealed (Diaz et al., 2010; Marik et al., 2011).

ALI was induced in GR^{spc} mice with a combined treatment of LPS and OA. LPS elicits a systemic inflammatory response whereas OA selectively targets the lung. Part of the mice was injected i.p. with Dex representing systemic GC-treatment. ALI led to a significant increase of inflammatory cells in the airways of both GR^{flox} and GR^{spc} mice which was characterized by neutrophilia in both mouse strains. Dex-treatment significantly repressed the number of inflammatory cells not only in GR^{flox} mice but also in GR^{spc} mice as revealed by flow cytometric and histological analysis. Serum analysis of IL-6, which is an important cytokine in the pathogenesis of ALI, demonstrated that GCs were effective in reducing its level in both mouse strains. Moreover, mRNA expression of IL-1β, MCP-1 and iNOS has been investigated in lung samples by qRT-PCR. These pro-inflammatory mediators drive the neutrophilic inflammation and promote tissue damage in ALI (Han and Mallampalli, 2015; Johnson and Matthay, 2010). Of note, AECs are known to express all of these mediators (Stellato, 2007). As expected, ALI induced a remarkable increase of IL-1β, MCP-1 and iNOS mRNA expression in lungs of both mouse strains. In line with the previous findings, Dex effectively repressed these inflammatory genes in wild type and mutant mice.

In contrast to AAI, these findings clearly demonstrated that AECs were dispensable for the GC-efficacy of ALI although both diseases were dependent on the transactivating mode of action (Vettorazzi et al., 2015). However, while GC repression of AAI depends at least in part on the GR in AT-II cells, macrophages were reported to be essential for the repression of ALI (Vettorazzi et al., 2015).

5.5 BNPs Are No Option to Optimize the GC-Treatment of Inflammatory Lung Diseases

Despite their beneficial effects, the awareness to induce severe side effects has limited the use of GCs in the treatment of inflammatory diseases. Therefore, the benefit-risk ratio of GC-treatment needs to be carefully taken into account. Over the past few years, many attempts have been made to optimize GC-treatment by enhancing the efficacy and drug safety.

The development of selective GR agonists (SEGRAS) or dissociated steroids is based on the suggestion that the anti-inflammatory effects rely on the transrepressing mechanism

while the undesirable adverse effects rely on the transactivating mechanism. Several substances have already been developed (Barnes, 2011b; Buttgereit et al., 2015; Stahn and Buttgereit, 2008). The efficacy of this strategy, however, has not been proven yet. Aside from this issue, the work at hand and other experimental findings contradict the concept of SEGRAS as transactivation has been shown to be essential to exert the anti-inflammatory activities of GCs in several disease models (Baschant et al., 2011; Kleiman et al., 2012; Tuckermann et al., 2007; Vandevyver et al., 2012; Vettorazzi et al., 2015).

The targeted delivery of GCs to the site of inflammation using liposomal formulations is another promising approach to optimize GC-treatment. In comparison to conventional GC-treatment, PEGylated GC liposomes were more effective and induced fewer side effects in murine models of multiple sclerosis and rheumatoid arthritis (Metselaar et al., 2003; Rauchhaus et al., 2009; Schmidt et al., 2003; Schweingruber et al., 2011). Despite being promising, these PEGylated liposomes can unfortunately cause hypersensitivity reactions by complement activation (van den Hoven et al., 2013).

Recently developed BNPs have been shown to be a novel interesting approach for optimized GC-therapy (Heck et al., 2015). These BNPs are based on inorganic-organic hybrid nanoparticles formed of cationic zirconium oxide together with anionic betamethasonephosphate and the green fluorescent dye flavinmononucleotide (Heck et al., 2015; Roming et al., 2010). In a murine model of multiple sclerosis, BNPs effectively repressed inflammatory responses and ameliorated disease symptoms (unpublished data).

As this work had demonstrated that GR-dependent gene regulation in AECs was a crucial mechanism for the therapeutic efficacy in AAI, target site-directed delivery of BNPs was investigated in the treatment of AAI. BNPs were conjugated with an anti-SPC antibody (BNPs-SPC) to selectively deliver GCs to AT-II cells. BNPs-SPC were applied topically by intranasal instillation to potentiate the efficacy. In comparison to antibody-coated nanoparticles, mice were also treated with BNPs via the same route.

As expected, Dex-treatment significantly diminished the AAI-induced increase of pulmonary infiltrates, but surprisingly, BNPs had no impact on BALF cell numbers whereas BNPs-SPC even caused an increase. The same tendencies were observed for eosinophil numbers in the BALF. Thus, neither BNPs nor BNPs-SPC were able to suppress AAI.

As BNPs-SPC were not effective to target AT-II cells by GCs, their uptake was investigated in LPC samples as well as in peritoneal macrophages *in vitro*. The MFI of the green fluorescent dye FMN contained in the nanoparticles was used as measure of uptake. $EpCAM^+$ LPCs were used as a representative population for AECs. BNP-SPC and BNP uptake occurred in a concentration-dependent manner in AECs as high nanoparticle concentrations correlated with high MFI values. In general, BNP-SPC uptake was more efficient than that of BNPs in AECs.

Interestingly, however, BNP and also BNP-SPC uptake could also be observed in peritoneal macrophages in a similar concentration-dependent manner. As macrophages were able to internalize both types of nanoparticles, macrophages presumably interfere with BNPs-SPC targeting to AECs *in vivo*. It is a well-described mechanism that nanoparticles that are deposited in the lung are rapidly removed by phagocytosis. Thus, nanoparticles have to circumvent the mucociliary and macrophage clearance to reach the AECs (Da Silva et al., 2013). In line with this notion, BNPs were shown to be preferentially taken up by macrophages in the treatment of the multiple sclerosis model (unpublished data). Thus, BNP treatment allows GC delivery specifically to macrophages. This is presumably why these nanoparticles were not effective in the treatment of AAI. Macrophages are dispensable in the GC-treatment of AAI (unpublished data) but at the same time, BNPs-SPC cannot reach AT-II cells as GC-target in AAI because of macrophage clearance.

Instead of BNPs-SPC, other approaches should be considered for the AT-II cell-directed delivery of GCs in AAI. Lipoplexes conjugated with the anti-SPC antibody have been shown to be promising drug carriers. These lipoplexes were able to specifically target AT-II cells without accumulating in other lung cells. Moreover, lipoplexes did not induce lung toxicity (Wu et al., 2015).

Since BNPs were shown to selectively target macrophages, their use in the treatment ALI was investigated. As mentioned before, macrophages are essential for the GC-efficacy in ALI rather than AECs. Analysis of pulmonary infiltrates expectedly demonstrated therapeutic efficacy of Dex in ALI therapy as BALF cell numbers were significantly reduced and neutrophilia efficiently repressed. Surprisingly, BNPs had no effect on total BALF cell and neutrophil numbers. In addition, IL-6 levels in serum were not diminished by BNPs in contrast to Dex. Thus, BNPs were not able to repress the inflammatory responses in ALI.

In contrast to Dex, BNPs were applied topically which might be another reason for the inefficacy in ALI. Systemic administration could presumably repress the inflammatory responses as ALI is characterized by systemic inflammation.

Even though macrophages are targets of BNPs and GC-efficacy in ALI, many factors can influence the nanoparticle effects in the lung. The occurrence of pulmonary disease can affect many physiological aspects of the lung like bronchoconstriction. This may prevent the deposition of nanoparticles into the desired regions of the lung or even prevent cellular uptake. Besides, nanoparticle properties can be influenced by e.g. low pH (Da Silva et al., 2013; Kuzmov and Minko, 2015). Hypoxia is a major symptom of ALI and might lead to degradation of BNPs. These pulmonary factors, however, need to be further investigated with regard to the BNP efficacy in ALI.

Taken together, target cell-directed delivery of BNPs failed in the treatment of both AAI and ALI. In the treatment of inflammatory lung diseases, these inorganic-organic hybrid nanoparticles are therefore not suitable for optimizing GC-treatment and other approaches thus need to be considered instead.

6. Conclusion

This work provides provocative new insights into the mechanisms of GCs in the treatment of asthma. It is the first example where GC-targeting of non-immune cells is required for therapeutic efficacy. Although GCs could partially repress the inflammatory responses in GR^{spc} mice, it is indisputable that AT-II cells are crucial targets of the beneficial effects of GC-therapy of AAI (**fig. 36**). Nevertheless, other structural cells of the lung such as airway smooth muscle cells and endothelial cells presumably contribute to the efficacy as well. So far, AT-II cells have only been linked to GC-therapy of AAI while they are dispensable for the treatment of ALI.

Furthermore, this work demonstrated that an intact GR-dimerization interface, which is responsible for the transactivation of many GC-target genes, is a prerequisite for the therapeutic efficacy in AAI, rather than the transrepressing mode of action. Thus, GR-dependent regulation of target genes in AECs is a critical mechanism of the therapeutic efficacy in AAI.

Although first approaches to selectively deliver GCs to AT-II cells using nanoparticles failed, target site-directed approaches might improve GC-treatment with fewer side effects. At the present time, the findings on the mechanisms of GCs in allergic asthma therapy are still limited to the mouse. However, it is likely that they will nonetheless pave the way for the development of improved asthma therapies in humans in the future.

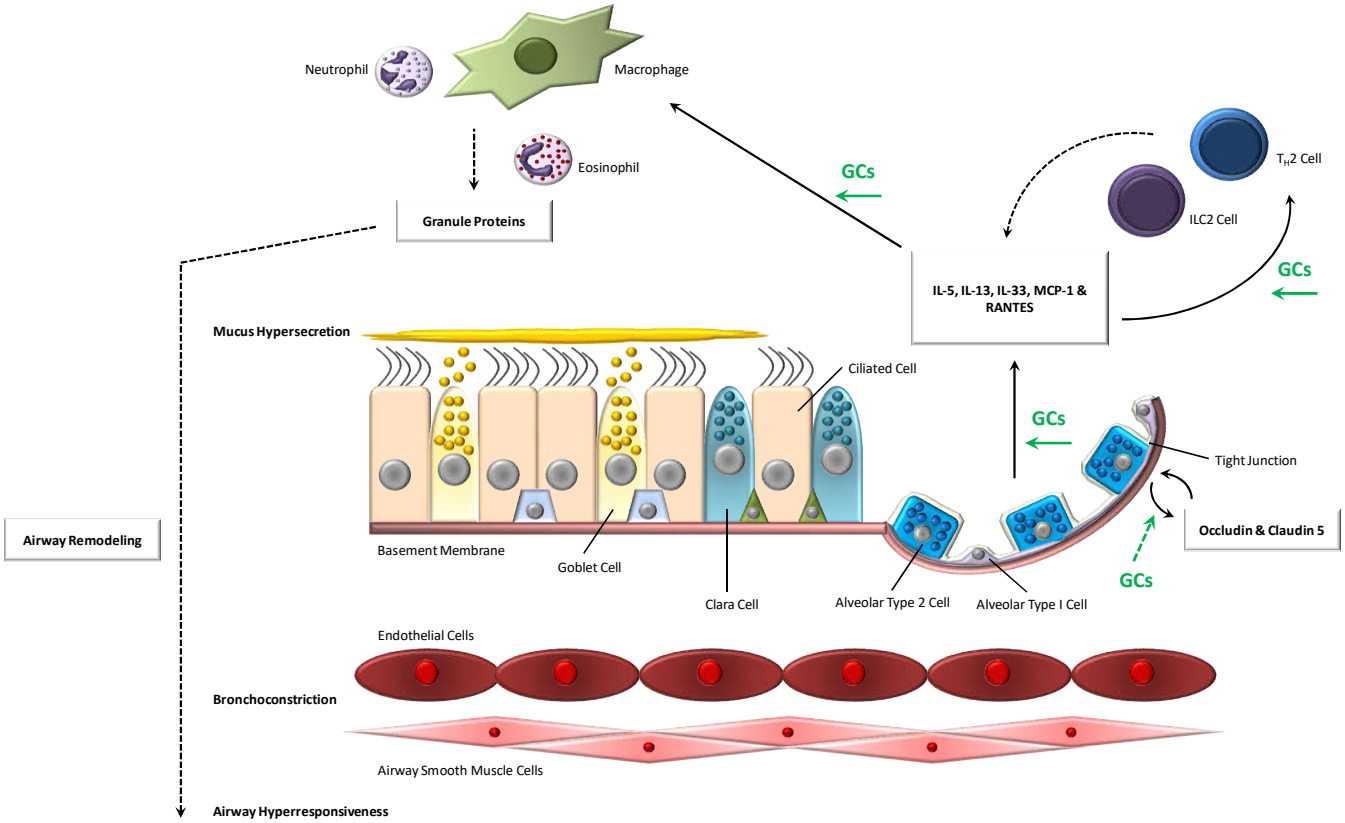

Figure 36: Model of GC activities in the treatment of allergic asthma. AECs are important targets of GCs in AAI. The conducting airways consist mainly of secretory goblet cells and clara cells as well as ciliated cells. The alveoli in the lung parenchyma are formed by AT-I and AT-II cells. Airway epithelial barrier function is regulated by tight junction proteins that are essential for the epithelial integrity. In response to allergen exposure, AT-II cells secrete a broad range of pro-inflammatory mediators including IL-33, MCP-1, RANTES and also the T_H2-specific cytokines IL-5 and IL-13. GCs repress the cytokine expression by AT-II cells. This impairs the activation of ILC2 cells and T_H2 cells while secretion of additional cytokines is also reduced. At the same time, GCs can interfere with the infiltration of eosinophils, macrophages and neutrophils. Release of granule proteins and other pro-inflammatory mediators that promote airway remodeling and tissue damage can be diminished. Expression of the tight junction proteins occludin and claudin 5 is controlled either directly or indirectly by GCs. GCs repress the AEC-secreted cytokines in a transactivating manner which reverses airway remodeling processes. Bronchoconstriction, mucus hypersecretion and AHR can be abolished. In addition to AT-II cells, GCs presumably also act on other structural cells of the lung such as airway smooth muscle cells and endothelial cells to improve asthma symptoms.

7. Appendix

7.1 References

Adcock, I.M., Gilbey, T., Gelder, C.M., Chung, K.F., and Barnes, P.J. (1996). Glucocorticoid receptor localization in normal and asthmatic lung. Am. J. Respir. Crit. Care Med. *154*, 771–782.

Alam, R., York, J., Boyars, M., Stafford, S., Grant, J.A., Lee, J., Forsythe, P., Sim, T., and Ida, N. (1996). Increased MCP-1, RANTES, and MIP-1alpha in bronchoalveolar lavage fluid of allergic asthmatic patients. Am. J. Respir. Crit. Care Med. *153*, 1398–1404.

Anders, S., and Huber, W. (2010). Differential expression analysis for sequence count data. Genome Biol. *11*, 1.

Anders, S., Pyl, P.T., and Huber, W. (2015). HTSeq--a Python framework to work with high-throughput sequencing data. Bioinformatics *31*, 166–169.

Annacker, O., Coombes, J.L., Malmstrom, V., Uhlig, H.H., Bourne, T., Johansson-Lindbom, B., Agace, W.W., Parker, C.M., and Powrie, F. (2005). Essential role for CD103 in the T cell–mediated regulation of experimental colitis. J. Exp. Med. *202*, 1051–1061.

Arora, N., and Kale, S. (2013). Airway epithelial cells: Barrier and much more. Indian J. Allergy Asthma Immunol. *27*, 95.

Ashbaugh, D., Boyd Bigelow, D., Petty, T., and Levine, B. (1967). ACUTE RESPIRATORY DISTRESS IN ADULTS. The Lancet *290*, 319–323.

Barnes, P.J. (1998). Anti-inflammatory actions of glucocorticoids: molecular mechanisms. Clin. Sci. Lond. Engl. 1979 *94*, 557–572.

Barnes, P.J. (2001). Molecular mechanisms of corticosteroids in allergic diseases. Allergy *56*, 928–936.

Barnes, P.J. (2003). How Do Corticosteroids Work in Asthma? Ann. Intern. Med. *139*, 359.

Barnes, P.J. (2011a). Biochemical basis of asthma therapy. J. Biol. Chem. *286*, 32899–32905.

Barnes, P.J. (2011b). Glucocorticosteroids: current and future directions: Glucocorticoids. Br. J. Pharmacol. *163*, 29–43.

Barnes, P.J. (2012). Severe asthma: advances in current management and future therapy. J. Allergy Clin. Immunol. *129*, 48–59.

Barnes, P.J. (2013). Corticosteroid resistance in patients with asthma and chronic obstructive pulmonary disease. J. Allergy Clin. Immunol. *131*, 636–645.

Baschant, U., Frappart, L., Rauchhaus, U., Bruns, L., Reichardt, H.M., Kamradt, T., Brauer, R., and Tuckermann, J.P. (2011). Glucocorticoid therapy of antigen-induced arthritis depends on the dimerized glucocorticoid receptor in T cells. Proc. Natl. Acad. Sci. *108*, 19317–19322.

Bastarache, J.A., and Blackwell, T.S. (2009). Development of animal models for the acute respiratory distress syndrome. Dis. Model. Mech. *2*, 218–223.

Bates, J.H.T., Rincon, M., and Irvin, C.G. (2009). Animal models of asthma. AJP Lung Cell. Mol. Physiol. *297*, L401–L410.

Benko, A.L., Olsen, N.J., and Kovacs, W.J. (2014). Glucocorticoid inhibition of activation-induced cytidine deaminase expression in human B lymphocytes. Mol. Cell. Endocrinol. *382*, 881–887.

Bernatchez, E., Gold, M.J., Langlois, A., Lemay, A.-M., Brassard, J., Flamand, N., Marsolais, D., McNagny, K.M., and Blanchet, M.-R. (2015). Pulmonary CD103 expression regulates airway inflammation in asthma. Am. J. Physiol. - Lung Cell. Mol. Physiol. *308*, L816–L826.

Bloemen, K., Verstraelen, S., Van Den Heuvel, R., Witters, H., Nelissen, I., and Schoeters, G. (2007). The allergic cascade: review of the most important molecules in the asthmatic lung. Immunol. Lett. *113*, 6–18.

Brandt, J. van den, Lühder, F., McPherson, K.G., de Graaf, K.L., Tischner, D., Wiehr, S., Herrmann, T., Weissert, R., Gold, R., and Reichardt, H.M. (2007). Enhanced Glucocorticoid Receptor Signaling in T Cells Impacts Thymocyte Apoptosis and Adaptive Immune Responses. Am. J. Pathol. *170*, 1041–1053.

Butt, Y., Kurdowska, A., and Allen, T.C. (2016). Acute Lung Injury: A Clinical and Molecular Review. Arch. Pathol. Lab. Med. *140*, 345–350.

Buttgereit, F. (2012). A fresh look at glucocorticoids how to use an old ally more effectively. Bull. NYU Hosp. Jt. Dis. *70 Suppl 1*, 26–29.

Buttgereit, F., Spies, C.M., and Bijlsma, J.W. (2015). Novel glucocorticoids: where are we now and where do we want to go? Clin. Exp. Rheumatol. *33*, 29.

Camelo, A., Dunmore, R., Sleeman, M.A., and Clarke, D.L. (2014). The epithelium in idiopathic pulmonary fibrosis: breaking the barrier. Front. Pharmacol. *4*.

Campo, P., Rodríguez, F., Sánchez-García, S., Barranco, P., Quirce, S., Pérez-Francés, C., Gómez-Torrijos, E., Cárdenas, R., Olaguibel, J.M., Delgado, J., et al. (2013). Phenotypes and endotypes of uncontrolled severe asthma: new treatments. J. Investig. Allergol. Clin. Immunol. *23*, 76–88; quiz 1 follow 88.

Chua, F. (2006). Neutrophil Elastase: Mediator of Extracellular Matrix Destruction and Accumulation. Proc. Am. Thorac. Soc. *3*, 424–427.

Conti, P., and DiGioacchino, M. (2001). MCP-1 and RANTES are mediators of acute and chronic inflammation. Allergy Asthma Proc. *22*, 133–137.

Corren, J. (2013). Role of interleukin-13 in asthma. Curr. Allergy Asthma Rep. *13*, 415–420.

Corti, M., Brody, A.R., and Harrison, J.H. (1996). Isolation and primary culture of murine alveolar type II cells. Am. J. Respir. Cell Mol. Biol. *14*, 309–315.

Cruz-Topete, D., and Cidlowski, J.A. (2015). One Hormone, Two Actions: Anti- and Pro-Inflammatory Effects of Glucocorticoids. Neuroimmunomodulation *22*, 20–32.

Cummins, P.M. (2012). Occludin: One Protein, Many Forms. Mol. Cell. Biol. *32*, 242–250.

Da Silva, A.L., Santos, R.S., Xisto, D.G., Alonso, S. del V., Morales, M.M., and Rocco, P.R.M. (2013). Nanoparticle-based therapy for respiratory diseases. An. Acad. Bras. Cienc. *85*, 137–146.

Dahl, R. (2006). Systemic side effects of inhaled corticosteroids in patients with asthma. Respir. Med. *100*, 1307–1317.

Davies, D.E. (2014). Epithelial Barrier Function and Immunity in Asthma. Ann. Am. Thorac. Soc. *11*, S244–S251.

Diaz, J.V., Brower, R., Calfee, C.S., and Matthay, M.A. (2010). Therapeutic strategies for severe acute lung injury: Crit. Care Med. *38*, 1644–1650.

Drazen, J.M., Postma, D.S., and Rabe, K.F. (2015). The Asthma–COPD Overlap Syndrome. N. Engl. J. Med. *373*, 1241–1249.

Durinck, S., Spellman, P.T., Birney, E., and Huber, W. (2009). Mapping identifiers for the integration of genomic datasets with the R/Bioconductor package biomaRt. Nat. Protoc. *4*, 1184–1191.

Fahy, J.V. (2015). Type 2 inflammation in asthma--present in most, absent in many. Nat. Rev. Immunol. *15*, 57–65.

Fehrenbach, H. (2001). Alveolar epithelial type II cell: defender of the alveolus revisited. Respir. Res. *2*, 33–46.

Felinski, E.A., Cox, A.E., Phillips, B.E., and Antonetti, D.A. (2008). Glucocorticoids induce transactivation of tight junction genes occludin and claudin-5 in retinal endothelial cells via a novel cis-element. Exp. Eye Res. *86*, 867–878.

Finkelman, F.D., Hogan, S.P., Hershey, G.K.K., Rothenberg, M.E., and Wills-Karp, M. (2010). Importance of Cytokines in Murine Allergic Airway Disease and Human Asthma. J. Immunol. *184*, 1663–1674.

Förster, C., Silwedel, C., Golenhofen, N., Burek, M., Kietz, S., Mankertz, J., and Drenckhahn, D. (2005). Occludin as direct target for glucocorticoid-induced improvement of blood-brain barrier properties in a murine *in vitro* system: Glucocorticoids induce occludin at blood-brain barrier. J. Physiol. *565*, 475–486.

Frijters, R., Fleuren, W., Toonen, E.J., Tuckermann, J.P., Reichardt, H.M., van der Maaden, H., van Elsas, A., van Lierop, M.-J., Dokter, W., de Vlieg, J., et al. (2010). Prednisolone-induced differential gene expression in mouse liver carrying wild type or a dimerization-defective glucocorticoid receptor. BMC Genomics *11*, 359.

Galli, S.J., Tsai, M., and Piliponsky, A.M. (2008). The development of allergic inflammation. Nature *454*, 445–454.

van de Garde, M.D.B., Martinez, F.O., Melgert, B.N., Hylkema, M.N., Jonkers, R.E., and Hamann, J. (2014). Chronic Exposure to Glucocorticoids Shapes Gene Expression and Modulates Innate and Adaptive Activation Pathways in Macrophages with Distinct Changes in Leukocyte Attraction. J. Immunol. *192*, 1196–1208.

Gereke, M., Jung, S., Buer, J., and Bruder, D. (2009). Alveolar Type II Epithelial Cells Present Antigen to CD4 $^{+}$ T Cells and Induce Foxp3 $^{+}$ Regulatory T Cells. Am. J. Respir. Crit. Care Med. *179*, 344–355.

Gereke, M., Autengruber, A., Gröbe, L., Jeron, A., Bruder, D., and Stegemann-Koniszewski, S. (2012). Flow Cytometric Isolation of Primary Murine Type II Alveolar Epithelial Cells for Functional and Molecular Studies. J. Vis. Exp.

Gonçalves-de-Albuquerque, C.F., Silva, A.R., Burth, P., Castro-Faria, M.V., and Castro-Faria-Neto, H.C. (2015). Acute Respiratory Distress Syndrome: Role of Oleic Acid-Triggered Lung Injury and Inflammation. Mediators Inflamm. *2015*, 1–9.

Gould, H.J., and Sutton, B.J. (2008). IgE in allergy and asthma today. Nat. Rev. Immunol. *8*, 205–217.

Guilbert, T.W., and Denlinger, L.C. (2010). Role of infection in the development and exacerbation of asthma. Expert Rev. Respir. Med. *4*, 71–83.

Gupta, P., and Bhatia, V. (2008). Corticosteroid physiology and principles of therapy. Indian J. Pediatr. *75*, 1039–1044.

Habermehl, D., Parkitna, J.R., Kaden, S., Brügger, B., Wieland, F., Gröne, H.-J., and Schütz, G. (2011). Glucocorticoid activity during lung maturation is essential in mesenchymal and less in alveolar epithelial cells. Mol. Endocrinol. Baltim. Md *25*, 1280–1288.

Han, S., and Mallampalli, R.K. (2015). The Acute Respiratory Distress Syndrome: From Mechanism to Translation. J. Immunol. *194*, 855–860.

Hasenberg, M., Stegemann-Koniszewski, S., and Gunzer, M. (2013). Cellular immune reactions in the lung. Immunol. Rev. *251*, 189–214.

Heck, J.G., Napp, J., Simonato, S., Möllmer, J., Lange, M., Reichardt, H.M., Staudt, R., Alves, F., and Feldmann, C. (2015). Multifunctional Phosphate-Based Inorganic–Organic Hybrid Nanoparticles. J. Am. Chem. Soc. *137*, 7329–7336.

Ho, I.-C., Tai, T.-S., and Pai, S.-Y. (2009). GATA3 and the T-cell lineage: essential functions before and after T-helper-2-cell differentiation. Nat. Rev. Immunol. *9*, 125–135.

Holgate, S.T. (2007). Epithelium dysfunction in asthma. J. Allergy Clin. Immunol. *120*, 1233–1244.

Holgate, S.T. (2011a). Asthma: a simple concept but in reality a complex disease: THE NEED FOR NEW ASTHMA TREATMENTS. Eur. J. Clin. Invest. *41*, 1339–1352.

Holgate, S.T. (2011b). The sentinel role of the airway epithelium in asthma pathogenesis. Immunol. Rev. *242*, 205–219.

Holgate, S.T. (2012a). Innate and adaptive immune responses in asthma. Nat. Med. *18*, 673–683.

Holgate, S.T. (2012b). Trials and tribulations in identifying new biologic treatments for asthma. Trends Immunol. *33*, 238–246.

Holgate, S.T. (2013). Stratified approaches to the treatment of asthma. Br. J. Clin. Pharmacol. *76*, 277–291.

Holgate, S.T., and Polosa, R. (2008). Treatment strategies for allergy and asthma. Nat. Rev. Immunol. *8*, 218–230.

Holgate, S.T., Bodey, K.S., Janezic, A., Frew, A.J., Kaplan, A.P., and Teran, L.M. (1997). Release of RANTES, MIP-1 α , and MCP-1 into Asthmatic Airways Following Endobronchial Allergen Challenge. Am. J. Respir. Crit. Care Med. *156*, 1377–1383.

Hollenhorst, M.I., Richter, K., and Fronius, M. (2011). Ion Transport by Pulmonary Epithelia. J. Biomed. Biotechnol. *2011*, 1–16.

Holt, P.G., Strickland, D.H., Wikström, M.E., and Jahnsen, F.L. (2008). Regulation of immunological homeostasis in the respiratory tract. Nat. Rev. Immunol. *8*, 142–152.

Holtzman, M.J., Byers, D.E., Alexander-Brett, J., and Wang, X. (2014). The role of airway epithelial cells and innate immune cells in chronic respiratory disease. Nat. Rev. Immunol. *14*, 686–698.

Hough, C.L. (2014). Steroids for Acute Respiratory Distress Syndrome? Clin. Chest Med. *35*, 781–795.

van den Hoven, J.M., Nemes, R., Metselaar, J.M., Nuijen, B., Beijnen, J.H., Storm, G., and Szebeni, J. (2013). Complement activation by PEGylated liposomes containing prednisolone. Eur. J. Pharm. Sci. Off. J. Eur. Fed. Pharm. Sci. *49*, 265–271.

Howell, D.C.J., and Bellingan, G.J. (2009). Acute Lung Injury and Acute Respiratory Distress Syndrome (ALI/ARDS). In Respiratory Disease and Its Management, A. McLuckie, ed. (London: Springer London), pp. 1–17.

Hsu, K.J., and Turvey, S.E. (2013). Functional analysis of the impact of ORMDL3 expression on inflammation and activation of the unfolded protein response in human airway epithelial cells. Allergy Asthma Clin. Immunol. *9*, 4.

Huber, W., Carey, V.J., Gentleman, R., Anders, S., Carlson, M., Carvalho, B.S., Bravo, H.C., Davis, S., Gatto, L., Girke, T., et al. (2015). Orchestrating high-throughput genomic analysis with Bioconductor. Nat. Methods *12*, 115–121.

Ishmael, F.T. (2011). The inflammatory response in the pathogenesis of asthma. J. Am. Osteopath. Assoc. *111*, S11-17.

Jabara, H.H., Brodeur, S.R., and Geha, R.S. (2001). Glucocorticoids upregulate CD40 ligand expression and induce CD40L-dependent immunoglobulin isotype switching. J. Clin. Invest. *107*, 371–378.

Johnson, E.R., and Matthay, M.A. (2010). Acute lung injury: epidemiology, pathogenesis, and treatment. J. Aerosol Med. Pulm. Drug Deliv. *23*, 243–252.

Kabata, H., Moro, K., Fukunaga, K., Suzuki, Y., Miyata, J., Masaki, K., Betsuyaku, T., Koyasu, S., and Asano, K. (2013). Thymic stromal lymphopoietin induces corticosteroid resistance in natural helper cells during airway inflammation. Nat. Commun. *4*.

Kadmiel, M., and Cidlowski, J.A. (2013). Glucocorticoid receptor signaling in health and disease. Trends Pharmacol. Sci. *34*, 518–530.

Kato, A., and Schleimer, R.P. (2007). Beyond inflammation: airway epithelial cells are at the interface of innate and adaptive immunity. Curr. Opin. Immunol. *19*, 711–720.

Kielgast, F., Schmidt, H., Braubach, P., Winkelmann, V.E., Thompson, K.E., Frick, M., Dietl, P., and Wittekindt, O.H. (2016). Glucocorticoids Regulate Tight Junction Permeability of Lung Epithelia by Modulating Claudin 8. Am. J. Respir. Cell Mol. Biol. *54*, 707–717.

Kips, J.C., Anderson, G.P., Fredberg, J.J., Herz, U., Inman, M.D., Jordana, M., Kemeny, D.M., Lötvall, J., Pauwels, R.A., Plopper, C.G., et al. (2003). Murine models of asthma. Eur. Respir. J. *22*, 374–382.

Kleiman, A., Hübner, S., Rodriguez Parkitna, J.M., Neumann, A., Hofer, S., Weigand, M.A., Bauer, M., Schmid, W., Schütz, G., Libert, C., et al. (2012). Glucocorticoid receptor dimerization is required for survival in septic shock via suppression of interleukin-1 in macrophages. FASEB J. Off. Publ. Fed. Am. Soc. Exp. Biol. *26*, 722–729.

Knight, D.A., and Holgate, S.T. (2003). The airway epithelium: Structural and functional properties in health and disease. Respirology *8*, 432–446.

Koga, H., Miyahara, N., Fuchimoto, Y., Ikeda, G., Waseda, K., Ono, K., Tanimoto, Y., Kataoka, M., Gelfand, E.W., Tanimoto, M., et al. (2013). Inhibition of neutrophil elastase attenuates airway hyperresponsiveness and inflammation in a mouse model of secondary allergen challenge: neutrophil elastase inhibition attenuates allergic airway responses. Respir. Res. *14*, 8.

Kowal, K. (2004). Expression of CD163 in asthmatic patients during specific bronchial challenge with dermatophagoides pteronyssinus (Dp) allergen*1. J. Allergy Clin. Immunol. *113*, S184.

Kowal, K., Moniuszko, M., and Bodzenta-Lukaszyk, A. (2014). The effect of inhaled corticosteroids on the concentration of soluble CD163 in induced sputum of allergic asthma patients. J. Investig. Allergol. Clin. Immunol. *24*, 49–55.

Kuzmov, A., and Minko, T. (2015). Nanotechnology approaches for inhalation treatment of lung diseases. J. Controlled Release *219*, 500–518.

Langen, U., Schmitz, R., and Steppuhn, H. (2013). [Prevalence of allergic diseases in Germany: results of the German Health Interview and Examination Survey for Adults (DEGS1)]. Bundesgesundheitsblatt Gesundheitsforschung Gesundheitsschutz *56*, 698–706.

Langmead, B., and Salzberg, S.L. (2012). Fast gapped-read alignment with Bowtie 2. Nat. Methods *9*, 357–359.

Laycock, H., and Rajah, A. (2010). Acute Lung Injury and Acute Respiratory Distress Syndrome: A Review. BJMP 3 (2); 324.

Lee, D.-H., Geyer, E., Flach, A.-C., Jung, K., Gold, R., Flügel, A., Linker, R.A., and Lühder, F. (2012). Central nervous system rather than immune cell-derived BDNF mediates axonal protective effects early in autoimmune demyelination. Acta Neuropathol. (Berl.) *123*, 247–258.

Lim, H.-W., Uhlenhaut, N.H., Rauch, A., Weiner, J., Hübner, S., Hübner, N., Won, K.-J., Lazar, M.A., Tuckermann, J., and Steger, D.J. (2015). Genomic redistribution of GR monomers and dimers mediates transcriptional response to exogenous glucocorticoid in vivo. Genome Res. *25*, 836–844.

Liu, A.H. (2015). Revisiting the hygiene hypothesis for allergy and asthma. J. Allergy Clin. Immunol. *136*, 860–865.

Lo, B., Hansen, S., Evans, K., Heath, J.K., and Wright, J.R. (2008). Alveolar Epithelial Type II Cells Induce T Cell Tolerance to Specific Antigen. J. Immunol. *180*, 881–888.

Mackay, A., and Al-Haddad, M. (2009). Acute lung injury and acute respiratory distress syndrome. Contin. Educ. Anaesth. Crit. Care Pain *9*, 152–156.

Makrinioti, H., Toussaint, M., Jackson, D.J., Walton, R.P., and Johnston, S.L. (2014). Role of interleukin 33 in respiratory allergy and asthma. Lancet Respir. Med. *2*, 226–237.

Marik, P.E., Meduri, G.U., Rocco, P.R.M., and Annane, D. (2011). Glucocorticoid Treatment in Acute Lung Injury and Acute Respiratory Distress Syndrome. Crit. Care Clin. *27*, 589–607.

Martinez, F.D., and Vercelli, D. (2013). Asthma. The Lancet *382*, 1360–1372.

Mason, R.J. (2006). Biology of alveolar type II cells. Respirology *11*, S12–S15.

Matute-Bello, G., Frevert, C.W., and Martin, T.R. (2008). Animal models of acute lung injury. AJP Lung Cell. Mol. Physiol. *295*, L379–L399.

Matute-Bello, G., Downey, G., Moore, B.B., Groshong, S.D., Matthay, M.A., Slutsky, A.S., and Kuebler, W.M. (2011). An Official American Thoracic Society Workshop Report: Features and Measurements of Experimental Acute Lung Injury in Animals. Am. J. Respir. Cell Mol. Biol. *44*, 725–738.

McGarvey, L.P.A., Dunbar, K., Martin, S.L., Brown, V., Macmahon, J., Ennis, M., and Elborn, J.S. (2002). Cytokine concentrations and neutrophil elastase activity in bronchoalveolar lavage and induced sputum from patients with cystic fibrosis, mild asthma and healthy volunteers. J. Cyst. Fibros. Off. J. Eur. Cyst. Fibros. Soc. *1*, 269–275.

Meduri, G.U., Schwingshackl, A., and Hermans, G. (2016). Prolonged Glucocorticoid Treatment in ARDS: Impact on Intensive Care Unit-Acquired Weakness. Front. Pediatr. *4*.

Metselaar, J.M., Wauben, M.H.M., Wagenaar-Hilbers, J.P.A., Boerman, O.C., and Storm, G. (2003). Complete remission of experimental arthritis by joint targeting of glucocorticoids with long-circulating liposomes. Arthritis Rheum. *48*, 2059–2066.

Michel, K.D., Uhmann, A., Dressel, R., van den Brandt, J., Hahn, H., and Reichardt, H.M. (2013). The Hedgehog Receptor Patched1 in T Cells Is Dispensable for Adaptive Immunity in Mice. PLoS ONE *8*, e61034.

Miller, M., Tam, A.B., Cho, J.Y., Doherty, T.A., Pham, A., Khorram, N., Rosenthal, P., Mueller, J.L., Hoffman, H.M., Suzukawa, M., et al. (2012). ORMDL3 is an inducible lung epithelial gene regulating metalloproteases, chemokines, OAS, and ATF6. Proc. Natl. Acad. Sci. *109*, 16648–16653.

Miller, M., Rosenthal, P., Beppu, A., Mueller, J.L., Hoffman, H.M., Tam, A.B., Doherty, T.A., McGeough, M.D., Pena, C.A., Suzukawa, M., et al. (2014). ORMDL3 Transgenic Mice Have Increased Airway Remodeling and Airway Responsiveness Characteristic of Asthma. J. Immunol. *192*, 3475–3487.

Nabe, T., Wakamori, H., Yano, C., Nishiguchi, A., Yuasa, R., Kido, H., Tomiyama, Y., Tomoda, A., Kida, H., Takiguchi, A., et al. (2015). Production of interleukin (IL)-33 in the lungs during multiple antigen challenge-induced airway inflammation in mice, and its modulation by a glucocorticoid. Eur. J. Pharmacol. *757*, 34–41.

Nadel, J.A., Takeyama, K., and Agustí, C. (1999). Role of neutrophil elastase in hypersecretion in asthma. Eur. Respir. J. *13*, 190–196.

Nakano, H., Free, M.E., Whitehead, G.S., Maruoka, S., Wilson, R.H., Nakano, K., and Cook, D.N. (2012). Pulmonary CD103+ dendritic cells prime Th2 responses to inhaled allergens. Mucosal Immunol. *5*, 53–65.

Nakawah, M.O., Hawkins, C., and Barbandi, F. (2013). Asthma, chronic obstructive pulmonary disease (COPD), and the overlap syndrome. J. Am. Board Fam. Med. JABFM *26*, 470–477.

Narasaraju, T., Yang, E., Samy, R.P., Ng, H.H., Poh, W.P., Liew, A.-A., Phoon, M.C., van Rooijen, N., and Chow, V.T. (2011). Excessive Neutrophils and Neutrophil Extracellular Traps Contribute to Acute Lung Injury of Influenza Pneumonitis. Am. J. Pathol. *179*, 199–210.

Nials, A.T., and Uddin, S. (2008). Mouse models of allergic asthma: acute and chronic allergen challenge. Dis. Model. Mech. *1*, 213–220.

Onofre, G., Kolácková, M., Jankovicová, K., and Krejsek, J. (2009). Scavenger receptor CD163 and its biological functions. Acta Medica (Hradec Kralove) *52*, 57–61.

Ponte, E.V., Cruz, A.A., Athanazio, R., Carvalho-Pinto, R., Fernandes, F.L.A., Barreto, M.L., and Stelmach, R. (2016). Urbanization is associated with increased asthma morbidity and mortality in Brazil. Clin. Respir. J.

Rauch, A., Seitz, S., Baschant, U., Schilling, A.F., Illing, A., Stride, B., Kirilov, M., Mandic, V., Takacz, A., Schmidt-Ullrich, R., et al. (2010). Glucocorticoids suppress bone formation by attenuating osteoblast differentiation via the monomeric glucocorticoid receptor. Cell Metab. *11*, 517–531.

Rauchhaus, U., Schwaiger, F., and Panzner, S. (2009). Separating therapeutic efficacy from glucocorticoid side effects in rodent arthritis using novel, liposomal delivery of dexamethasone phosphate: long-term suppression of arthritis facilitates interval treatment. Arthritis Res. Ther. *11*, R190.

Reddy, A.J., and Kleeberger, S.R. (2009). Genetic polymorphisms associated with acute lung injury. Pharmacogenomics *10*, 1527–1539.

Reichardt, H.M., Kaestner, K.H., Tuckermann, J., Kretz, O., Wessely, O., Bock, R., Gass, P., Schmid, W., Herrlich, P., Angel, P., et al. (1998). DNA Binding of the Glucocorticoid Receptor Is Not Essential for Survival. Cell *93*, 531–541.

Rhen, T., and Cidlowski, J.A. (2005). Antiinflammatory action of glucocorticoids—new mechanisms for old drugs. N. Engl. J. Med. *353*, 1711–1723.

van Rijt, L., von Richthofen, H., and van Ree, R. (2016). Type 2 innate lymphoid cells: at the cross-roads in allergic asthma. Semin. Immunopathol.

Rock, J.R., Barkauskas, C.E., Cronce, M.J., Xue, Y., Harris, J.R., Liang, J., Noble, P.W., and Hogan, B.L.M. (2011). Multiple stromal populations contribute to pulmonary fibrosis without evidence for epithelial to mesenchymal transition. Proc. Natl. Acad. Sci. *108*, E1475–E1483.

Roming, M., Lünsdorf, H., Dittmar, K.E.J., and Feldmann, C. (2010). ZrO(HPO4)1−x(FMN)x: Quick and Easy Synthesis of a Nanoscale Luminescent Biomarker. Angew. Chem. Int. Ed. *49*, 632–637.

Ronchetti, S., Migliorati, G., and Riccardi, C. (2015). GILZ as a Mediator of the Anti-Inflammatory Effects of Glucocorticoids. Front. Endocrinol. *6*.

Rothe, T. (2013). Asthma-Phänotypen und die Phänotyp-spezifische Therapie. PRAXIS *102*, 211–218.

Rubenfeld, G.D., Caldwell, E., Peabody, E., Weaver, J., Martin, D.P., Neff, M., Stern, E.J., and Hudson, L.D. (2005). Incidence and outcomes of acute lung injury. N. Engl. J. Med. *353*, 1685–1693.

Saguil, A., and Fargo, M. (2012). Acute respiratory distress syndrome: diagnosis and management. Am. Fam. Physician *85*, 352–358.

Sanderson, M.J. (2011). Exploring lung physiology in health and disease with lung slices. Pulm. Pharmacol. Ther. *24*, 452–465.

Sandhaus, R.A., and Turino, G. (2013). Neutrophil Elastase-Mediated Lung Disease. COPD J. Chronic Obstr. Pulm. Dis. *10*, 60–63.

Scanlon, S.T., and McKenzie, A.N.J. (2012). Type 2 innate lymphoid cells: new players in asthma and allergy. Curr. Opin. Immunol. *24*, 707–712.

Schäcke, H., Döcke, W.-D., and Asadullah, K. (2002). Mechanisms involved in the side effects of glucocorticoids. Pharmacol. Ther. *96*, 23–43.

Schleimer, R.P., Kato, A., Kern, R., Kuperman, D., and Avila, P.C. (2007). Epithelium: At the interface of innate and adaptive immune responses. J. Allergy Clin. Immunol. *120*, 1279–1284.

Schmidt, J., Metselaar, J.M., Wauben, M.H.M., Toyka, K.V., Storm, G., and Gold, R. (2003). Drug targeting by long-circulating liposomal glucocorticosteroids increases therapeutic efficacy in a model of multiple sclerosis. Brain J. Neurol. *126*, 1895–1904.

Schweingruber, N., Haine, A., Tiede, K., Karabinskaya, A., van den Brandt, J., Wüst, S., Metselaar, J.M., Gold, R., Tuckermann, J.P., Reichardt, H.M., et al. (2011). Liposomal encapsulation of glucocorticoids alters their mode of action in the treatment of experimental autoimmune encephalomyelitis. J. Immunol. Baltim. Md 1950 *187*, 4310–4318.

Sharp, C., Millar, A.B., and Medford, A.R.L. (2015). Advances in Understanding of the Pathogenesis of Acute Respiratory Distress Syndrome. Respiration *89*, 420–434.

Shen, C.H., and Stavnezer, J. (1998). Interaction of stat6 and NF-kappaB: direct association and synergistic activation of interleukin-4-induced transcription. Mol. Cell. Biol. *18*, 3395–3404.

Shifren, A., Witt, C., Christie, C., and Castro, M. (2012). Mechanisms of remodeling in asthmatic airways. J. Allergy *2012*, 316049.

Shin, Y.S., Takeda, K., and Gelfand, E.W. (2009). Understanding asthma using animal models. Allergy Asthma Immunol. Res. *1*, 10–18.

Smyth, L.J.C., Kirby, J.A., and Cunningham, A.C. (2007). Role of the mucosal integrin alpha(E)(CD103)beta(7) in tissue-restricted cytotoxicity. Clin. Exp. Immunol. *149*, 162–170.

Soini, Y. (2011). Claudins in lung diseases. Respir. Res. *12*.

Stahn, C., and Buttgereit, F. (2008). Genomic and nongenomic effects of glucocorticoids. Nat. Clin. Pract. Rheumatol. *4*, 525–533.

Stellato, C. (2007). Glucocorticoid actions on airway epithelial responses in immunity: Functional outcomes and molecular targets. J. Allergy Clin. Immunol. *120*, 1247–1263.

Tan, C.K., and Wahli, W. (2016). A trilogy of glucocorticoid receptor actions. Proc. Natl. Acad. Sci. *113*, 1115–1117.

Theiss-Suennemann, J., Jörß, K., Messmann, J.J., Reichardt, S.D., Montes-Cobos, E., Lühder, F., Tuckermann, J.P., AWolff, H., Dressel, R., Gröne, H.-J., et al. (2015). Glucocorticoids attenuate acute graft-versus-host disease by suppressing the cytotoxic capacity of CD8(+) T cells. J. Pathol. *235*, 646–655.

Tronche, F., Kellendonk, C., Kretz, O., Gass, P., Anlag, K., Orban, P.C., Bock, R., Klein, R., and Schütz, G. (1999). Disruption of the glucocorticoid receptor gene in the nervous system results in reduced anxiety. Nat. Genet. *23*, 99–103.

Tuckermann, J.P., Kleiman, A., Moriggl, R., Spanbroek, R., Neumann, A., Illing, A., Clausen, B.E., Stride, B., Förster, I., Habenicht, A.J.R., et al. (2007). Macrophages and neutrophils are the targets for immune suppression by glucocorticoids in contact allergy. J. Clin. Invest. *117*, 1381–1390.

Van der Velden, J.L., Bertoncello, I., and McQualter, J.L. (2013). LysoTracker is a marker of differentiated alveolar type II cells. Respir. Res. *14*, 123.

Vandevyver, S., Dejager, L., Van Bogaert, T., Kleyman, A., Liu, Y., Tuckermann, J., and Libert, C. (2012). Glucocorticoid receptor dimerization induces MKP1 to protect against TNF-induced inflammation. J. Clin. Invest. *122*, 2130–2140.

Vandevyver, S., Dejager, L., Tuckermann, J., and Libert, C. (2013). New Insights into the Anti-inflammatory Mechanisms of Glucocorticoids: An Emerging Role for Glucocorticoid-Receptor-Mediated Transactivation. Endocrinology *154*, 993–1007.

Verstraelen, S., Bloemen, K., Nelissen, I., Witters, H., Schoeters, G., and Heuvel, R.V.D. (2008). Cell types involved in allergic asthma and their use in in vitro models to assess respiratory sensitization. Toxicol. In Vitro *22*, 1419–1431.

Vettorazzi, S., Bode, C., Dejager, L., Frappart, L., Shelest, E., Klaßen, C., Tasdogan, A., Reichardt, H.M., Libert, C., Schneider, M., et al. (2015). Glucocorticoids limit acute lung inflammation in concert with inflammatory stimuli by induction of SphK1. Nat. Commun. *6*, 7796.

Wang, Y., Bai, C., Li, K., Adler, K.B., and Wang, X. (2008). Role of airway epithelial cells in development of asthma and allergic rhinitis. Respir. Med. *102*, 949–955.

Warnes, M.G.R. (2016). Package “gplots.”

Weitnauer, M., Mijošek, V., and Dalpke, A.H. (2016). Control of local immunity by airway epithelial cells. Mucosal Immunol. *9*, 287–298.

Wenzel, S.E. (2012). Asthma phenotypes: the evolution from clinical to molecular approaches. Nat. Med. *18*, 716–725.

Whitsett, J.A., and Alenghat, T. (2014). Respiratory epithelial cells orchestrate pulmonary innate immunity. Nat. Immunol. *16*, 27–35.

World Health Organization (2013). WHO Asthma Fact Sheet No. 307. http://www.who.int/mediacentre/factsheets/fs307/en/ [cited November 24th, 2016]

Williams, C.M.M., Rahman, S., Hubeau, C., and Ma, H.-L. (2012a). Cytokine Pathways in Allergic Disease. Toxicol. Pathol. *40*, 205–215.

Williams, J.W., Tjota, M.Y., and Sperling, A.I. (2012b). The contribution of allergen-specific IgG to the development of th2-mediated airway inflammation. J. Allergy *2012*, 236075.

Wu, Y., Ma, J., Woods, P.S., Chesarino, N.M., Liu, C., Lee, L.J., Nana-Sinkam, S.P., and Davis, I.C. (2015). Selective targeting of alveolar type II respiratory epithelial cells by anti-surfactant protein-C antibody-conjugated lipoplexes. J. Controlled Release *203*, 140–149.

Wüst, S., van den Brandt, J., Tischner, D., Kleiman, A., Tuckermann, J.P., Gold, R., Lühder, F., and Reichardt, H.M. (2008). Peripheral T cells are the therapeutic targets of glucocorticoids in experimental autoimmune encephalomyelitis. J. Immunol. Baltim. Md 1950 *180*, 8434–8443.

Young, M.D., Wakefield, M.J., Smyth, G.K., and Oshlack, A. (2010). Gene ontology analysis for RNA-seq: accounting for selection bias. Genome Biol. *11*, 1.

Zhang, Z., Chen, L., and Ni, H. (2015). The effectiveness of Corticosteroids on mortality in patients with acute respiratory distress syndrome or acute lung injury: a secondary analysis. Sci. Rep. *5*, 17654.

Zheng, D., Limmon, G.V., Yin, L., Leung, N.H.N., Yu, H., Chow, V.T.K., and Chen, J. (2013). A Cellular Pathway Involved in Clara Cell to Alveolar Type II Cell Differentiation after Severe Lung Injury. PLoS ONE *8*, e71028.

Zhou, Z., Kozlowski, J., and Schuster, D.P. (2005). Physiologic, Biochemical, and Imaging Characterization of Acute Lung Injury in Mice. Am. J. Respir. Crit. Care Med. *172*, 344–351.

Zosky, G.R., and Sly, P.D. (2007). Animal models of asthma. Clin. Exp. Allergy J. Br. Soc. Allergy Clin. Immunol. *37*, 973–988.

7.2 List of Abbreviations

AAI	Allergic Airway Inflammation
Acc.	According
ACE	Angiotensin Converting Enzyme
ACOS	Asthma-COPD Overlap Syndrome
ACTH	Adrenocorticotropic Hormone
AECs	Airway Epithelial Cells
AF	Activation Function
AHR	Airway Hyperresponsiveness
ALI	Acute Lung Injury
Alum	Aluminum Hydroxide
AP-1	Activator Protein-1
APC	Antigen-Presenting Cell
APRIL	A Proliferation Inducing Ligand
APS	Ammonium Persulfate
ARDS	Acute Respiratory Distress Syndrome
ATF-6	Activating Transcription Factor
AT-I Cell	Alveolar Type I Epithelial Cell
AT-II Cell	Alveolar Type II Epithelial Cell
BAFF	B Cell Activating Factor
BAL	Bronchoalveolar Lavage
BALF	Bronchoalveolar Lavage Fluid
BMP	Betamethasonephosphate
BNP	Betamethasonephosphate Nanoparticle
bp	Base Pairs
BSA	Bovine Serum Albumine
CCL	CC Chemokine Ligand
CD	Cluster of Differentiation
cDNA	Complementary DNA

COX-2	Cyclo-Oxygenase-2
CREB	cAMP Response Element-Binding Protein
CRH	Corticotropin-Releasing Hormone
CSR	Class-Switch Recombination
Ctrl	Control
CXC	CXC Chemokine Ligand
Da	Dalton
DAMP	Danger-Associated Molecular Pattern
DBD	DND-Binding Domain
DC	Dendritic Cell
Dex	Dexamethasone
DMEM	Dulbecco's Modified Eagle Medium
DMSO	Dimethyl Sulfoxide
DNA	Deoxyribonucleic Acid
DNase	Deoxyribonuclease
dNTP	Deoxyribonucleotide Triphosphate
DUSP1	Dual Specificity Protein Phosphatase 1
e.g.	Exempli Gratia
ECM	Extracellular Matrix
ECP	Eosinophilic Cationic Protein
EDN	Eosinophil-Derived Neurotoxin
EDTA	Ethylendiaminetetraacetic Acid
ELANE	Elastase Neutrophil-Expressed
ELISA	Enzyme-Linked Immunsorbent Assay
EMA	European Medicines Agency
EMTU	Epithelial Mesenchymal Trophic Unit
ENI	European Neuroscience Institute
eNOS	Endothelial Nitric Oxide Synthase
EP	Eosinophil Peroxidase
et al.	Et Alii

FACS	Fluorescence Activated Cell Sorting
FasL	Fas Ligand
FBS	Fetal Bovine Serum
FDA	Food and Drug Administration
FGR	Familial GC-Resistance
FMN	Flavinmononucleotide
FSC	Forward Scatter
g	Gram
GC	Glucocorticoid
GILZ	Glucocorticoid-Induced Leucine Zipper
GM-CSF	Granulocyte-Macrophage Colony-Stimulating Factor
GR	Glucocorticoid Receptor
GRE	Glucocorticoid-Responsive Elements
GWAS	Genomewide-Association Study
HAT	Histone-Acetyltransferase
HDAC	Histone-Deacetylase
H & E	Hemalum and Eosin
HPA	Hypothalamus-Pituitary-Adrenal
HPRT	Hypoxanthine Phosphoribosyl Transferase
HSD	Hydroxysteroid Dehydrogenase
Hsp	Heat Shock Proteins
i.e.	Id Est
i.p.	Intraperitoneal
i.v.	Intravenous
IAV	Influenza A Virus
ICs	Inhaled GCs
IFN	Interferon
Ig	Immunoglobulin
IL	Interleukin

iNOS	Inducible Nitric Oxide Synthase
ITGAE	Integrin α E
IVC	Individually Ventilated Cage
JAM	Junctional Adhesion Molecule
k	Kilo
l	Liter
LABA	Long-Acting β_2-Agonist
LAVES	Lower Saxony State Office for Consumer Protection and Food Safety
LBD	C-Terminal Ligand-Binding Domain
LPC	Lung Parenchymal Cell
LPS	Lipopolysaccharide
m	Milli/ Meter
M	Molar
MACS	Magnetic Cell Separation
MBP	Major Basic Protein
MCP	Monocyte Chemoattractant Protein
MFI	Mean Fluorescence Intensity
MHC	Major Histocompatibility Complex
min	Minute
mRNA	Messenger RNA
n	Nano
NEB	Neuroepithelial Bodies
NET	Neutrophil-Extracellular Trap
NF-κB	Nuclear Factor Kappa-Light-Chain-Enhancer of Activated B Cells
nGRE	Negative Glucocorticoid-Responsive Elements

NLR	Nod-Like Receptor
NO	Nitric Oxide
NTD	N-Terminal Transactivation Domain
OA	Oleic Acid
OD	Optical Density
OVA	Ovalbumine
PAF	Platelet-Activating Factor
PAMP	Pathogen-Associated Molecular Pattern
PBS	Phosphate-Buffered Saline
PCR	Polymerase Chain Reaction
PFA	Paraformaldehyde
PI3K	Phosphatidylinositol-3-Kinase
PRR	Pattern Recognition Receptor
PTM	Post-Transcriptional Modifications
qRT-PCR	Quantitative Real-Time PCR
RANTES	Regulated upon Activation, Normal T Cell-Expressed, and Secreted
RNA	Ribonucleic Acid
RNase	Ribonuclease
RNA-Seq	RNA Sequencing
ROS	Reactive Oxygen Species
RSV	Respiratory Syncytial Virus
RT	Room Temperature
Sec	Seconds
SABA	Short-Acting β_2-Agonist
SDS	Sodium Dodecylsulfate
SEGRA	Selective GR Agonist
SEM	Standard Error of the Mean

SLPI	Secretory Leukocyte Inhibitory Protein
SP	Surfactant Protein
SPC	Surfactant Protein C
SPF	Specific Pathogen-Free
SSC	Sideward Scatter
TEMED	Tetramethylethylenediamine
TGF	Transforming Growth Factor
T_H	T Helper Cell
TLR	Toll-Like Receptor
TMB	Tetramethylbenzidine
TNF	Tumor Necrosis Factor
T_{reg}	Regulatory T Cell
TSLP	Thymic Stromal Lymphopoietin
U	Unit
VEGF	Vascular Endothelial Growth Factor
WHO	World Health Organization
ZO	Zonula Occludens
α	Alpha
β	Beta
Δ	Delta
ε	Epsilon
λ	Gamma
µ	Mikro
p	Piko

7.3 List of Figures

7.4 List of Tables

7.5 Acknowledgements

An erster Stelle möchte ich meinem Doktorvater Prof. Dr. Holger M. Reichardt danken, der mir die Erstellung meiner Dissertation in seiner Arbeitsgruppe ermöglicht hat. Ich danke ihm für die Betreuung meiner Arbeit, für seine Unterstützung und fachlichen Rat in den letzten Jahren.

Besonderer Dank gilt den Mitgliedern meines Thesis-Komitees Prof. Dr. Uwe Groß und Prof. Dr. Frauke Alves, sowie den Mitgliedern meines Prüfungsausschusses Prof. Dr. Lutz Walter, Prof. Dr. mult. Thomas Meyer und Prof. Dr. Hubertus Jarry.

Desweiteren möchte ich den Kollaborationspartnern des Karlsruher Instituts für Technologie Prof. Dr. Claus Feldmann und Dr. Joachim Heck für die Bereitstellung der Nanopartikel danken.

Zusätzlich bedanke ich mich bei dem Transkriptomanalyselabor von Dr. Gabriela Salinas-Riester für die Durchführung der RNA-Sequenzierung und der bioinformatischen Datenanalyse.

Darüber hinaus möchte ich mich bei sämtlichen Mitgliedern und Ehemaligen meiner Arbeitsgruppe bedanken - ganz besonders bei Anna, Kai, Xiao, Katharina, Eric, Milena, Ann-Kathrin, Sarah, Nicky und Elena A. Besonderer Dank gilt Amina - die mir im Labor immer treu zur Seite stand und auf deren Unterstützung ich immer zählen konnte. Deine tröstenden Worte konnten mich immer wieder aufbauen. Julian - ohne Dich würden mir die Mäuse immer noch um die Ohren fliegen. Außerdem möchte ich mich bei meiner "Leidensgenossin" Elena bedanken. Seit dem Masterstudium standest Du mir stets zur Seite, ohne Dich wäre die Zeit nur halb so schön gewesen.

Danke sagen möchte ich auch Robyn, Julius, Jule und allen meinen anderen Freunden, die mich in den letzten Jahren unterstützt haben und die mir zeigten, dass es auch noch ein Leben außerhalb des Labors gibt.

Zu guter Letzt möchte ich mich ganz herzlich bei meinen Eltern Uwe und Marieta bedanken, ohne deren Hilfe ein Studium und eine Promotion niemals möglich gewesen wären. Meinen Eltern, meinem Bruder André und ganz besonders Jens, möchte ich für den Rückhalt in den letzten Jahren danken. Ihr habt meine Launen jahrelang ertragen und mich dennoch immer wieder neu aufgerichtet.